Universität für Bodenkultur Wien
University of Natural Resources and Life Sciences, Vienna

Department of Civil Engineering and Natural Hazards,
Institute of Applied Geology (IAG)

Detecting the equifinality of r.avaflow regarding entrainment and input discharge: a case study of the 2010 jökulhlaup at Eyjafjallajökull (Iceland)

Masterarbeit / Master thesis
Angestrebter akademischer Grad / In partial fulfilment of the requirements for the degree of
Diplomingenieur / graduate engineer

submitted by:
KRIECHBAUM, ULRICH

Supervisor: Priv.-Doz. Dr. Mergili, Martin
Co-Supervisor: Dipl.-Phys. Dr. techn. Fischer, Jan-Thomas

Student number 01140928 07.05.2020

Acknowledgements

First of all I want to thank my parents who made it possible for me to attend University and always supported me. Thank you for your patience, support, encouragement in harder times and everything else. Thank you for the opportunity to find my own way in life.

Thanks to Martin Mergili for supervising. He was a wonderful mentor, always there if needed and a huge help with his vast knowledge. I always could rely on his help which was needed quite a lot sometimes. It was great working with you.

Thanks to Jan-Thomas Fischer for co-supervising this thesis. Thanks for the possibility to conduct my simulations at the BfW in Innsbruck in my own office. Thank you for always having an open door for me, listening to my questions. Your motivation was always a huge help.

Thanks to BOKU and all its people for all the great times. It was a special place and a special time for me, and my time would have definitely not been the same at a different university.

Thanks to my girlfriend Sarina, who was always supporting and motivating me, especially in hard times. Your kindness and loving support helped me to push through until the end and finish this thesis.

Thanks to my sister, which made time at university such a fun one. I always could rely on you if I need anything which was a big help throughout University.

I want to thank all my study colleagues I met throughout University, which became great friends. You all made University a special time for me. Especially Fruchti, Jonas and Uschi from my masters and Benji and Lisi from my bachelors.

Last but nor least I want to thank Eyjafjallajökull for providing an interesting topic for my master thesis. It was a pleasure exploring you.

Abstract (English)

The main goal of this thesis is to determine, if equifinality plays an important role simulating jökulhlaups with the underlying model, with respect to different mass sources as initial and boundary conditions, utilized in the simulation tool r.avaflow regarding entrainment and the input discharge. Used in the present work was the version r.avaflow_20181022.
A short-lived eruption on the southern flank of the Eyjafjallajökull volcano 2010 burst through the glacier cover and produced a sudden outburst flood that descended the southern slopes of the mountain. The flood almost breached the main ring road along the south coast of Iceland, caused damage to fields, and vegetated land along its way. The flood entrained volcanic tephra and debris and contained a substantial proportion of solid material in the lower part of the path. The characteristics of this event are relevant for simulations of mixed mass flows involving several types of materials and their interactions. The simulation tool r.avaflow allows assessing this type of complex, multi-phase processes, combining different types of mass materials including ice, snow, water and rock in the form of avalanches, debris flows and flood waves. Thus, we explore the potential use of r.avaflow to simulate this event, based on available data of the entrained volume, maximum flow height of the flood and assumptions of the time till the flow reached the lowlands. 121 simulations with different combinations of entrainment-coefficient and input-hydrograph were conducted to detect, if equifinality issues arise using r.avaflow.
This simulation approach holds considerable potential to assess possible impacts of hyperconcentrated jökulhlaups at other locations in Iceland that pose hazard to people and property, including jökulhlaups from the Katla volcano in Mýrdalsjökull ice cap and the Öraefajökull volcano in S-Vatnajökull ice cap, which are known to produce floods that are a mixture of water, debris and ice fragments.

Abstract (Deutsch)

Der Fokus der vorliegenden Arbeit liegt darauf zu überprüfen, ob Äquifinalität eine wichtige Rolle spielt bei Simulation von Jökulhlaups mit dem zugrunde liegenden, in r.avaflow implementierten, Modell in Bezug auf das Entrainment und den Abfluss. Verwendet wurde die Version r.avaflow_20181022.

Im April 2010 ereignete sich ein Vulkanausbruch am Eyjafjallajökull, welcher einen Jökulhlaup zur Folge hatte, der die südlichen Hänge hinabströmte. Der Jökulhlaup erreichte beinahe die Hauptstraße, die entlang der Südküste von Island verläuft, beschädigte Felder sowie landwirtschaftliche Flächen entlang des Fließpfades. Entlang des Fließpfades wurden Tephra und Geröll erodiert, was zu einem erhöhten Anteil an festem Material in dem Jökulhlaup führte. Die Charakteristika dieses Ereignisses sind relevant für Simulationen von Massenbewegungen von verschiedenen Materialien und deren Wechselwirkungen. Es ist möglich, mit r.avaflow solche komplexen, mehrphasigen Ereignisse zu simulieren welche aus verschiedenen Materialien wie Eis, Schnee, Wasser und Geröll bestehen und in Form von Lawinen, Muren und Flutwellen potentiellen Schaden anrichten können. Aus diesem Grund untersuchen wir r.avaflows´s Möglichkeiten dieses Ereignis zu simulieren, basierend auf vorhandenen Daten zu erodiertem Volumen, maximaler Fließhöhe und Schätzungen zur Fließzeit bis der Jökulhlaup die Ebene erreicht. 121 Simulationen mit unterschiedlichen Kombinationen von Entrainment-Koeffizient und Input-Hydrographen wurden durchgeführt um zu veranschaulichen, ob Äquifinalität Probleme verursachen kann, wenn man dieses Ereignis mit r.avaflow simuliert.

Mit dem Ergebnis dieser Simulationen ist es eventuell möglich, Auswirkungen anderer potentieller Jökulhlaups abzuschätzen. Es gibt in Island mehrere Standorte, wie den Katla Vulkan auf der Mýrdalsjökull Eiskappe und den Öraefajökull Vulkan auf der S-Vatnajökull Eiskappe, die bekannt sind für solche Ereignisse, deren Folgen man hiermit eventuell besser abschätzen kann.

List of contents

1 Introduction

Interactions of lava with ice and snow are often the result following eruptions of ice-covered volcanoes. These type of events, often called jökulhlaups (glacial outburst floods), have caused more than 37.000 fatalities, in more than 40 historical eruptions, globally, especially in Iceland, Alaska, the northwest USA and parts of the Andes (Dunning et al., 2013; Magnusson et al., 2012).

In Iceland, jökulhlaups are the most frequently occurring volcanic hazard. Usually, the magnitude is relatively small, while major events, which are much less frequent, can reach peak discharges of order 10.000 – 100.000 m^3/s. Mostly, these major events, are following large eruptions under glaciers. Recent eruptions in Iceland, with interactions of volcanic eruptions with a surrounding glacier, have been under investigation, notably the eruptions at Gjálp in 1996, Grímsvötn in 1998 and 2004 and minor eruptions in the Katla caldera. These investigations have shown a coherence of glacier response to rapid melting for ice thicknesses and proved, that a highly efficient heat transfer occurs from lava to ice, during the subglacial stage of an eruption (Magnusson et al., 2012).

Eyjafjallajökull's peak is 1666 m a.s.l., the southern slopes are cultivated with agricultural land, with the closest farms 7 km to the summit caldera. Because under recent investigation, there are various types of monitoring systems installed at Eyjafjallajökull.

Figure 1: Overview of the Eyjafjallajökull ice cap. Source: Martin Mergili, 11 November 2018

On April 14th 2010, a flooding proceeded down the southern side of the ice cap, during which a jökulhlaup carved a 3 km trench in the ice surface (M. Gudmundsson et al., 2011; Roberts et al., 2011).

Jökulhlaups can be the result of more than one trigger mechanism (see Table 1), thus are complex processes. To investigate jökulhlaups, which pose an increasing threat to people and property, researchers mainly use assessments and simulations (Kattel et al., 2016; Xin et al., 2008).

Modelling of complex mass flow processes is only at the beginning. Well documented events are needed, coupled with physically based models, to allow a realistic reproduction using a simulation tool. r.avaflow is capable of reproducing such complex events by implementing the Pudasaini (2012) two-phase flow model and explicitly considering entrainment, and the corresponding change of basal topography (M. Mergili, Fischer, Krenn, et al., 2017; Schneider et al., 2014).

By entraining bed material they encounter, mass flows, such as debris flows, avalanches, jökulhlaups, can increase vastly in size and destructive potential (Iverson & Ouyang, 2015). Because of the poor understanding of the mechanical processes of entrainment in geophysical mass flows, it is one of the greatest challenges in modelling flow dynamics (Crosta et al., 2009; Hungr et al., 2005; Shiva P. Pudasaini & Fischer, 2016).

Different methodologies have been evolved over the past decades to better treat model and /or data uncertainties. One method to treat this uncertainties is the equifinality thesis. The equifinality thesis states that there are multiple acceptable models or parameter sets, not only process parameters but initial (e.g. discharge) and boundary (e.g. topography) conditions, within a model that operate as representation. In the context of deterministic simulation, these models or parameter sets represent, equally good (or poor), the observed event. With an increasing number of unknowns, the results using the equifinality thesis become more and more unstable (Beven, 1993, 2012; Beven & Freer, 2001; Ebel & Loague, 2006).

Jökulhlaups are not only triggered by volcanic eruptions but can origin from different sources (see Sect. 3.1). However, despite different trigger mechanisms, all jökulhlaups are released from a glacial source. Most of the newer research believes, that jökulhlaups, and their attendant hazards, will be more frequent events in the future, due to climate warming and accompanying glacier thinning, in the regions of the world, that are mentioned above. Therefore, anticipation of events will become more and more important in the future to manage the potential risks regarding people and infrastructure. As mentioned above, with an increasing number of unknown parameters, results produced with the equifinality thesis can´t be taken in consideration. It could possibly hamper reliable simulations, therefore it is crucial to better understand the ongoing mechanisms during jökulhlaups to be able to get meaningful results using simulations. The number of glacier lakes will increase along with the volume of these glacial lakes. The melting rates of mother glaciers will rise and moraine dams may become instable due to climate warming. Lakes, which are dammed by moraines, have increased in number and size in the last 40 years,

worldwide. If these moraine dams collapse, glacial lake outburst floods (GLOFs/jökulhlaups) will be the consequence, resulting in possible massive and devastating debris flows (Anacona et al., 2015; Awal et al., 2010; Bajracharya et al., 2007; Breien et al., 2008; Dunning et al., 2013; Kattel et al., 2016; Lecomte et al., 2008; Mool et al., 2001; S. Pudasaini & Hutter, 2007; Worni et al., 2012; Xin et al., 2008).

Research questions:
1: Is equifinality an important aspect simulating jökulhlaups with the underlying model implemented in r.avaflow, with respect to initial and boundary conditions?

2: Can the software tool r.avaflow be used to simulate the 2010 jökulhlaup at Eyjafjallajökull in an empirically adequate way, and how large are the accompanying uncertainties and how can we quantify them?

2 Aim

The main goal of this thesis is, if equifinality issues arise in jökulhlaup simulations, using the underlying model, with respect to initial and boundary conditions, implemented in the simulation tool r.avaflow. In this context the main objective of the thesis is to determine, if different parameter sets, for the same event, can show equally good (or poor) results, for the same observed event. More in detail, the implemented Pudasaini(2012) two-phase mass-flow model will be used to reproduce a jökulhlaup event. Eleven values will be assigned to the two input parameters entrainment-coefficient and input-hydrograph (Discharge), between an upper and lower threshold, to reproduce the observed event. By the means of entrained volume, flow-height at a certain point and flow-time until a certain point is reached, the capability of the underlying model implemented r.avaflow regarding equifinality will be detected. These three control quantities were chosen, because there were reasonable observations.
For the entrained volume, a post-event DEM was available, which was created from an air-bourne laserscan of the area prepared by the Icelandic Meteorological Office. Using this post-event DEM, it was possible to create a pre-event DEM, and furthermore to estimate the total entrained volume. Another reason for the entrained volume as control quantity was, that a good comparison with the simulations was possible. For each simulation, r.avaflow creates a validation file stating

the exact solid and fluid entrained volume of the simulation, which then could be compared to the observed entrained volume.
The flow height was chosen, because measurement devices were installed prior to the event, measuring the flow heights at different points along the flow path. At the end of the southern gully (see Fig. 20) two measurement points were installed close-by, so, for the observation value the mean of these two measurements was chosen. To compare the observation with the simulations, regarding the flow height, a control-point was installed in r.avaflow. This control-point was installed at roughly the same location as the two measurement points, and measured the maximum flow height for each simulation, which then was compared to the observation value.
At last, the flow time was chosen as control quantity. There are different sources of information regarding the observation value. Pictures made by the Icelandic Meteorological Office out of a helicopter and statements by witnesses, which have seen or heard the flow at a certain time at a certain point. Using all this information, the flow time was reconstructed, choosing two points at which the flow appeared after 45, respectively 60 minutes. To compare the observation with the simulations, two output-hydrographs were installed at the two chosen points. Analyzing these two hydrographs, the time the simulated flow needed to reach the two points could be extracted to compare it to the observation.

The second aspect of this thesis is the replication of jökulhlaups in general, which will also be detected, and, simultaneously, inhowfar equifinality issues emerge in jökulhlaup simulations with r.avaflow. 121 simulations will be executed in total, all with different input-parameter combinations regarding the entrainment-coefficient and the input-hydrograph. After all simulations are conducted, heatmaps will be created to compare the observations with the simulations and, furthermore, show if r.avaflow is capable of, empirically adequately, simulate jökulhlaups.

3 Background

3.1 Jökulhlaups

Jökulhlaups are sudden outbursts of floods that are released from a glacial source, regardless of their origin, or a moraine-dammed lake (Fig. 2; Table 1). It is an icelandic term which does not differentiate between water flows and lahars.
Lahars are mud- or debris flows streaming down volcanoes that always contain water as a component. In this thesis the term jökulhlaup further will relate to water flows (Carrivick, 2011; M. Gudmundsson, 2015; Roberts, 2005).
They can be divided in nonvolcanic and volcanogenic events. For this Thesis events of volcanogenic origin are important, which can be separated in two types:

- originating from subglacial lakes, where geothermics melt the base of the ice. Events of this type usually drain periodically and are common in Iceland. Minor events have a duration of hours to days, with peak discharges around 100m³/s. Bigger reservoirs can yield peak discharges of 1000-10000 m³/s. Because of their usually periodic drain events of this kind usually do not cause major hazards.
- The second type of volcanogenic jökulhlaups occur as a result of direct melting during volcanic eruptions. Floods of this type usually contain more sediment load and have higher peak discharge than events with a geothermal origin. Jökulhlaups breaking through the glacier and reaching the surface of it, are capable of entraining lots of snow and/or firn, especially if the eruption occurs in the winter. The result of this entrainment can be a slurry of water, slush, tephra and ice blocks (M. Gudmundsson, 2015).

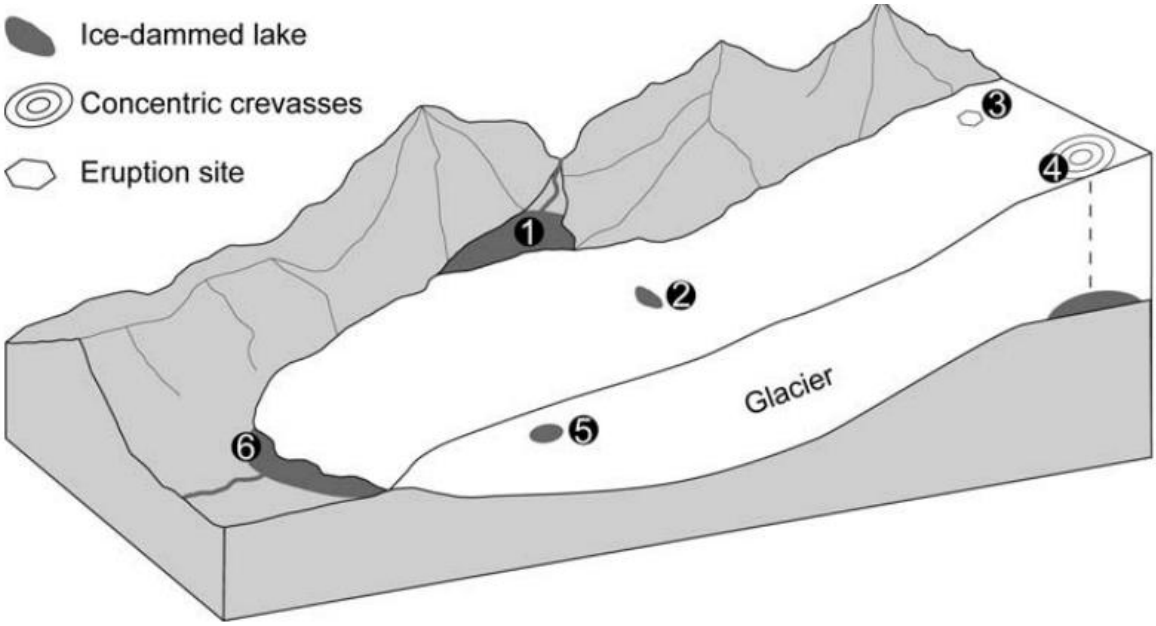

Figure 2: Reservoir sites and meltwater sources for jökulhlaups. See Table 1 for a summary about each numbered location. Source: Roberts 2005

Table 1: Recognized types of jökulhlaups and candidate trigger mechanisms. Source: Roberts 2005

Recognized types of jökulhlaups	**Postulated trigger mechanisms**
Type 1, drainage of an ice-marginal, ice-dammed lake	Hydrostatic stress causes ice dam to float (Thórarinsson, 1939) Mechanical damage of the dam base caused by enhanced glacier sliding (Liestøl, 1956) Increased hydrodynamics due to the growth of the breach between glacier ice and substrate (Walder & Costa, 1996)
Type 2, drainage of a supraglacial lake	Hydraulic tapping of a meltwater reservoir by intraglacial drainage (Anderson et al., 2003; Fisher, 1973) Intraglacial release of meltwater (Björnsson, 1976; Boon & Sharp, 2003)
Type 3, volcanically induced jökulhlaup	Ice melt due to subglacial volcanism, causing either subglacial ponding (see type 4 for trigger mechanisms) or immediate drainage of floodwater with no significant storage (Björnsson, 1988; Pierson, 1989)
Type 4, drainage of a subglacial lake	Hydrostatic stress causes ice dam to float (Thórarinsson, 1939)
Type 5, drainage of an intraglacial cavity	Shattering of a water-filled cave (Haeberli, 1983) Intraglacial drainage of a meltwater teservoir (Anderson et al., 2003; Fisher, 1973)
Type 6, drainage of a moraine-dammed lake, including those dammed by ice cored moraines	Lake level rises suddenly, spillway increases (Clague & Evans, 2000; Haeberli, 1983)
Type 7, meltwater release during surge termination	Abrupt evacuation of stored meltwater due to change of subglacial drainage distribution(Björnsson, 1988; Kamb et al., 1985)

There have been documented jökulhlaups all around the world. Major events can release millions of cubic meters in a short period of time (minutes to hours). Due to their high erosive and transport capacity deep, high-velocity flows can be generated (Breien et al., 2008). Thus, jökulhlaups constitute a severe hazard to communities in mountainous regions. Due to an increasing population and higher tourism activities in mountainous areas, people have settled in regions, which are highly exposed to natural hazards (Anacona et al., 2015; Bajracharya et al., 2007).

The physics of the flow of water is a complex topic with a rich variety of interesting problems. To exemplify this complexity, Nye (1976), who was one of the first to investigate jökulhlaups on a scientific base, provided this illustrative example: Water flow through a subglacial tunnel can generate enough heat by friction to enlarge the tunnel in a catastrophic way; but water flow through the vein system, if it occurs, evidently does not normally do this. Why should this be so? In his jökulhlaup theory, Nye (1976) states, that water from a flood lake drains in a subglacial channel who grows in size to operate the drainage hydrograph. However, in his theory, he ignores glacier flow due to basal sliding, which may occur due to changing subglacial water pressures during floods.

Alpine marginal lakes and supraglacial lakes are both reservoirs whose water balance depends on the current climate, and the drainage-ice-flow coupling in both types of system involves rapid, high-magnitude variations in subglacial discharge. Nye (1976) offered a foundation for modelling the physics of this coupling with his theory. To simulate jökulhlaups discharge full coupling

between subglacial drainage and the lake is required, which is defined by two conditions: (i) water flux at the channel inlet equals the lake outflow, and (ii) the lake-water depth controls the water pressure at the channel inlet.
A circumstance, which makes simulating jökulhlaups rather diffcult, is the variability in the hydrodynamic behaviour of different jökulhlaup systems that origin from their glaciological and environmental factors, factors which may be difficult to straighten with field data (Kingslake & Ng, 2013; Nye, 1976).

3.1.1 Jökulhlaups in Iceland

In Iceland exist six subglacial geothermal areas, beneath ice cauldrons, where jökulhlaups originate from (Fig. 3). From the 1940s on, jökulhlaups were registered at an interval of 4 to 6 years, with peak discharges of 600 to 10000 m³/s, lasting 2 to 3 weeks, reaching volumes of 0.5 to 3.0 km³. Before the 1940s, about one jökulhlaup per decade was recorded, with volumes of estimated 5 km³ and peak discharges of roughly 300000 m³/s (Björnsson, 1992, 2003).

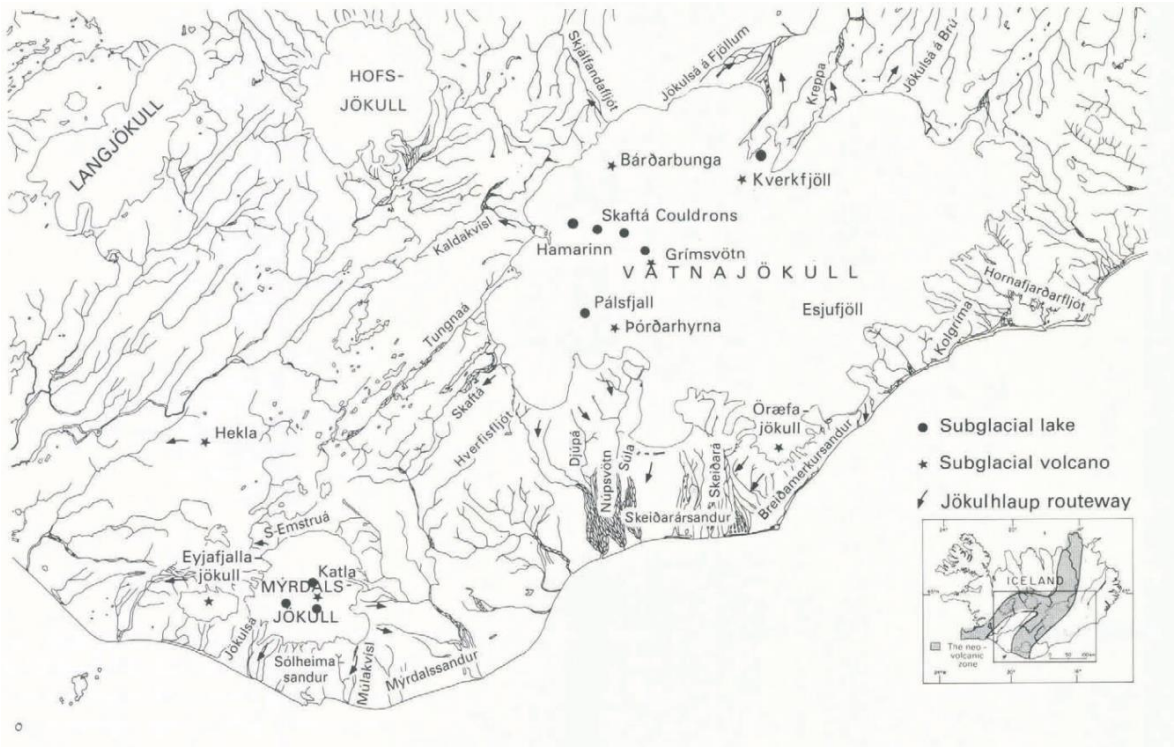

Figure 3:Location of subglacial lakes at geothermal areas and sites of subglacial volcanic eruptions in Iceland, and rivers affected by jökulhlaups in historical times. The small frame in the bottom right is Fig.4. Source: Björnsson 2003

At least 80 subglacial volcanic eruptions have been reported, since Iceland was settled around 870 AD. Many of these jökulhlaups reached enormous size with fierce impact on inhabitated areas and landforms. The largest known flood originated from Katla volcano, which is east of Eyjafjallajökull, lasted 3 to 5 days, reached peak discharges of 100000 – 300000 m^3/s and had a total volume of ~ 1 km^3. What is now known is, that the largest possible jökulhlaups are situated in northern Vatnajökull (Bardharburnga and Kverkfjöll) and would be caused by eruptions in the big ice-filled calderas. Researchers believe, that they could be the source of prehistoric jökulhlaups, which reached peak discharges up to 400000 m^3/s. This kind of events have had huge impact in Iceland, causing the loss of lives, ruined farms and cultivated land, devastating large areas of vegetated land, threatening and destroying roads, bridges and hydroelectric power plant on glacier-fed rivers. Large canyons have been eroded and sediment transported and deposited over outwash plains, as effects of jökulhlaups on the Icelandic landscape. Research and better understanding of jökulhlaups are essential for advance warnings, preventive measures and civil defence.

The first attempts to simulate Icelandic jökulhlaups were made by Nye (1976), Spring and Hutter (1981) and Clarke (1982). Partly, because Iceland is a unique and valuable study site for glaciovolcanic interactions. 10 % (~11200 km^2) of the area is ice-covered, of which 60 % are overlying the active volcanic zone (Fig.4). 15 subglacial volcanic eruptions took place in the 20th century (10 major and 5 minor events), of which one-third happened in Iceland. Another reason is, that the Icelandic community has a big archive of documented natural hazards, such as volcanic eruptions, earthquakes, snow avalanches and jökulhlaups, since the beginning of the settlement. Because of this exact documentation natural events can be investigated quite well to some extent (Björnsson, 1992, 2003; Johannesdottir & Gisladottir, 2010).

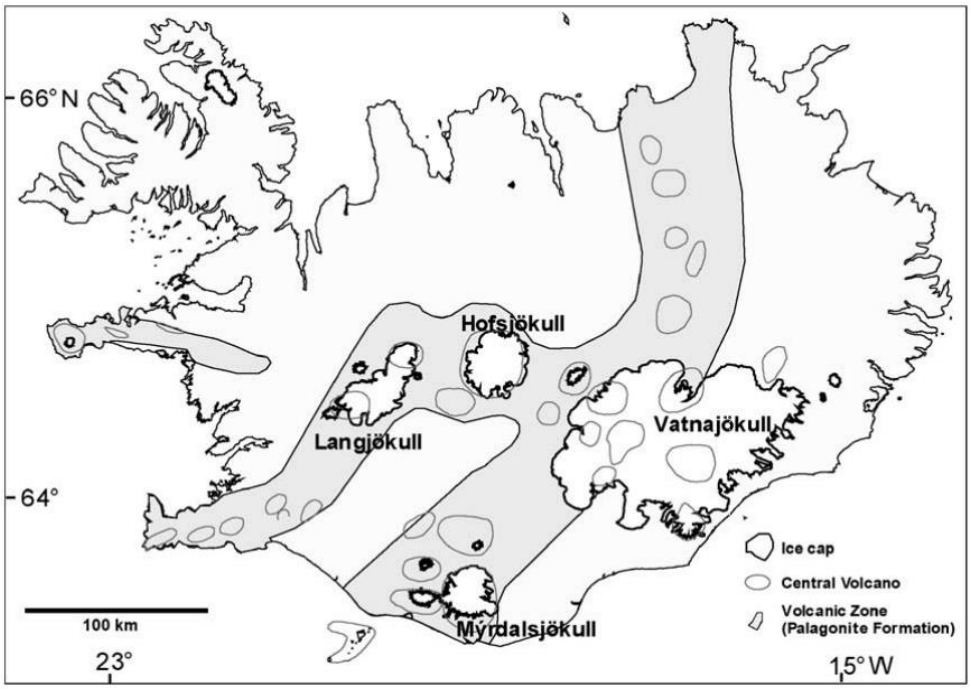

Figure 4: Location map of iceland showing icecaps, the volcanic zone (The Palagonite Formation) and the central volcanoes. Source: Björnsson 2003

3.2 Eyjafjallajökull 2010

Eyjafjallajökull is approximately located in the center of the southern coast of Iceland. The Mid-Atlantic plate boundary, which runs through Iceland, is uttered as a series of seismic and volcanic zones. It is divided into two parts, the Western and Eastern Volcanic Zones (Karlsdottir et al., 2012).

The Eyjafjallajökull eruption in 2010 is probably most famous for the disruption to international air traffic that it caused, cancelling about 100000 commercial flights, costing the aviation industry 250 million US-dollars per day during April 15th-20th. Not so well documented is the impact that it had on local residents, caused by ash fall to the south and east of the crater. In the course of the summit eruption, intensive volcano-ice interactions occurred during the first few days. These interactions produced rapid melting of ice, formation of ice cauldrons and sediment-laden outburst floods during April 14th – 16th. Jökulhlaups were of primary concern for officials, who tried to protect the local population prior and during the eruption (Bird & Gisladottir, 2012; Magnusson et al., 2012).

The eruption was preceded by almost 20 years of intermittent unrest, indicated by earthquake swarms in 1994 (middle to upper crust), 1996 (base of the crust), 1999 and 2009-2010 (shallower swarms). Definite signs that an eruption was imminent, were intense seismic activity and crustal deformation around the Eyjafjallajökull ice cap in 2009 and 2010 (Dunning et al., 2013; M. Gudmundsson et al., 2011).

The Eyjafjallajökull volcano rises from sea level to about 1666 m a.s.l. and is a central volcano. It was built through numerous eruptions over the last 800-thousand years. From an elevation of 1000 m a.s.l. on, the volcano is covered by an ice cap of approximately 80 km² and typically less than 100 m thick on the slopes. The small, ice-filled, summit caldera is about 2,5 km across with a 1,4 km wide breach towards north. In the west part of the summit caldera the ice is ~200 m thick, in the east part up to 400 m. With a relief of about 1,5 km, a length of 27 km in east-west direction and a maximum width of 14 km in north-south direction, the Eyjafjallajökull is located at the eastern margin of the southern lowlands, with an area of ~300 km² (Karlsdottir et al., 2012; Magnusson et al., 2012).

The eruption of Eyjafjallajökull in April 2010 was the largest eruption in iceland since Hekla 1947. It took place within the summit caldera, initially beneath around 150 m of ice. The event lasted 39 days and generated multiple jökulhlaups, which were caused by localised melting of glacier ice. Most of the ice was melted during the first couple of days, with melting rates ~300 – 500 m³/s, melting up to 200 m thick glacier ice at the eruption sites. Compared to other recent jökulhlaup events in Iceland, the melting was rather slow. In the early hours of April 14th, the first visible sign was an eruption plume, while the first signs of floodings on the glaciers were seen around 0650 UTC at a gauging station north of the volcano. This first flood, flowing down the Gígjökull outlet glacier, reached peak discharges of 2500 – 3000 m³/s, at the main road, 20 km downstream. A

maximum height of 10 km was reached by the eruption plume on the first day. After five days the main eruption was over, with explosive power, plume height, and ash production significantly decreasing. Between April 21nd – May 2nd, lahars flowed down northward from the crater, streaming down the valley glacier Gígjökull, with ice being melted along their paths. The size of the eruption is classified as moderate, producing 0,27 km³ of tephra and the volcanic plume never exceeding a height of 10 km a.s.l., most of the time staggering between 4 and 8 km a.s.l. Still, ash was transported thousands of kilometers over the Atlantic Ocean and parts of Europe (the reason so many flights had to be cancelled) (M. Gudmundsson et al., 2011; Jensen et al., 2013; Karlsdottir et al., 2012; Roberts et al., 2011).

Eruptions of the Eyjafjallajökull have always been accompanied by jökulhlaups. Around 700 AD occurred the oldest known jökulhlaup, while an eruption ~920 AD produced a jökulhlaup flowing down the northern slope of the volcano. Since the 10th century, Eyjafjallajökull erupted three times: 1612, 1821 – 1823, where all eruptions were accompanied by disastrously jökulhlaups and most recently, the event described above, 2010 (Bird & Gisladottir, 2012; Björnsson, 1992, 2003; Karlsdottir et al., 2012).

Due to their history of eruptions, an automatic monitoring system has been installed in 1999 for Eyjafjallajökull and Katla (25 km east of Eyjafjallajökull). The monitoring system includes an automated, 56-station seismic network; a continuous Global Positioning System (GPS) network of more than 70 stations; a network of automated hydrological stations for monitoring runnof in regions close to glaciers and a regional network of six borehole strainmeters, which monitor deformation of the Earth's crust in their vicinity. Three institutes are responsible for the monitoring system and further to provide relevant information for officials and the general public: (i) the Icelandic Meteorological Office (IMO), (ii) the Institute of Earth Sciences (IES) of the University of Iceland and (iii) the Department of Civil Protection and Emergency Management of the National Commisioner of the Icelandic Police (NCIP-DCPEM). Alongside that, a risk assessment and an evacuation plan were established in 2005 for the close communities. In 2006 a public awareness campaign took place and, because of a possible eruption of the Katla volcano, an evacuation drill was conducted, where all inhabitants of nearby areas participated (Bird & Gisladottir, 2012; M. Gudmundsson et al., 2011; Karlsdottir et al., 2012).

Witnessing the eruption of Eyjafjallajökull in 2010 provided an exceptional opportunity to observe the evolution of glacial/proglacial geomorphology during a series of volcanogenic jökulhlaups (>140 events). This enabled a special possibility to (i) survey potential jökulhlaup routes immediately prior to the eruption and (ii) quantify during-event and post-event landscape-scale changes with the goal of defining the relationship between a well-constrained sequence of jökulhlaups, which were generated volcanically, and the evolution of the proglacial landscape (Dunning et al., 2013).

Residents, officials and researchers have, without a doubt, learned essential lesson from the 2010 Eyjafjallajökull eruption. Researchers had an unique opportunity to witness an event of this

type live, while officials and residents developed new response procedures and strategies, which are appropiate to vulnerable communities (Bird & Gisladottir, 2012).

3.2.1 Event description

The Eyjafjallajökull volcano, with its included ice cap, is located in southern Iceland (Fig. 5). On April 14th there was an eruption induced flood on the southern side of the ice cap, down the Svadbaelisá river, which carved a 3km trench in the ice surface (Fig. 6) and inundating farmland (~1,5 km²) in the lowlands with a sediment-laden floodwater, also destroying ~70m of levees (Roberts et al., 2011). It was not the main eruption of the Eyjafjallajökull event causing the flood down the Svadbaelisá river, but one of many small eruptions.

Figure 5: Study area located in southern Iceland. The green field marks the area impacted by the described event. Source: Google Maps

The flood almost breached the main ring road along the south coast of Iceland and caused damage to fields and vegetated land along its way (Fig.7). The flood entrained volcanic tephra and debris and contained a substantial proportion of solid material (tens of percentages according to Tómas Jóhannesson from the Icelandic Meteorological Office) in the lower part of the path. The

characteristics of this event are relevant for simulations of mixed mass flows involving several types of materials and their interactions. The simulation tool r.avaflow allows to assess this type of complex, multi-phase processes, combining different types of mass materials including ice, snow, water and rock.

Figure 6: Trench carved in the ice surface. Source: Tómas Jóhannesson

Figure 7: Inundated farmland. The red-dotted line is indicating the main ring road. Source: Tómas Jóhannesson

According to radar images from the Icelandic Coast Guard a path had formed in the glacier at 10:23 GMT, reaching “far down” from the top caldera. Just before 10:30 the jökulhlaup was heard flowing down the gully at the bottom of the valley (Núpakotsdalur, which was quite noisy and good to hear according to a local farmer (Ólafor Eggertsson), who was interviewed shortly after the event. On a photo (Fig. 7) taken from a helicopter at 11:02 GMT the flood has reached about 100m below the main ring road. The farmer stated in his interview, that the estimated time from the gully to the bridge to be around 15-18 minutes.

Fig. 8 shows a DEM after the event of the study area. Marked as red, is the area of extent. A month after the event a lahar came down the river path and deposited great amounts of debris. Also, a number of floods occurred during the summer. The DEM was measured after these events, so it shows a different landscape, especially for the lowlands, than at the time of the jökulhlaup. Therefore, the present work focuses more on flow time and flow height than the area of extent.

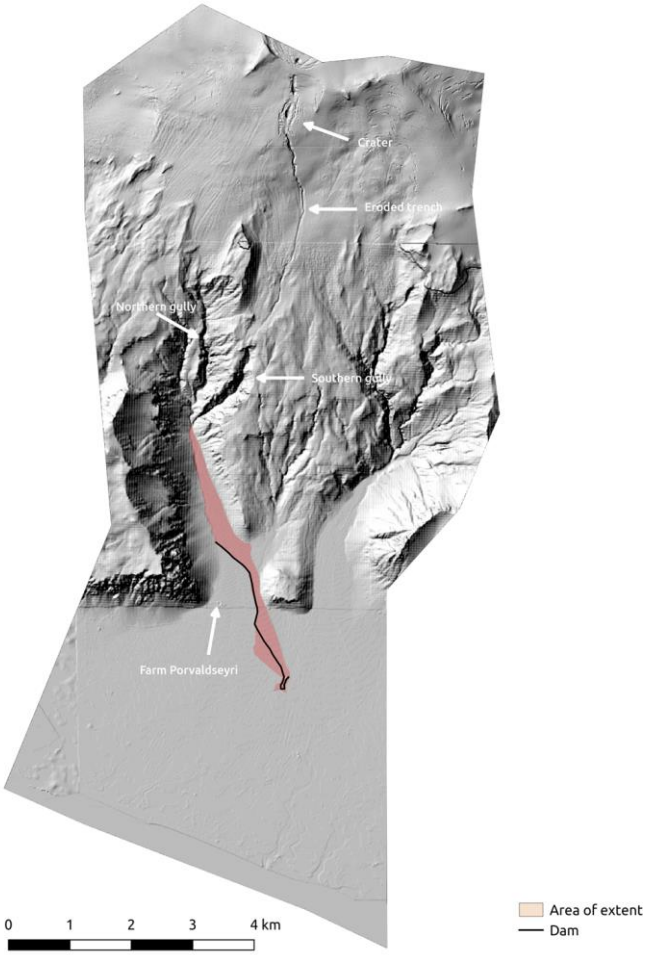

Figure 8: DEM of study area.

3.3 Simulation tools for gravitational mass flows

Nowadays, the most used simulations tools for gravitational mass flows, such as rockslides, rock avalanches and avalanches, are effectively single-phase. Most used are Coulomb- or Voellmy-type models for single-phase flows, e.g. dry rock and snow avalanches(Fischer et al., 2012; Sosio et al., 2012; Voellmy, 1955). These models (single-phase Voellmy- or Coulomb-type models) are not able to adequately simulate complex events, such as process chains of two-phase mass flows (Hungr & Evans, 2004; Schneider et al., 2010; Sosio et al., 2012). Real two-phase flow models (such as Pudasaini, 2012) are better suitable for simulating complex process interactions of solid (rock and/or ice) and fluid (water, snow, slurry) phases (S. Pudasaini & Krautblatter, 2014).

One of the main purposes of mass flow models is hazard mapping, which gained more and more importance in the last decades (Fischer et al., 2012; Gruber & Margreth, 2001; S. Pudasaini & Hutter, 2007). Hazard mapping is the process, where endangered areas, i.e. areas which are exposed to natural hazards, are defined and furthermore the necessary requirements are specified, under which new infrastructure or civil engineering work is allowed to be created. For areas, where the defined risk is too high, it is possible that further infrastructure is prohibited at all. If there already constructions on the area under investigation, additional mitigation measures are taken into account. For a sophisticated risk assessment and evaluate the right mitigation measures, and the reasonable dimensions of those, simulation models became an important tool for practicioners and decision makers. Simulations models provide flow heights, flow velocities, total runout distances and with these parameters the potential impact area, destructive impact forces and deposition characteristics. Using all these information defense structures, hazard maps and risk assessments can be evaluated (Bottino et al., 2002; Chen & Lee, 2000; Crosta et al., 2006; S. Pudasaini & Hutter, 2007; S. Pudasaini & Krautblatter, 2014; Schneider et al., 2010; Sosio et al., 2012).

GLOFs are a present natural hazard all around the globe. Millions of cubic metres of water can be released in a short period of time (minutes to hours) creating deep, high-velocity flows with major erosive and transport capacity (Breien et al., 2008; Costa & Schuster, 1988). For this reason, GLOFs are a great threat to mountain communities and their infrastructure. As with all other mass flows endangering people and infrastructure, the scientific community tries to better understand the complex events occurring during a GLOF and try to enhance simulation models to better predict possible future events. One way to increase simulations of GLOFs, which got more and more important in recent years, was to couple remote sensing data with a GIS model (Carrivick, 2006; Huggel et al., 2003). Before the Pudasaini (2012) two-phase mass flow model, some

single-phase models, both empirical and physically based models, were developed and used for simulating high-mountain mass movements, such as GLOFs (Kingslake & Ng, 2013; Osti & Egashira, 2009; Worni et al., 2012). The most recent scientific approaches simulating GLOFs were almost all executed with the Pudasaini (2012) two-phase mass flow model, as it has a couple of advantages compared to other models. It considers the strong interactions between the solid phase and fluid phase, also buoyancy along with other crucial aspects of mass flows, such as enhanced non-Newtonian viscous stress, virtual mass force and generalized drag (Anacona et al., 2015; Fread, 1988; Kattel et al., 2016; Schneider et al., 2014).

One important aspect for the future, as GLOFs and rock-ice avalanches will occur more often in the future, will be, to get a better understanding of the process transformations and interactions during the event itself. Using that knowledge, more sophisticated models, which are capable to reproduce these complex events, can be developed and used to predict the outcomes of potential GLOFs/rock-ice avalanches more efficiently. A major challenge of simulating GLOFs is the ongoing fluidization during the process. Lubrication and fluidization factors are functions of different physical parameters and dynamical/mechanical variables. This highly influences the overall dynamics of the mass flow, resulting in more rapid flows and large runout distances. The snow and ice melt during the event due to frictional heating producing fluid, i.e. importing water in the mass flow, which changes the flow behaviour completely. Observations, in the field and the laboratory, clearly show the changing flow properties from a solid-like to fluid-like flow. Single-phase models are not capable of reproducing such mass flows, so more sophisticated models are needed. Pudasaini and Krautblatter (2014) enhanced the original Pudasaini (2012) model, so fluidization and lubrication effects are taken into account, which is a first step in simulating GLOFs more accurately (Anacona et al., 2015; S. Pudasaini & Krautblatter, 2014; Schneider et al., 2010, 2014; Xin et al., 2008).

3.3.1 r.avaflow

r.avaflow is an open-source (www.avaflow.org) computational tool, which was developed to simulate mass flows, avalanches and process chains originating from a defined release area down a topography to a deposition area. It is available in two versions, r.avaflow [EXPERT] and r.avaflow [PROFESSIONAL]. r.avaflow [PROFESSIONAL] is a version with reduced functionalities, developed for practicioners, but currently not available. The simulations for this work were all conducted with r.avaflow [EXPERT], which is implemented as a raster module of the open-source software package GRASS GIS 7(GRASS Development Team, 2016; Neteler & Mitasova, 2007). What is distinguishing r.avaflow from other computational tools is: “r.avaflow (i)

employs a two-phase, interacting solid and fluid mixture model (S. P. Pudasaini, 2012); (ii) is suitable for modelling more or less complex process chains and interactions; (iii) explicitly considers both entrainment and stopping with deposition, i.e. the change of basal topography; (iv) allows for the definition of multiple release masse, and/or hydrographs; and (v) serves with built-in functionalities for validation, parameter optimization, and sensitivity analysis" (M. Mergili, Fischer, Krenn, et al., 2017; M. Mergili, Frank, et al., 2018).

The key input and output parameters that are necessary for a simulation with r.avaflow are stated in Table 3 (M. Mergili, Fischer, Krenn, et al., 2017).

Table 2: Key input and output parameters of r.avaflow.

Parameter	**Unit**	**Symbol**	**Format**
Initial surface elevation	m	Z_0	Raster
Solid and fluid release height	m	$H_{0,s}$, $H_{0,f}$	Raster
Total release height	m	H_0	Raster
Solid concentration of total release	-	$\alpha_{s,0}$	Value
Entrainable total height	m	H_{Emax}	Raster
Solid concentration of the entrainable mass	-	$\alpha_{s,Emax}$	Value
Hydrograph tables: solid and fluid flow height and velocities at defined time steps	m, m/s	-	Tables
x and y coordinate, width and aspect of the input hydrographs	-, -, m, rad	-	Values
Flow parameters	-	-	Values
Entrainment coefficient	-	C_E	Value
Time interval for output maps and stopping time	s, s	Δt_{out}, Δt_{max}	Values
Observed impact and deposition area	-	OIA, ODA	Raster
Output (validation and visualization are not included)			
Maximum flow height	m	H_{Max}	Raster
Maximum kinetic energy	J	T_{Max}	Raster
Maximum pressure (for solid, fluid and total)	Pa	P_{Max}	Raster
Flow velocities (x and y direction, total values) for solid and fluid	ms^{-1}	v_x, v_y, v	Raster
Change of basal topography (for solid, fluid and total)	m	H_C	Raster
Impact indicator index, deposition indicator index	-, -	III, DII	Raster
Flow height at each output time step (for solid, fluid and total)	m	H_{tout}	Raster
Flow kinetic energy at each output time step (for solid, fluid and total)	J	T_{tout}	Raster
Flow pressure at each output time step (for solid, fluid and total)	Pa	P_{tout}	Raster

Most important for r.avaflow are a digital terrain model (DTM) representing the pre-event topography, solid and fluid release heights (raster maps) or hydrographs containing solid and fluid release, and a set of flow parameters (see Table 3)(M. Mergili, Fischer, Krenn, et al., 2017).

Table 3: Required flow parameters.

Flow parameter	**Unit**
Solid material density	Kg m^{-3}
Fluid material density	Kg m^{-3}
Virtual mass	-
Internal friction angle	Degree
Basal friction angle	Degree
Exponent for drag (1 = linear, 2 = quadratic)	-
Quasi-Reynolds number	-
Mobility number	-
Terminal velocity	m s^{-1}
Parameter for combination of solid- and fluid-like contributions to drag resistance	-
Particle Reynolds number	-
Mobility number	-
Ambient drag coefficient	-
Entrainment coefficient	kg^{-1}
Viscous shearing coefficient for fluid	-
Solid concentration distribution with depth	-

Important for this work is the functionality of hydrographs, as they are used for the release masses instead of raster maps with solid and fluid heights. As Fig. 9 shows, a hydrograph in r.avaflow consists of a solid and fluid part. In the middle of the hydrograph the solid and fluid height can be defined, as can the velocities for the solid and fluid parts of the flow. The hydrograph has a defined maximum profile length, which can be shortened, if it intersects with the basal topography of the DTM (M. Mergili, Fischer, Krenn, et al., 2017).

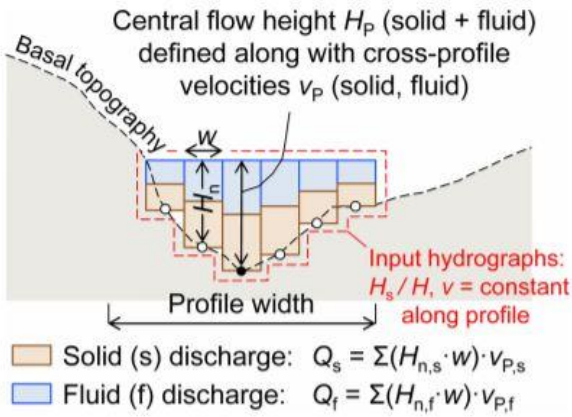

Figure 9: Sketch of a hydrograph profile. The flow surface of input hydrographs is defined by Hp and is extended in cross-profile direction either to the edge of the profile or until it intersects with the basal topography (M. Mergili, Fischer, Krenn, et al., 2017).

With r.avaflow, the user has the option to run a single model run or multiple model runs. For this current work, only single model runs have been used. Using multiple model runs, the results of all single runs get combined to impact or deposition indicator indices, which will not be explained in more detail because they have no importance for this work. The results of a single model run are "raster maps of solid, fluid and total flow heights, flow velocities in x and y direction and in absolute terms, pressures and kinetic energies and the change of the basal topography" (M. Mergili, Fischer, Krenn, et al., 2017). Before every single model run, T_{out} is defined, which indicates at which time steps all raster maps are produced. Another possible output are tables with the maximum solid and fluid flow heights and velocities. Also important for this work, is the possibility to install output hydrographs on a user-chosen point of the DTM, which show the solid and fluid flow heights and velocities at every time step. Fig. 10 is showing the framework of r.avaflow (M. Mergili, Fischer, Krenn, et al., 2017).

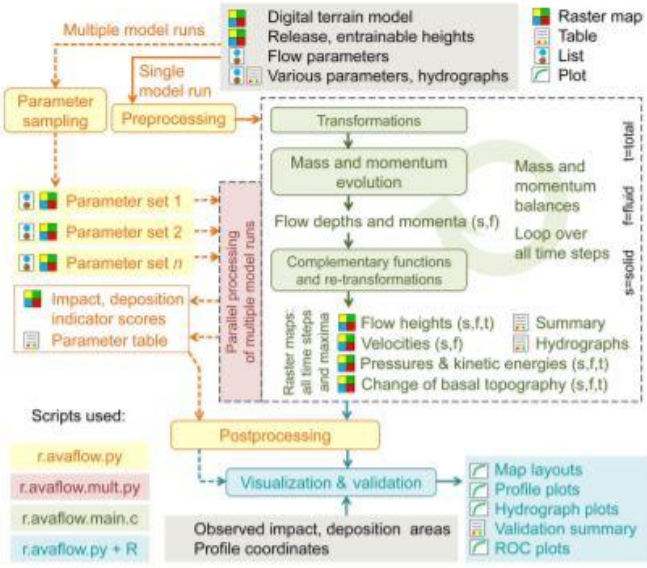

Figure 10: Framework of r.avaflow (M. Mergili, Fischer, Krenn, et al., 2017).

The essential function of r.avaflow is the possibility to redistribution mass and momentum, using a dynamic flow model and a numerical scheme. Two kinds of models can be used, – depending which model is in use, the required flow parameters differ – either a single-phase shallow water model with Voellmy friction relation (Christen et al., 2010; Fischer et al., 2012), or the Pudasaini (2012) two-phase flow model with ambient drag (Kattel et al., 2016). For this work, the Pudasaini (2012) two-phase model was chosen. Additionally, to the model, six complementary functions are implemented in r.avaflow to make the models more reliable and easier to use for the final user. The user defines, which of the following six complementary functions are suitable for his/her simulation:

- Conversion of release heights into release depths
- Diffusion control: If the velocity of the flow is not high enough, the movement of the flow from one cell to the next one is suppressed; this function should reduce numerical diffusion
- Conservation of volume: If the flow loses volume due to numerical reasons, it is compensated after each time step
- Surface control: Numerical oscillations are prevented from flat surfaces (e.g. water surfaces)
- Entrainment: Empirical approach of computing entrainment, i.e. changes in the basal topography
- Stopping and deposition: energy balance method for stopping and deposition of flow material (M. Mergili, Fischer, Krenn, et al., 2017)

For the validation and visualization of the simulations, r.avaflow is employing Python and R programming language (R Core Team, 2016). r.avaflow is only possible to validate simulations if one of the following three parameters is given:

- a raster map of the observed impact or deposition area,
- a profile along the flow path defined by the user, or
- measured values of H or v at certain time steps or coordinates.

Comparing the observation with the simulation, four validation scores can be evaluated, which are shown in Figure 11:

- true positive (TP): observation and simulation of the event
- true negative (TN): no observation and simulation of the event
- false positive (FP): no observation but simulation of the event
- false negative (FN): observation but no simulation of the event

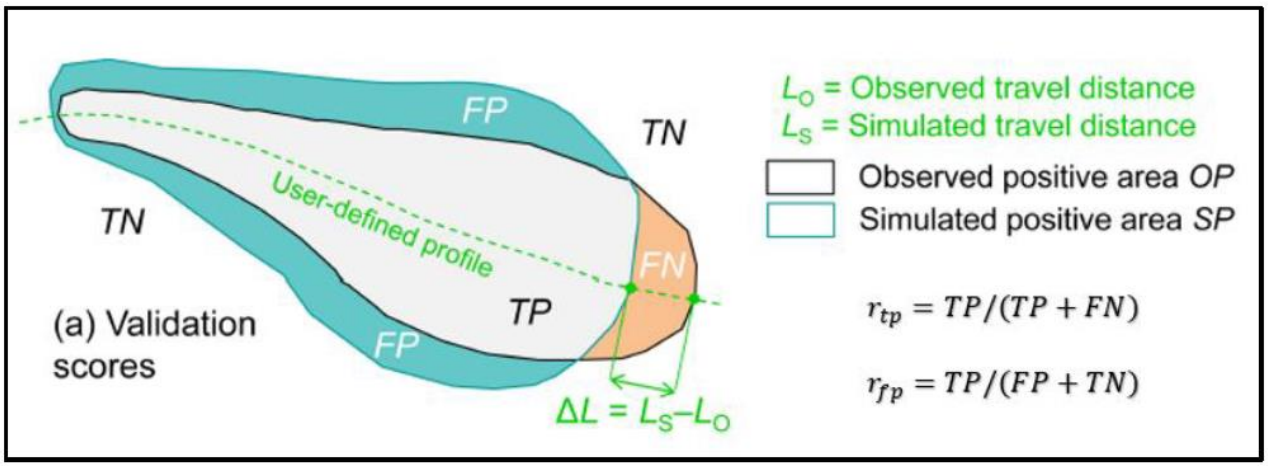

Figure 11: Validation scores for single model run(M. Mergili, Fischer, Krenn, et al., 2017).

Using these four validation scores, different values can be calculated in order to evaluate the difference between the observation and the simulation (Table 4).

Table 4: Validation parameters used in r.avaflow.

Name	Definition	Possible range	Optimum
Excess travel distance (*ΔL*)	L_S - L_O	[-L_O, ∞]	0
Factor of conservativeness (*FoC*)	$FoC = \frac{TP + FP}{TP + FN}$	[0, ∞]	0
Critical success index (*CSI*)	$CSI = \frac{TP}{TP + FP + FN}$	[0, 1]	1
Distance to perfect classification (*D2PC*)	$D2PC = \sqrt{(1 - r_{tp})^2 + r_{FP}^2}$	[0, 1]	0

Because TN is strongly dependent of the size of the area of interest, it is regulated with 5*(TP+FN)-FP to achieve meaningful results. The four validation scores TP, TN, FP and FN are used to calculate the parameters 2-4 shown in Table 4. In contrast to that, the first parameter (Excess travel distance), is based only on the user-defined longitudinal profile. ΔL and FoC indicate at the conservativeness of the results, where ΔL > 0 and FoC > 1 indicate conservative results (meaning the simulated area of interest is larger than the observed one), while ΔL < 0 and FoC < 1 incivate non-conservative results. CSI and D2PC do not allow conclusions on the conservativeness of the simulation, but to quantify the differences between the observed and simulated impact and deposition areas (M. Mergili, Fischer, Krenn, et al., 2017).

In general, r.avaflow is considered potentially suitable for simulating process chains. However, there are certain difficulties, are currently investigated to make r.avaflow fit for forward simulations. One of the main challenges is, that results have shown a high sensitivity of certain parameters highly influencing the simulation results. To appropriately deal with these

uncertainties, it will be necessary to perform a multi-parameter sensitivity analysis and optimization campaign with various, well-documented events of all sizes and varieties. Well-documented two-phase events are therefore essential for developing r.avaflow, to gain guiding values for uncertain parameters, back-calculating these events (Fischer et al., 2015; Krenn et al., 2016; M. Mergili, Emmer, et al., 2018; M. Mergili, Frank, et al., 2018; M. Mergili, Jaboyedoff, et al., 2020; M. Mergili, Pudasaini, et al., 2020; Martin Mergili et al., 2016). The two main issues here are the rare, well-documented, two-phase events and the complex parameter interactions. Another key factor will be, to replace the empirical entrainment model with a mechanical model for erosion, entrainment, and deposition (for example Pudasaini and Fischer, 2016) (M. Mergili, Emmer, et al., 2018; M. Mergili, Fischer, Krenn, et al., 2017; M. Mergili, Fischer, & Pudasaini, 2017; M. Mergili, Frank, et al., 2018)

3.4 Entrainment

One major factor, which is largely unclear, regarding the size, speed and destructive potential of geophysical mass flows is the entrainment of bed material they encounter. There exist several hypotheses explaining the possible bed erosion mechanics. However, how, where and when the erodible material enters the moving mass is still a largely unanswered question, due to a lack of high-resolution, field-scale data, and presents significant modeling and computational challenges. While descending steep slopes and channels, gravity-driven flows of solid-fluid mixtures, that entrain bed material, have a large-scale impact in geomorphology, volcanology, hydrology, and civil engineering. Some of these are jökulhlaups, debris flows, rock avalanches, lahars, ground-hugging pyroclastic flows, and avalanches (McCoy et al., 2012; J. D. Rogers et al., 2010; Scott et al., 2005; Sovilla et al., 2006; Sparks et al., 1997). Many of those appear abruptly, reach peak speeds ranging from 10 to 100 m/s, with volumes up to >1 km³. Field observations exhibit increasing flow volumes (V) by many factors due to entrainment (Hungr & Evans, 2004; Pierson, 1989; Wang et al., 2003), while inundated downslope areas tend to increase in proportion to V^(2/3) (Griswold & Iverson, 2008; Legros, 2002; Vallance & Scott, 1997). Also, drastically increasing flow momentum due to decreasing friction can be a feedback of entrainment. Understanding the detailed mechanics of entrainment has been impeded by the violent nature of full-scale geophysical mass flows and the difficulty of taking direct measurements at their evolving basal boundaries. Various methods have been employed to determine the maximum depth of channel bed erosion. Some examples are scour chains (Leopold et al., 1964) and painted tracer stones (Einstein, 1937; Leopold et al., 1966; Wilcock et al., 1996). These techniques served as a basis for different approaches, such as radioactive, fluorescent, magnetic, or radio transmitting tracers. Other methods like buried and tethered ping-pong balls (Lisle & Eads, 1991; Moring &

Lantz, 1975), sliding-bead monitors (Nawa & Frissell, 1993), or the “Tausendfüssler” of De Jong (1992) have also been successfully used. Shown in some of these experiments is the fact, that high bed-water contents increase flow velocity and mass entrainment in gravity-driven mass flows (Berger et al., 2010; Iverson & Ouyang, 2015; A. Mangeney, 2011; A. Mangeney et al., 2007; Shiva P. Pudasaini & Fischer, 2016).

Relatively high amounts of water in the pores seem to play a key role in the entrainment of material along the slope, which is suspected to highly impact flow dynamics, possibly driving mass flows over unusually long distances. Though measurements of material entrainment in natural flows is very difficult, the entrainment of sediments or debris into gravity flows seems to be crucial to the dynamics of the flow. The eroded tracks are mostly hidden by subsequent flows, and in general differentiating flow deposit from the underlying erodible layer is quite hard because they are usually composed of the same material. Occurring entrainment can either decrease or increase deposit extent and flow velocity, which is dependent on the type of gravitational flow and the geological setting. Concluding, material entrainment in natural gravitational flows is most likely dependent on a combination of both physics of granular material and pore water pressure, among many other processes. Regarding glacial lake outburst floods (GLOFs), which represent a major hazard in mountainous regions like the Alps, the Himalayas, the Andes and Iceland (Cenderelli & Wohl, 2003; Kattelmann, 2003; Kershaw et al., 2005; Vilímek et al., 2005), surface water flow is one of the most common triggering mechanisms. These water masses, often flowing at high velocities, can possibly erode and transport vast amounts of sediment when they pass erodible material (A. Mangeney, 2011; A. Mangeney et al., 2007; McDougall & Hungr, 2005; Sovilla et al., 2006).

Indicating the causes and effects of entrainment is one of the most challenging tasks in modelling flow dynamics (Crosta et al., 2009; Hungr et al., 2005) There exists potential comparing measurements of evolving flow velocities and depths to model predictions to constrain entrainment mechanics. This approach is only applicable if the models themselves are soundly grounded (Iverson et al., 2011). Therefore, it is essential for dynamic models to be based on physical conservation laws that are properly formulated. Several mechanical and numerical models have included entrainment (Armanini et al., 2009; Bouchut et al., 2008; Brufau et al., 2000; Chen et al., 2006; Crosta et al., 2009; Fischer et al., 2015; Fraccarollo & Capart, 2002; Iverson, 2012; Le & Pitman, 2009; A. Mangeney et al., 2007; McDougall & Hungr, 2005; Tai & Kuo, 2008).

3.4.1 Entrainment in gravitational mass flows simulation

In general, there are two types of erosion models in use: empirical and mechanical ones. Empirical models are the ones that are most used in practical tasks and are evolved from experience. Yield and/or erosion rates are the base of empirical models (Shiva P. Pudasaini & Fischer, 2016).

Mechanical models, however, are process-based and consider the mass and momentum exchanges between a gravitational mass flow and the underlying erodible bed. An erosion rate is the result, that is proportional to the shear stress difference between entraining and resisting stresses (Issler, 2014; Iverson, 2012). Based on this mechanical erosion rate, a singularity emerges, showing that the erosion-rate is inversely proportional to the velocity. Iverson 2012 shows, for bulk-, or solid-type models, erosion-rates become indefinitely large for decelerating or stopping flows, and almost insignificant for mass flows with very high velocities. This stays in contrast to observations in nature, which clearly show the opposite (Iverson, 2012; Iverson & Ouyang, 2015; Shiva P. Pudasaini & Fischer, 2016).

Another classification of erosion models is the amount of phases considered by them: single-phase or mixture models. Erosion models are commonly developed for a viscous fluid presented as a single-phase fluid. Erosion rates, the result of these erosion models, are usually used for landslides, rock and debris avalanches (Bouchut et al., 2008; Le & Pitman, 2009; A. Mangeney et al., 2010; Naaim et al., 2003). Armanini et al. (2009) was one of the first presenters of mixture simulations, considering erosion, but solely for single-phase material. Entrainment/deposition in simulations for rock/debris-avalanches was firstly presented by McDougall and Hungr (2005), Crosta et al., (2009) and Pirulli and Pastor (2012). Only few erosion models exist that take into account fluid-grain mixture (Fraccarollo & Capart, 2002), saturated entrained materials (Crosta et al., 2009) and debris mixture (Armanini et al., 2009; Iverson, 2012). However, all the mentioned models are not fully coupled and true two-phase model. Pudasaini (2012) introduced a general two-phase mass flow model, which is implemented in r.avaflow, the simulation tool used for the simulations in this thesis.

As mentioned above (see Sect. 3.4), a clear understanding of the basic process of entrainment still remains vague due to a lack of high-quality data, although entrainment is one of the key factors to hazard assessment and landscape evolution. Numerical simulations, which are based on physics, may be one way to pass these limitations and create a more, clear understanding, examining broader aspects of the flow parameters, erosion, mobility and deposition. Even the basic mechanism of erosion in the presence of both solid and fluid has not yet been investigated, because more advanced models would be needed to undergo such investigations. Another

mechanism almost not investigated yet, due to the true two-phase nature of flows, are the evolving contrast between the densities of solid and fluid that leads to a change in buoyancy and the change of the basal surface/the whole system due to erosion/deposition. Changes in basal surface have slightly been included recently by Fraccarollo and Capart (2002) and Le and Pitman (2009). This is why it is of high importance to appropriately model two-phase bed and flow properties that highly influence the appearance and rates of entrainment, and mobility. Five crucial aspects have to be considered in modelling geophysical flows regarding erosion/deposition:

- Erosion rate
- How to model the real erosion process
- Proper knowledge of the velocities of the fluid and solid particles that have just been eroded
- Momentum productions/losses resulting from the mass productions/losses
- Erosion induced mobility

(Shiva P. Pudasaini & Fischer, 2016)

Pudasaini & Fischer, 2016 presented a mechanical erosion model that shows, that erosion is not possible by setting the zero velocity of the eroded particle. The velocities of the particles across the interface are a product in terms of the density and volume fraction contrasts. If the basal substrate is weaker in these terms, compared to the flow, the particles that are eroded move relatively faster. Relatively slower velocities occur, if the basal substrate is stronger than the flow. When there are no contrasts along the interface, there are clear results that show, that the bottom of the flow moves twice as fast as the eroded particles on the other side of the interface. For erosion to take even place, one of the four following parameters, at least, must have a distinction along the interface:

- the buoyancies
- the densities
- the friction coefficients
- the volume fractions

Erosion only occurs, when the flow is mechanically stronger than the basal substrate. Moreover, if mass is added into the flow, it is promptly accelerated due to the gravity load. Added mass means added potential energy, which leads to increasing flow mobility. Summarizing all these facts, the higher mobility of mass flows which entrain basal substrate can be explained (S. P. Pudasaini & Fischer, 2016).

3.4.2 Entrainment in r.avaflow

As stated above, entrainment is a major aspect in modelling natural hazards, because solid and fluid material entrained and integrated in the flow can vastly change the dynamics and consequences of a flow, hence r.avaflow is particularly considering both entrainment and stopping with deposition, i.e. the change of basal topography (Fraccarollo & Capart, 2002; Hungr & Evans, 2004; Le & Pitman, 2009; M. Mergili, Fischer, & Pudasaini, 2017; M. Mergili, Frank, et al., 2018). In r.avaflow, an empirical approach is used to compute entrainment. An entrainment coefficient C_e (kg^{-1}) (see Table 2), which is one of the input parameters of r.avaflow, can be defined by the user, and further is multiplied with the total solid and fluid momentum at each raster cell at each time step (M. Mergili, Fischer, Krenn, et al., 2017; M. Mergili, Frank, et al., 2018).

Table 5: Input parameters of r.avaflow.

Parameter	**Unit**	**Symbol**	**Format**
Initial surface elevation	m	Z_0	Raster
Solid and fluid release height	m	$H_{0,s}$, $H_{0,f}$	Raster
Total release height	m	H_0	Raster
Solid concentration of total release	-	$\alpha_{s,0}$	Value
Entrainable total height	m	H_{Emax}	Raster
Solid concentration of the entrainable mass	-	$\alpha_{s,Emax}$	Value
Hydrograph tables: solid and fluid flow height and velocities at defined time steps	m, m/s	-	Tables
x and y coordinate, width and aspect of the input hydrographs	-, -, m, rad	-	Values
Flow parameters	-	-	Values
Entrainment coefficient	-	C_E	Value
Time interval for output maps and stopping time	s, s	Δt_{out}, Δt_{max}	Values
Observed impact and deposition area	-	OIA, ODA	Raster

After a single model run is completed, the output concerning entrainment, are raster maps, that show the change of the basal topography. The input parameter T_{out} (see Table 2) is defining the time steps, at which this raster maps are produced. So, for example, if $T_{out} = 20$, r.avaflow produces a raster map for every 20 seconds of the simulation. Furthermore, one raster map is produced for the maximum over all time steps(M. Mergili, Fischer, Krenn, et al., 2017).

r.avaflow consists of complementary functions (see Sect.3.3.1 : r.avaflow) to make the model more reliable and easier to use for the final user:

- Conversion of release heights into release depths
- Diffusion control: the flow does not propagate from one pixel to another if the velocity is too low, avoiding numerical diffusion
- Conservation of volume: losses of volume due to numerical reasons get compensated
- Surface control: numerical oscillations of flat surfaces (especially water bodies) get suppressed
- Entrainment: computing entrainment of basal material
- Stopping and deposition: Stopping and deposition of flow material,

one of which is entrainment. Pudasaini (2012) does not originally include entrainment, so it is a dynamic function executed at the end of each time step.

However, the time steps at which is the numerical is updated is equivalent to the time steps at which the entrainment and change of basal topography are updated. As mentioned before, the user-defined empirical entrainment coefficient C_e (see Table 2) is multiplied with the solid and fluid momentum, which results in the potential solid and fluid entrainment rates $q_{E,s}$ and $q_{E,f}$. These entrainment rates are assumed perpendicular to the basal topography. Furthermore, we suppose a vertically homogeneous solid fraction $\alpha_{s,Emax}$ within the entrainable material, which gives us the following equations for $q_{E,s}$ and $q_{E,f}$:

$$q_{E,s} = C_E |M_s + M_f| \alpha_{s,Emax},$$
$$q_{E,f} = C_E |M_s + M_f| (1 - \alpha_{s,Emax}).$$

Usually the depth-averaged velocities are higher than the basal velocities, which are relevant for entrainment, but, r.avaflow does not explicitly consider this circumstance. However, it is represented, as C_e, $q_{E,s}$ and $q_{E,f}$ are always positive. This leads to the solid and fluid changes of basal topography, happening due to entrainment, $H_{E,s}$ and $H_{E,f}$, which are:

$$H_{E,s,t} = \min\left(H_{E,s}(t - \Delta t) + \frac{q_{E,s}\Delta t}{\cos\beta}, H_{Emax,s}\right),$$
$$H_{E,f,t} = \min\left(H_{E,f}(t - \Delta t) + \frac{q_{E,f}\Delta t}{\cos\beta}, H_{Emax,f}\right),$$

“where HE,s (t – Δt) and HE,f (t – Δt) are the change of the basal topography at the start of the time step, HEmax,s and HEmax,f are the maximum entrainable depths at the given cell, t is the time passed at the end of the time step, delta t is the time step length, and beta is the local slope of the basal surface. The division by cos(β) approximates from depths to heights”(M. Mergili, Fischer, Krenn, et al., 2017). Resulting are the solid and fluid entrained depths

$$D_{E,s} = (H_{E,s}(t) - H_{E,s}(t - \Delta t))\cos\beta$$

and

$$D_{E,f} = \left(H_{E,f}(t) - H_{E,f}(t - \Delta t)\right) \cos\beta$$

Which are added to the existing solid and fluid flow depths. Fig. 12 shows the interactions of the flow with the basal topography.

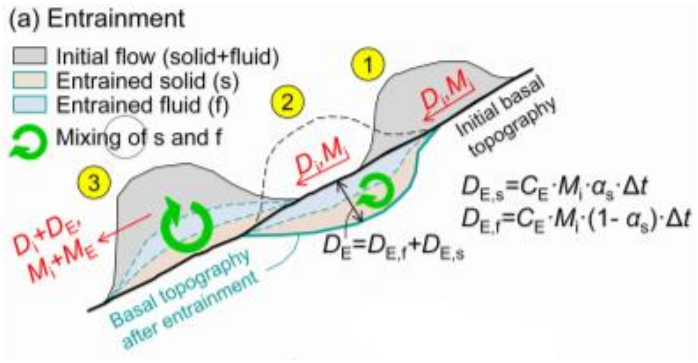

Figure 12: Interactions of the flow with the basal topography: (a) entrainment, assuming that HEmax,s and HEmax,f are not limiting; Di: total initial flow depth (s+f); Mi: total initial momentum (s+f); De: entrained depth; ME: total increase in momentum due to entrainment (s+f). Source: (M. Mergili, Fischer, Krenn, et al., 2017)

Another assumption made is, that the entrainment increases both momenta (solid and fluid) “in each direction by the product of the entrained solid and fluid depth and the velocity in the given direction. The basal topography and, consequently, the x and y cell sizes, cell areas, and gravitational acceleration components in x, y and z direction are updated after each time step” (M. Mergili, Fischer, Krenn, et al., 2017).

A problem that might occur with the entrainment coefficient C_e is, that with higher values the momentum of the flow is increased, while the fluid content, and hence the fluidity, may be decreased, so the combined effect has to be looked at carefully. Another effect, which has to thought about, is the spatial pattern of the intensity of the impact changed due to entrainment. Higher entrainment rates increase the flow height and momentum, which leads to higher possible damages, but as mentioned before, reduce the fluidity and therefore the intensity of the impact of the intensity farther away may be decreased, because the higher entrainment rates reduce the spreading of the flow. This aspect has to be interpreted carefully, as r.avaflow (at the moment) is not explicitly considering the separation of the solid and fluid phases (M. Mergili, Fischer, Krenn, et al., 2017; M. Mergili, Fischer, & Pudasaini, 2017; M. Mergili, Frank, et al., 2018).

At the moment the empirical entrainment model used for r.avaflow is a rough approach. In the future, it is planned to substitute the empirical entrainment model with a physically-based model (for example Pudasaini & Fischer, 2016). This will be one of the key challenges to evolve r.avaflow and make it even more precise. Right now, the empirical approach might inadequately represent the physical processes: that is why sometimes the entrained volume does not scale correctly with the flow magnitude in some examples (M. Mergili, Frank, et al., 2018). The Pudasaini & Fischer (2016) model mentioned above, is directly relating the entrainment

coefficient to the basal friction, which may lead to more accurate results (M. Mergili, Emmer, et al., 2018; M. Mergili, Fischer, Krenn, et al., 2017; M. Mergili, Fischer, & Pudasaini, 2017; M. Mergili, Frank, et al., 2018; Shiva P. Pudasaini & Fischer, 2016).

3.5 Equifinality

In the past decades, different methodologies have been established to better counteract uncertainty, one of which is the equifinality thesis. Approaches for uncertainty still used recently, like the equifinality thesis, require a significant knowledge of statistics and mathematics, together with the ability of implement these in a simulation model (Vrugt et al., 2008). Equifinality is not only limited to earth sciences. Other fields, for example biology (A. R. Rogers, 2000)n management (Doty et al., 1993), psychology (Gottlieb, 2001) and geomorphology (Haines-Young & Petch, 1983) have been using the equifinality thesis for their researches. In geomorphology, for example, equifinality has a long history, stating that alike landforms might originate from different histories and processes. Hence, by only seeing the landform on its own, it might be difficult to tag the explicit set of processes that caused the landform. This usage implies the assumption, that a single correct representation of the reality cannot be derived from the usually available data (Beven, 1993, 2006).

Equifinality, in terms of mass flow models, states, that many different models or different parameter sets within a model, lead to an accurate representation compared to observations. It is replacing the idea, that there is only one optimal model or parameter set within that model to accurately simulate an actual event. In fact, the decision to only rely on one optimal model or one optimal parameter set within a model, is a poor one regarding to the equifinality thesis. The equifinality approach especially has been used in different hydrology models, such as rainfall-runoff modelling (Liu et al., 2009), hydraulic modelling (Pappenberger et al., 2007), water equality modelling (Dean et al., 2009) and mixing models (Iorgulescu et al., 2007) to develop the certainty of simulation models (Beven, 2006, 2012; Hauffe et al., 2016).

One major aspect the equifinality thesis is approaching, is the uncertainty of certain parameters within a model structure based on often not sophisticated data available or a, to this day, not complete understanding of complex interactions occurring during mass flows. During a mass flow event, countless interactions between the different including substances occur. So, unless the underlying physical theory is entirely correct, many representations of the event may be equally good. That is, why equifinality is not a surprising concept, as the underlying physical processes of mass flows/process chains are still not understood completely. Complex models contain many

components and parameters, to reflect the understanding of the underlying processes, including aspects about which the scientific community has a relatively poor understanding (Beven, 2018). For the specification of certain parameter values, the scientific community usually conducts back-calculation of events or calibration of parameters, assuming the underlaying equations are correct (Beven, 1993). This is the reason, why a single optimum parameter set can only be known with some degree of uncertainty. What is paradox, is, the greater the understanding of the different processes underlying mass flows is, which is implemented in simulation models, the number of parameters usually increase and more parameters to be calibrated result in more uncertainties regarding the simulation model (Beven, 2012; Ebel & Loague, 2006). When using a specific model, many model runs can be performed using different combinations of parameter sets, which are chosen randomly from a prior parameter range. Afterwards, the simulated results get compared to the observed event. For each parameter set, a likelihood value can be determined, which states, how well the parameter set simulated the event. The higher the likelihood value, the higher the simulation fits the observation. In conclusion, it can be stated, that parameterization of a physics-based model, especially with poor input data, is not a trivial task at all (Beven, 1993, 2006, 2012, 2018; Ebel & Loague, 2006; Vrugt et al., 2008).

Although equifinality is mostly known in the scientific community, there are still a lot of modellers not adopting the equifinality thesis. The modelling philosophy applied by this group of scientists is, that science is supposed to reproduce the reality in a single correct description, that is why the equifinality thesis is not accepted, as science should not provide multiple possible descriptions of reality, even at the risk of avoiding model acceptability and uncertainty. Often, it is not even considered, that a single optimal description is not possible. That is exactly what the equifinality thesis tries to avoid by stating that there are many acceptable representations of reality and this fact should be highly considered regarding predictions (Beven, 1993, 2006; Beven & Freer, 2001).

Sceptics have called for simpler models, responding to the issues with the equifinality thesis (Kirkby, 1996; Young et al., 1996). Nevertheless, certain systems, e.g. process chains, are just not simple enough to only use simple models to reproduce them. A simple model cannot sophistically replicate processes and interactions that are not included in its mathematical or physical background (Ebel & Loague, 2006; Hauffe et al., 2016).

4 Methods

Several different methods were used to approach the research questions (see Fig. 13). Firstly, it was necessary to create a pre-event DEM, which could be implemented in r.avaflow to run meaningful simulations. It was created editing the post-event DEM, which was provided by the Icelandic Meteorological Office. The editing was conducted with QGIS, which was also used to produce a shapefile containing the maximum possible entrainment area and depth. Furthermore, triangular input-hydrographs were established, to simulate the floods streaming down the glacier. Using all these inputs, first meaningful simulations could be realised.

To compare the simulations with the observations, different methods were conducted. First, using the pre-event DEM and post-event DEM the entrained volume during the actual event was estimated to be compared with the simulated entrained volume. Also, two output-hydrographs were installed in r.avaflow to measure the time at which the flow reaches a certain area. Finally, a control point was added in r.avaflow, which measures the maximum flow height, to compare observed and simulated maximum flow heights at a certain point.

After all the 121 simulations were successfully simulated, using Python 3.7, heatmaps were created, to show, how well each simulation corresponds with the observations regarding entrained volume, flow height, flow time and the combination of these three parameters.

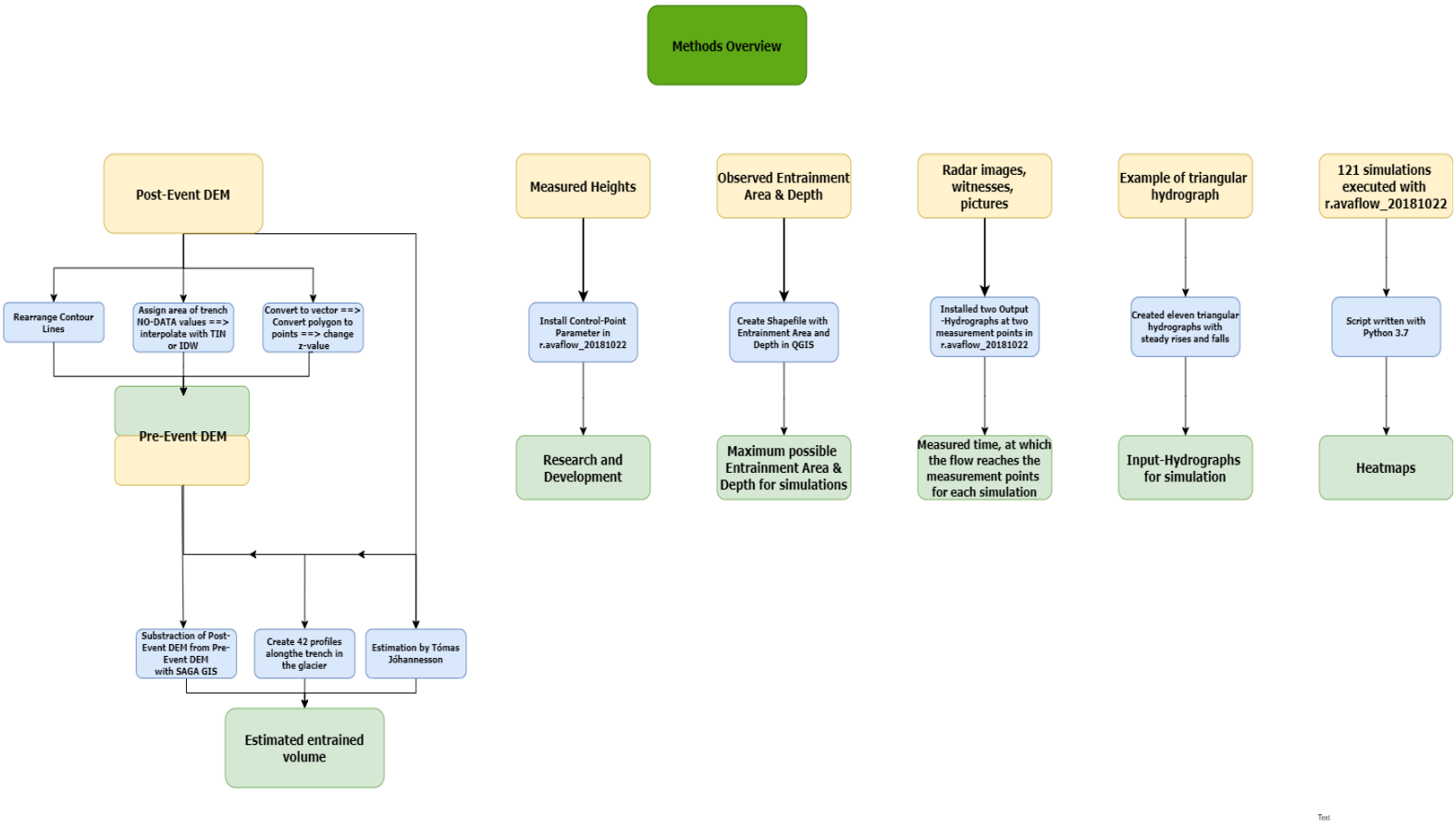

Figure 13: Overview of applied methods.

4.1 Data

Table 6 summarizes the data which was used as input, including the applied methods and the output. In the following Sect. 4.2, each method will be explained in detail.

Table 6: Input- Data used for the simulations, including applied methods and output.

Input	Methods	Output
Post-Event DEM	Rearrange Contour Lines Assign area of trench NO-DATA values ➔ interpolate with TIN or IDW Convert to vector ➔ Convert polygon to points ➔ change z-value (elevation)	Pre-Event DEM
Pre-Event DEM & Post-Event DEM	Substraction of Post-Event DEM from Pre-Event DEM with SAGA GIS Create 42 profiles along the trench in the glacier Estimation by Tómas Jóhannesson	Estimated entrained volume
Measured Heights	Install Control-Point Parameter in r.avaflow	Maximum flow height for each simulation
Observed Entrainment Area & Depth	Create shapefile with Entrainment Area & Depth in QGIS	Maximum possible Entrainment Area & Depth for simulations
Radar images, witnesses, pictures	Installed two Output-Hydrographs at two measurement points in r.avaflow	Measured time, at which the flow reaches the measurement points for each simulation
Triangular hydrograph as example	Created eleven triangular hydrographs with steady rises and falls	Input-hydrographs for simulations
121 simulations executed with r.avaflow	Script written with Python 3.7	Heatmaps

4.2 Methods

4.2.1 Pre-Event DEM

As described in chapter 3.2.1 the jökulhlaup eroded a trench of approx. 3 km of length with a maximum depth of ~ 50 m. After the event the Icelandic Meteorological Office created an airborne laser-scan of the area, which, after georeferencing the pointcloud, was transformed to a 5 m resolution DEM. To run meaningful simulations with r.avaflow, a DEM of the topography before the event, is required. Only then, the entrainment of the trench in the glacier can be displayed accurately and compared to the actual event. Prior to all the following methods, it is important to not work with the whole DEM, but only with the area of the trench and the surrounding area. Otherwise these methods would not only change the area of interest, but would also change other areas of the DEM, which should be avoided. Once finished with manipulating the DEM, the changed area can be merged with the rest of the DEM and the result is a pre-event DEM, that now can be used to work with. In order to obtain such a pre-event DEM three different methods were tested and compared with QGIS:

1. Create the contour lines with the “Contour”-function in QGIS and then manually correct them, to realign the area of the trench and furthermore remove it from the DEM. After finishing this working process, the contour lines can be re-converted to a raster.

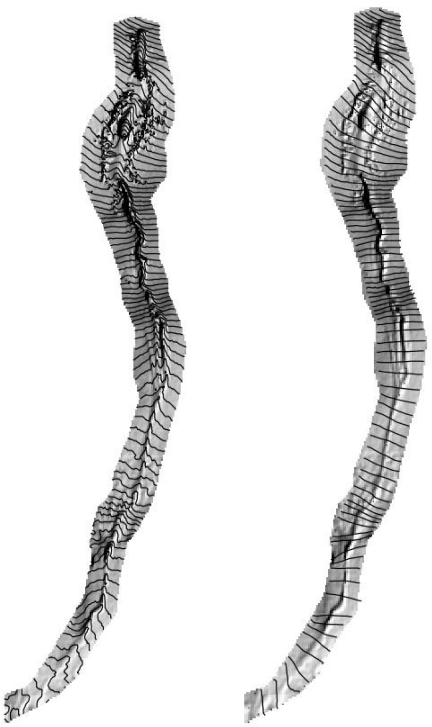

Figure 14: Contour lines after the event (left), and modified contour lines to represent the pre-event topography (right).

2. Convert the DEM, which is in raster format, to a vector and then with the “Extract Nodes”-function, convert the polygon to points. In the area of the trench, the z-values (elevation) of the points can now, manually, be changed, to regain the topography before the event. The next step would be, as in method 1, to re-convert the points to a raster.

Figure 15: Nodes of the post-event DEM that can furthermore be manipulated.

3. Clip the area of the trench out of the DEM, so that all values for the trench are NO-DATA values. Then interpolate with either TIN (Triangular Irregular Networks) or IDW (Inverse Distance Weighting) to receive values for the area of the trench.

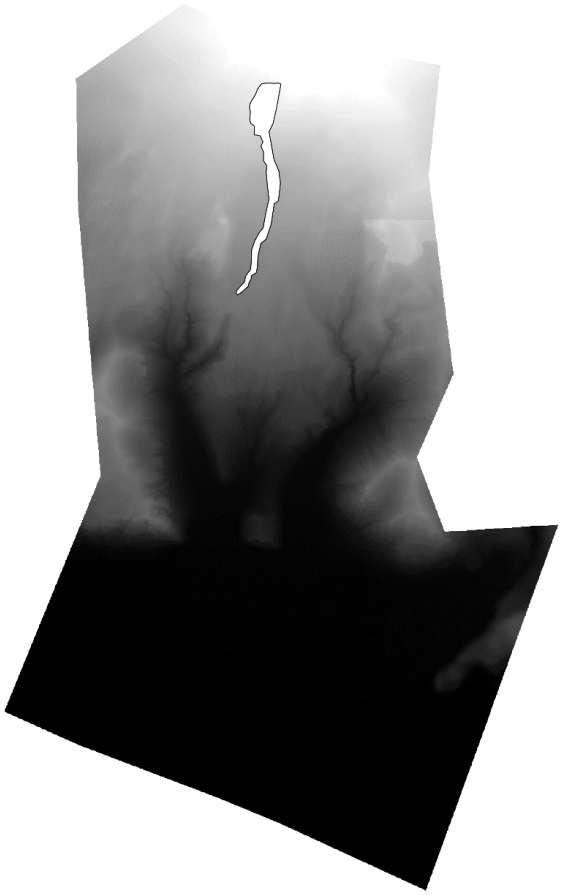

Figure 16: DEM with area of trench cut out.

After using and comparing all these methods, method one was chosen for all the furthermore work, because the attained results looked the most promising to obtain meaningful simulations with r.avaflow.

4.2.2 Entrainment

4.2.2.1 Entrained volume

To reproduce the entrained trench with r.avaflow, it was necessary to create a pre-event DEM (see Sect. 4.2.1). This DEM is the input for all the r.avaflow simulations executed for this work. Three estimations of the volume of the trench were consulted, whereby the second and third estimations verified, if the first estimation is meaningful:

1.) Using SAGA GIS, the post-event laserscan DEM was subtracted from the pre-event DEM to attain the volume of the trench. This method is fairly straightforward, since the tool just creates the difference between the two DEM´s. If a pre-event DEM would have existed, in theory no verification would have been needed, because, if done right, this method would have computed the volume of the trench exactly. However, practically verification is mandatory to make sure if the used method produces reliable results. Since there was no pre-event DEM available, the main focus of verification was to check if the created pre-event DEM was useful or not. Resulting was a volume of $2*10^6$ m³.

2.) With QGIS the eroded trench was separated from the DEM, thereafter 42 profiles were laid through the trench. Due to the often trapezial-like shape (see Fig. 18) of the profiles the volume was calculated as for a rectangle with V=x*h*L (see Fig. 17), where L is the distance between the two profiles. For simplification x was always slightly underestimated to obtain meaningful results. This approach is only acceptable because the goal is an estimated volume to verify the estimation attained with SAGA GIS. This is necessary, because the first method is using the pre-event DEM, which is not 100% accurate, due to the fact, because it was created using the post-event DEM (see Sect. 4.2.1). So a verification is needed, to validate the correctness of the interpolated pre-event DEM. Using this method, the resulting volume was $2{,}4*10^6$ m³.

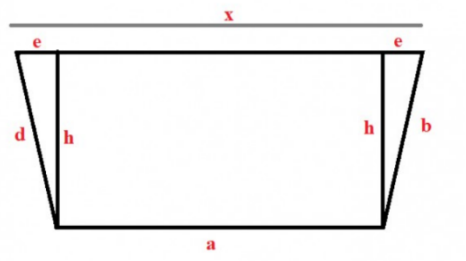

Figure 17: General shape of a trapeze.

Figure 18: Usual profile of eroded trench.

3.) For the second verification I contacted Tómas Jóhannesson from the Icelandic Meteorological Office, which created the post-event DEM. Using a GIS program, he estimated a volume of 2.7 $*10^6$ m³.

Considering that these approaches are all estimations, it is not important, that all the resulting volumes are exactly the same, but are in the same range of value, which they are. Differences between the estimations might origin from various reasons. One factor of uncertainty is the pre-event DEM. Since it had to be created artificially, it will never reproduce reality perfectly. All methods used produce slightly different results, which, presumably, is one of the reasons why the estimation of Tómas Jóhannesson is different. Furthermore, the second approach with the

created profiles is not perfectly accurate due to its estimating nature regarding the area of the profiles.
In conclusion, due to the fact that all three results are in the same range, the first estimation generated a meaningful result for the eroded volume of the trench. For the results, regarding the Entrainment (see Sect. 5.2), the value the simulations are compared with, will be $2*10^6$ m³, because the initial phase of the simulations will be the pre-event DEM.

4.2.2.2 Entrainment Area/Depth

Using r.avaflow, the area where entrainment is possible must be defined precisely. Usually, when back-calculating an event, entrainment should be possible over the whole area of interest, in this case the whole area until the flow reaches the southern gully. This approach is used, when the aim of the simulation is to replicate the event as accurate as possible, to see, if entrainment only occurs at the same areas as it occurred during the event, or if other areas are also impacted by entrainment. Since the aim of this work is not to replicate the event as accurate as possible, but to compare measured observations with simulations, the entrainment area was modified (see Fig. 19) to the area surrounding the trench. Entrainment in other areas than in the trench could not be evaluated because of lacking observations. Thus, it would not be possible to compare the simulations with the observation because of the missing data.
Looking at the depth of the entrained trench, ~50 m was the maximum depth entrained during the event. When back-calculating an event, the maximum possible entrainment depth for the simulation should be fairly high, so that the simulated flow can entrain as much as possible without getting restricted by simulation settings. After testing different maximum entrainment depths, 100 m were chosen to be the maximum depth that can possibly be entrained. Some of the simulations with higher entrainment-coefficients got restricted, as they reached the maximum entrainment depth. However, these simulations already overestimated the observations by factors from 6 up to 8 (see Fig. 25), so allowing more entrainment due to a deeper maximum entrainment depth, would not have made any difference regarding the equifinality. Another reason for limiting the maximum entrainment depth was the computing time of the simulations, as the simulations with high entrainment-coefficients and input-hydrographs needed up to 96 hours of computing time to be done. Increasing the maximum entrainment depth would have led to even higher computing times that would have exceeded the frame of this work.

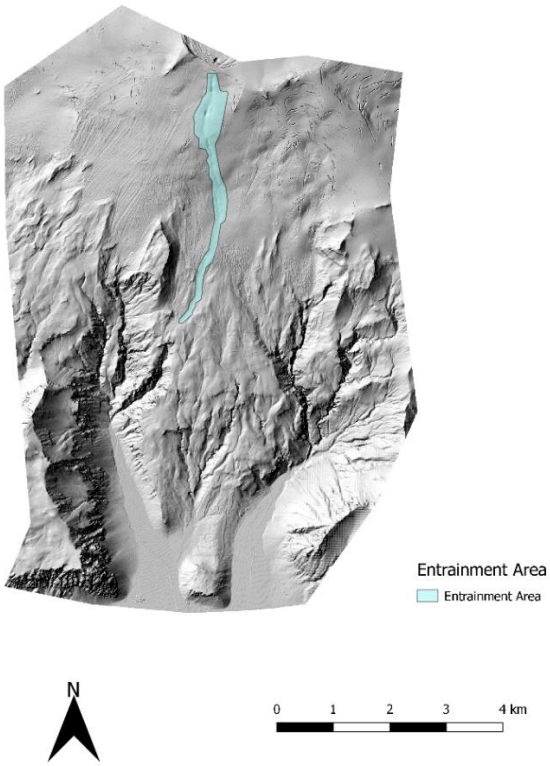

Figure 19: Area of possible entrainment.

4.2.3 Flow Height

For the original event in 2010, there exist measurements of the maximum flow height at certain points (Gíslason, 2012). Table 7 displays the measured maximum flow height at each point, whereas Fig. 20 is pointing out the location of the measurement points. The measurement points are numbered from 1, at the bottom of the valley, up to 10 at the mouth of the gully.

Table 7: Measured maximum flow heights for the original event (Gíslason, 2012).

Mæling nr.	Hámarksdýpi (m)
1	3
2	3
3	3
4	4,3
5	4
6	5
7	5
8	5,1
9	6
10	8

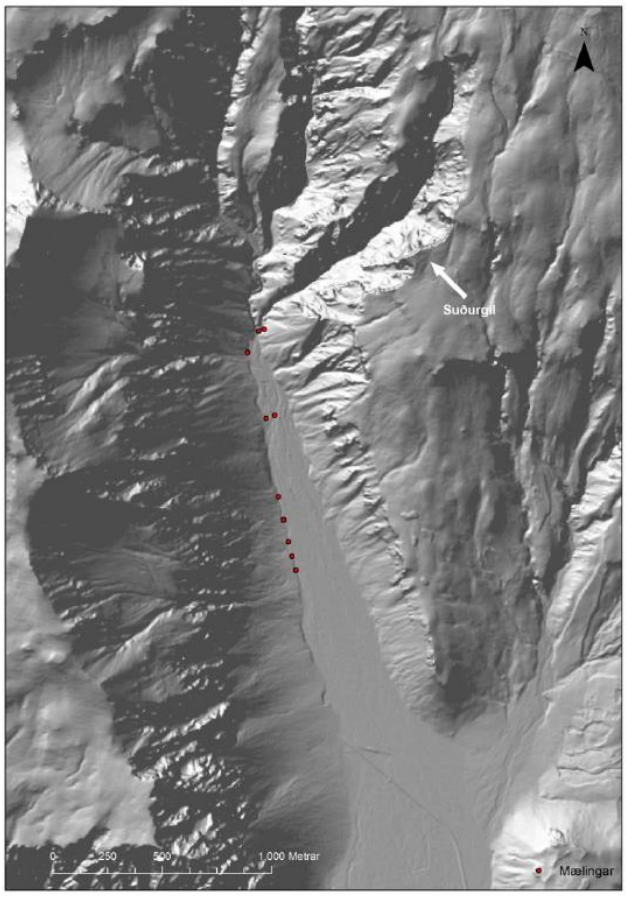

Figure 20: Locations of the measurement points (Gíslason, 2012).

Comparing the simulations with the observation, the control-point-parameter implemented in r.avaflow was used. This parameters output is the maximum flow height for each time step and the maximum flow height for the whole simulation. Using the maximum flow height of the simulation and comparing it to the observation results in a relationship between simulation and observation, that can be evaluated. For the location of the control-point, the area where the southern and the northern gully reach the valley bottom, is chosen. Firstly, because at all meaningful simulations, the whole flow is passing this area and due to its narrowness, the control-point is measuring the whole flow and not only part of it. Another reason for choosing this location is, that there are two measurements on this area, that are fairly nearby, indicating rather meaningful measurements. As a value for comparison, 7 meters of flow are height are opted, which is the mean value of observation points 9 and 10 (Table 7).

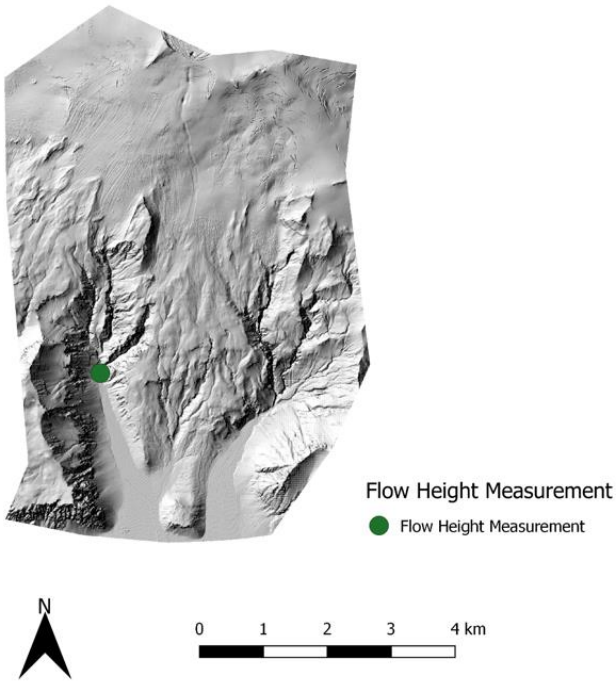

Figure 21: Location of the control-point for the simulations.

4.2.4 Duration of flow

Regarding the flow time, several sources of information are available. The Icelandic Coast Guard produced radar images, according to which at 10:23 GMT the flow had formed a path, which at that point was already way below the top caldera. Using this radar images, a starting time of around 10:00 GMT was estimated. According to a local farmer (Ólafur Eggertson), just about at 10:30 GMT, the jökulhlaup was heard flowing down the gully at the bottom of the valley, which was, as stated by the farmer, quite noisy, thus recognized by him. Estimated by the farmer, the flow needed approximately 15-18 minutes from the bottom of the gully until it reached the bridge further down the valley. On a photo from a helicopter at 11:02 GMT the flood had reached about 100m below the main road.

Summarizing all this information, two measurement points for the flow time can be extracted. The first one at the bottom of the southern gully after 30 minutes, and the second one at the bridge after 45 minutes (see Fig. 22). To evaluate the simulations in reference to the observation, two output-hydrographs were installed in the simulations with r.avaflow. The output of these hydrographs are the solid and fluid heights of the flow at every time step. If there is no solid or fluid flow passing through the hydrograph, the values are zero. That implies the first time step the hydrograph is displaying values other than zero, is the time the flow needed to reach that hydrograph. For the evaluation with Python 3.7, the second measurement point was used to

compare the simulations with the observations. The first measurement point got interpreted separately by analysing the flow times after 30 minutes in QGIS.

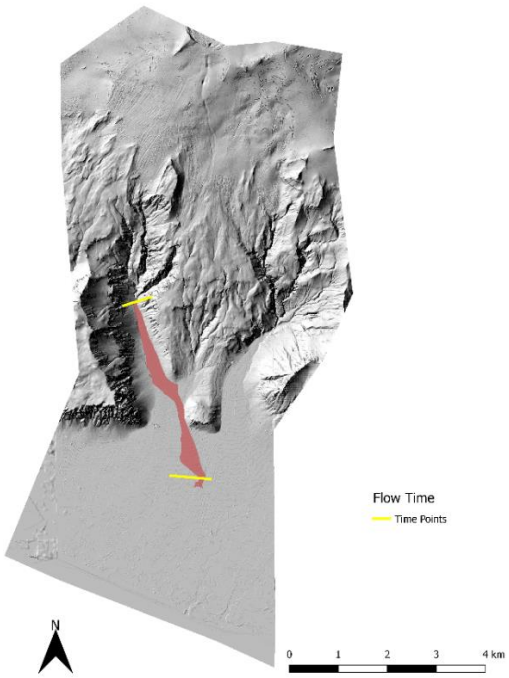

Figure 22: Installed output-hydrographs for measuring the flow time.

4.2.5 Input Hydrograph

To verify the equifinality of the numerical models implemented in r.avaflow, several input-hydrographs had to be created. On the other side of the volcano, a much bigger jökulhlaup took place caused by the Eyjafjällajökull eruption. For this jökulhlaup, discharge measurements on the top of the glacier exist, which could be scaled to fit the Svadbaelisa jökulhlaup (Gíslason, 2012). However, this could be misleading, as it can give the impression of being actual measurements. So, artificial input-hydrographs were created, with steady rises and falls (see Fig. 23, Table 8). The maximum height (solid + fluid height) got increased by 17,5 cm for every input-hydrograph, where 35% of the maximum height was solid and 65% of the maximum height fluid. This composition was chosen, due to the fact that visual observations of the jökulhlaup and the depositions suggested “tens of percent” (Tómas Jóhannesson) solid stake. Because no information of the pace of the jökulhlaup was available, the velocities, in the input-hydrograph, of the solid and fluid component were chosen to be consistently 10 m/s for all time steps. H(max) from all input-hydrographs ranged from 17,5 cm up to 1,925m. After running test simulations for all these input-hydrographs with different entrainment-coefficients, no results could be achieved with the two lowest input-hydrographs, regarding H(max), independently of the entrainment-

coefficient. One reason for this circumstance might be, that the numerical model was not able to calculate with such shallow flow depths and therefore the simulations all resulted in a “Numerical Error” (r.avaflow). Due to that fact, these simulations were not considered for the equifinality/results.

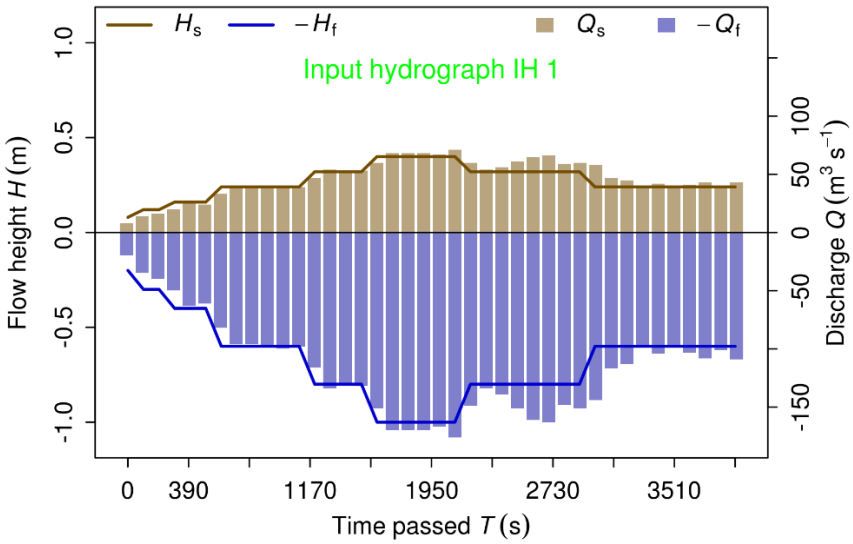

Figure 23: Example of an input-hydrograph.

Table 8: Example of an input-hydrograph.

T	H(s)	V(s)	H(f)	V(f)
0	0,05	10	0,125	10
100	0,075	10	0,188	10
200	0,075	10	0,188	10
300	0,1	10	0,25	10
400	0,1	10	0,25	10
600	0,15	10	0,375	10
1000	0,15	10	0,375	10
1200	0,2	10	0,5	10
1400	0,2	10	0,5	10
1600	0,25	10	0,625	10
1800	0,25	10	0,625	10
2000	0,25	10	0,625	10
2200	0,2	10	0,5	10
2600	0,2	10	0,5	10
3000	0,15	10	0,375	10
3500	0,15	10	0,375	10
4000	0,1	10	0,25	10

4.2.6 Heatmaps

To evaluate the equifinality of the numerical models implemented in r.avaflow 121 simulations were executed, where every entrainment-coefficient got combined with every input-hydrograph. As explained in Sect. 4.2.5, after seeing the results from each simulation, the simulations using the two input-hydrographs with the least H(max) were cancelled. To display these results properly, a heatmap for the entrainment, flow height, flow time and the combination of these three parameters was created, using the programming language Python 3.7. In these heatmaps, the observed values for the entrainment, flow height and flow time got compared to the simulated values, resulting in a deviation ratio α indicating how alike the observation and the simulation are. To calculate the deviation ratio α, the following equation was used:

$$\alpha = \frac{Simulation - Observation}{Observation}$$

Using that equation, a value of 0 is the optimum, meaning, that the observed and simulated value coincide perfectly.

For the entrainment, r.avaflow creates a validation file for each simulation, which displays several validation features, including the solid and fluid entrained volume. Added up, these two values result in the total entrainment of the simulation. As stated in Sect. 4.2.2.1 an observation value of $2*10^6$ m³ was assumed. This value was used in the stated equation above. The result for each simulation was the relative ratio of deviation, regarding the entrainment.

As explained in Sect. 4.2.3, a control-point was installed to measure the maximum flow height at a certain position. r.avaflow creates an output file for each simulation, displaying the results for this control-point. These are the flow height for every time step and the overall maximum flow height. For the observation value 7m were chosen (see Sect. 4.2.3) to attain, as for the entrainment, the relative ratio of deviation.

Regarding the duration of the flow two output-hydrographs were installed (see Sect. 4.2.4). These display the time until the flow reached the locations of the hydrographs. To obtain the relative ratio of deviation for the flow time, using the equation above, an observation value of 45 minutes was assumed.

For the absolute ratio of deviation the equation used for the entrainment, flow height and flow time got slightly changed to:

$$\alpha\_abs = \sqrt{\frac{(Simulation - Observation)^2}{Observation^2}}$$

With that change, only positive values will be achieved, which can be further used to calculate an overall goodness of fit. To determine the overall goodness of fit of each simulation, the three ratios of deviation of entrainment, flow height and flow time got combined, where each ratio got multiplied with a quantifier regarding the quality of the observation. While the entrainment got a quantifier of 0.5, the flow height and flow time each got a quantifier of 0.25, because the

observation of the entrainment is the most valid observation, since several approaches led to similar results.

$$\alpha\_abs\_combined = \alpha_{entrainment} * 0{,}5 + \alpha_{flowheight} * 0{,}25 + \alpha_{flowtime} * 0.25$$

Added up, this equation results in an absolute ratio of deviation for each simulation, displaying the compliance of each simulation with all three observations.
With these created heatmaps, the simulations with the least/most absolute ratio of deviation could be chosen, to display the results in more detail (see Sect. 5). Attachment A shows the script written in Python 3.7, which was used to create the heatmaps.

5 Results

5.1 Combined deviation of entrainment, flow height and flow time

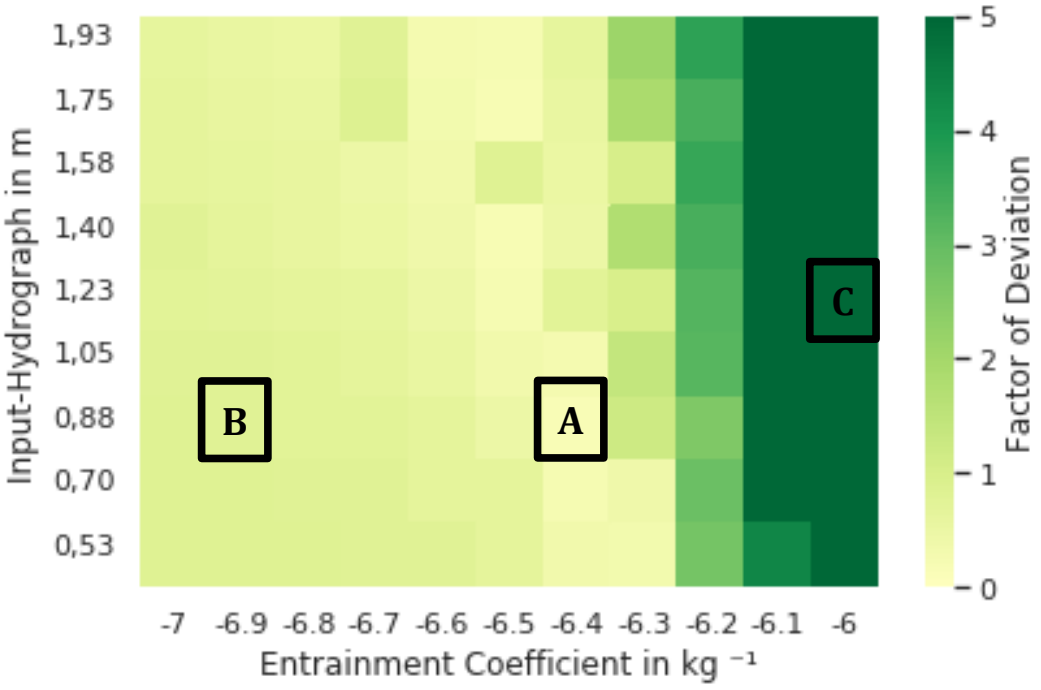

Figure 24: Heatmap with the three chosen simulations a, b and c.

Three simulations were chosen from the combined heatmap, to adequately display the results, regarding their deviation. The simulation A (Input-hydrograph = 0.88m; C_e = -6.4 kg^{-1}) showed the best combined result with the least absolute deviation of all simulations. Further, one simulation

was chosen, that underestimated the observation, and one that overestimated the observation. For the underestimation the simulation B (Input-hydrograph = 0.88m; C_e = -6.9 kg^{-1}) was chosen, for the overestimation simulation C (Input-hydrograph = 1.23m; C_e = -6 kg^{-1}). These three simulations show similar results, regarding the deviation, in all heatmaps (entrainment, flow height, flow time), which was the crucial facet of their selection, to properly display the results. Additionally, the simulation with the least deviation in each of the single heatmaps, is also displayed, to evaluate two similar results close to the observation.

5.2 Entrainment

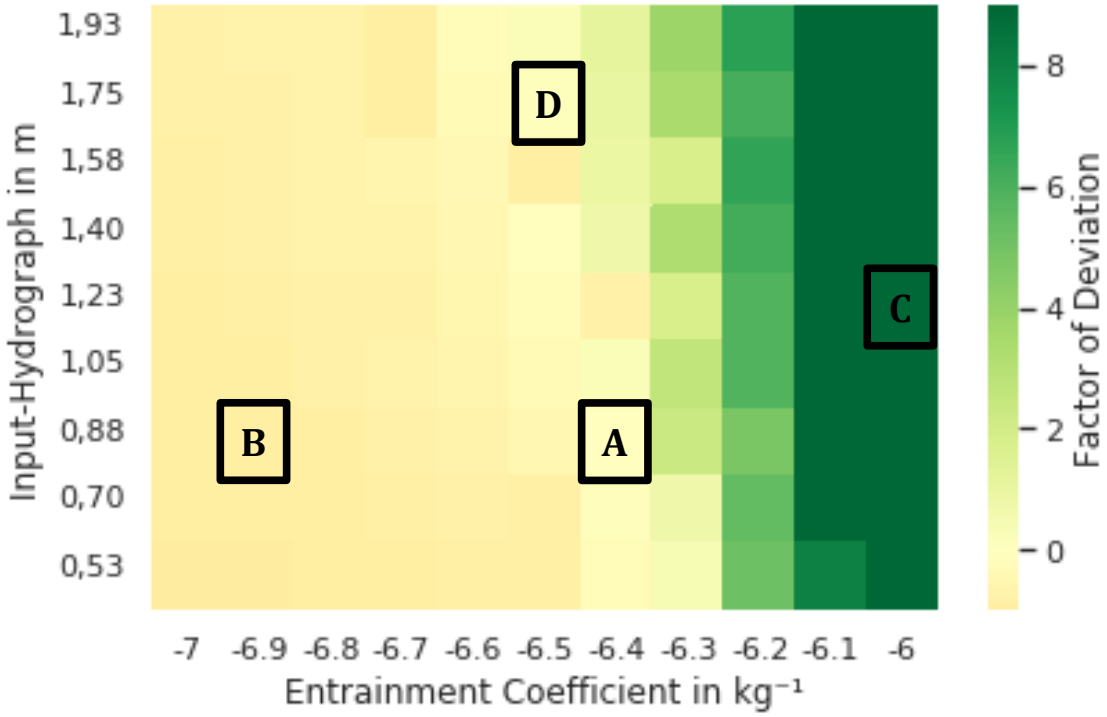

Figure 25: Heatmap of the deviation regarding the entrainment volume.

For the entrained volume the simulation A (Input-hydrograph = 0.88m; C_e = -6.4^{-1}) was the closest one to the assumed entrainment. So, the simulation with the second least deviation was added to the existing three simulations, which is simulation D (Input-hydrograph = 1.75m; C_e = -6.5 kg^{-1}).

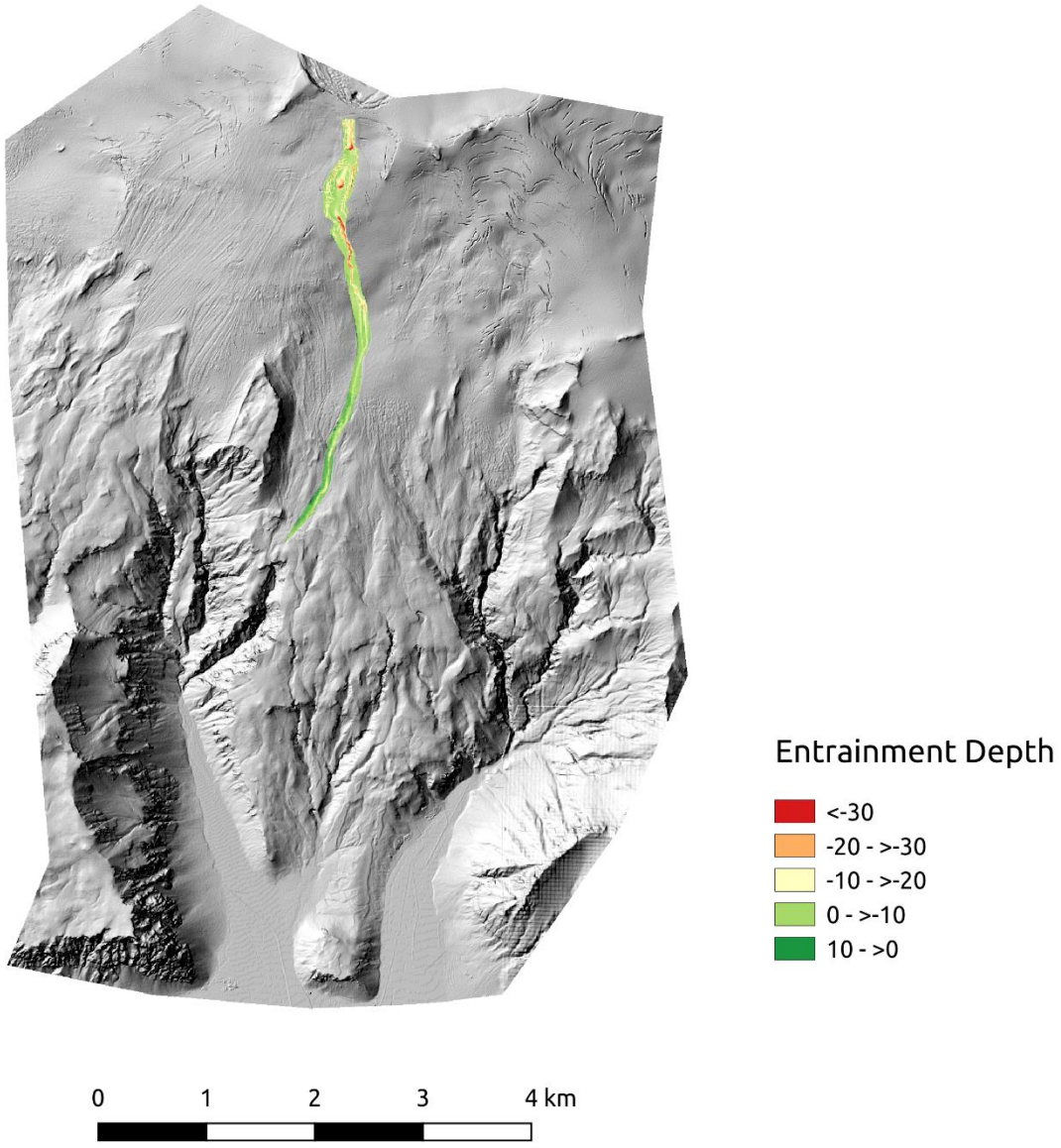

Figure 26: Observed entrainment of the event under investigation.

Figure 26 shows the observed entrainment depths in meters, that occurred during the event under investigation. The most entrainment, concerning the depth, happened in the first third of the trench (~ 1km). In this part of the trench, the entrainment depths go up to over 30 m. In the middle part of the trench, the entrainment depths range between 0 – 20 m, with a big portion between 10 – 20m. Reaching the end of the trench the entrainment depths mostly range between 0 – 10m. Looking at the end of the trench on the orographic right, there even are some depositions of entrained material, up to 10 m high.

The slope of the topography declines from the beginning of the trench to its end. Because of that the original jökulhlaup plus the entrained material reach high velocities at the beginning and then slow down over time and space. This might be one of the reasons why the entrained depths have their peak in the first third of the trench and decline, the further down the flow propagates. The

width of the trench also decreases from top to bottom, probably due to the decrease of velocity of the flow. At the end of the trench, where it reaches the southern gully, the slope is fairly plain, the trench rather narrow causing material to be deposited at the orographic right of the trench. Entering the southern gully, the width of the trench gets so narrow and the flow cannot flow through completely, causing the depositions.

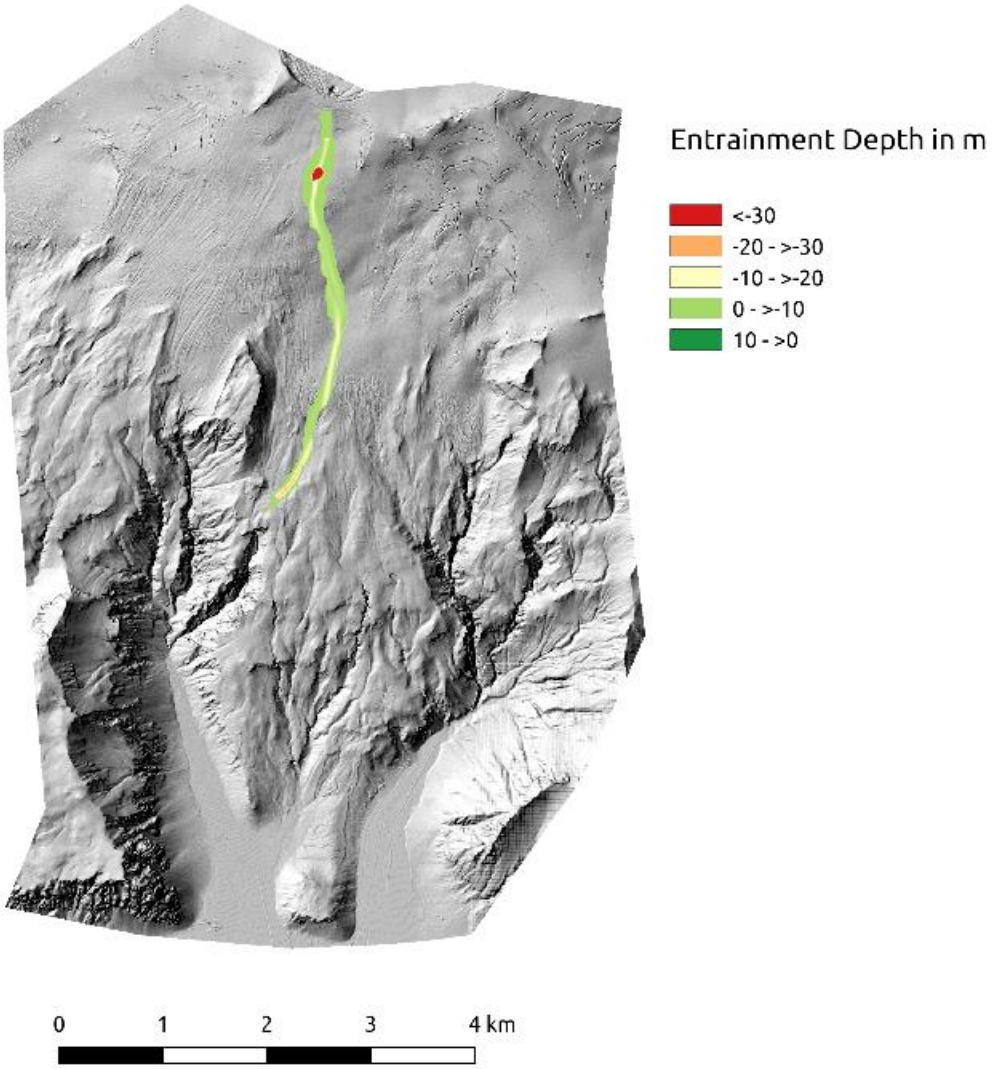

Figure 27: The best simulation regarding the entrained volume.

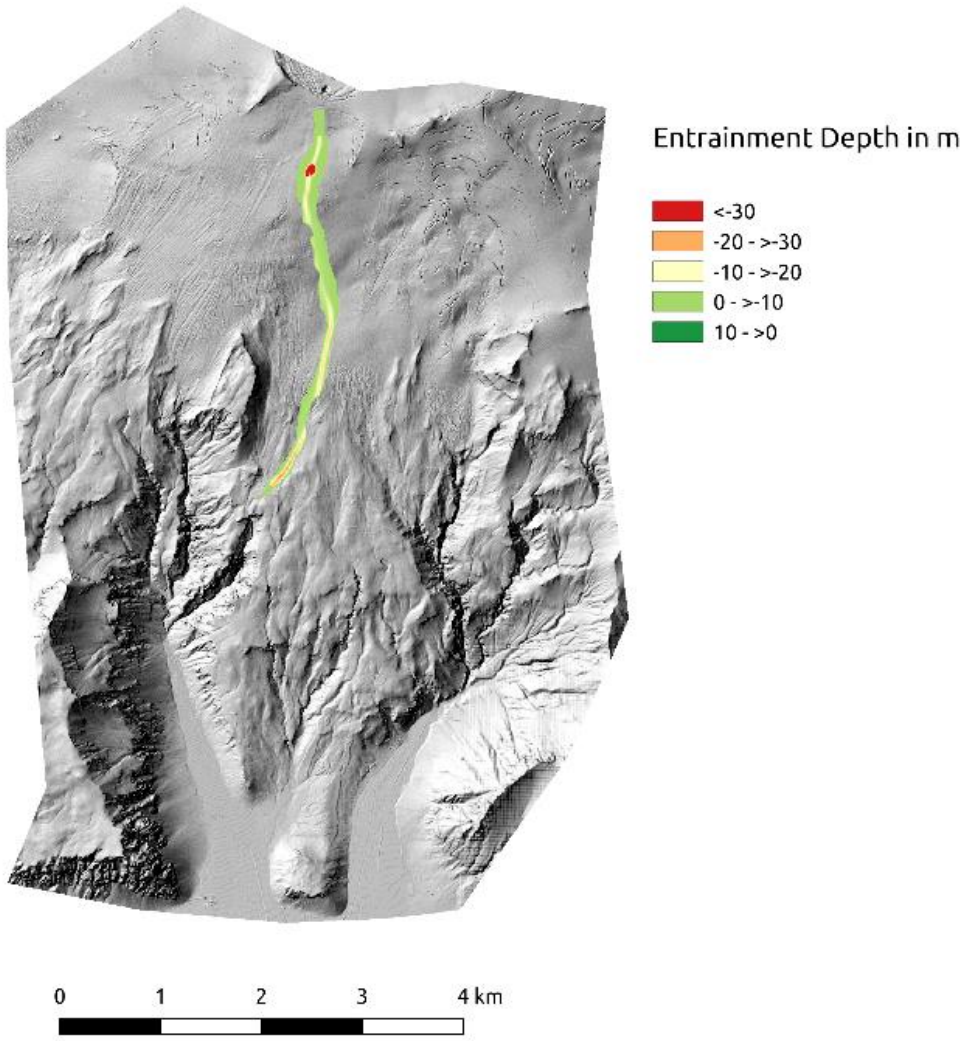

Figure 258: The second-best simulation regarding the entrained volume.

Figure 27 and 28 show the two simulations A and D (Input-hydrograph = 0.88m; C_e = -6.4 kg^{-1} and Input-hydrograph = 1.75m; C_e = -6. kg^{-1}) with the least deviation with reference to the actual entrained volume. Like in Fig. 26 the maximum entrained depths appear in the upper part of the trench, with the slight difference that entrained depths over 30 m are only observed in the crater, created due to the jökulhlaup, and not further downstream in the actual trench itself. Also, the entrainment depth is not continuously decreasing downwards the trench. Before reaching the southern gully, the entrained depths increase again in the last part of the trench. Another aspect which is remarkable is the structure of the entrained depths. In contrast to Figure 26, where the entrained depths are heavily structured and heterogeneous, the simulations show rather homogeneous entrainment, with only a couple of separated areas.

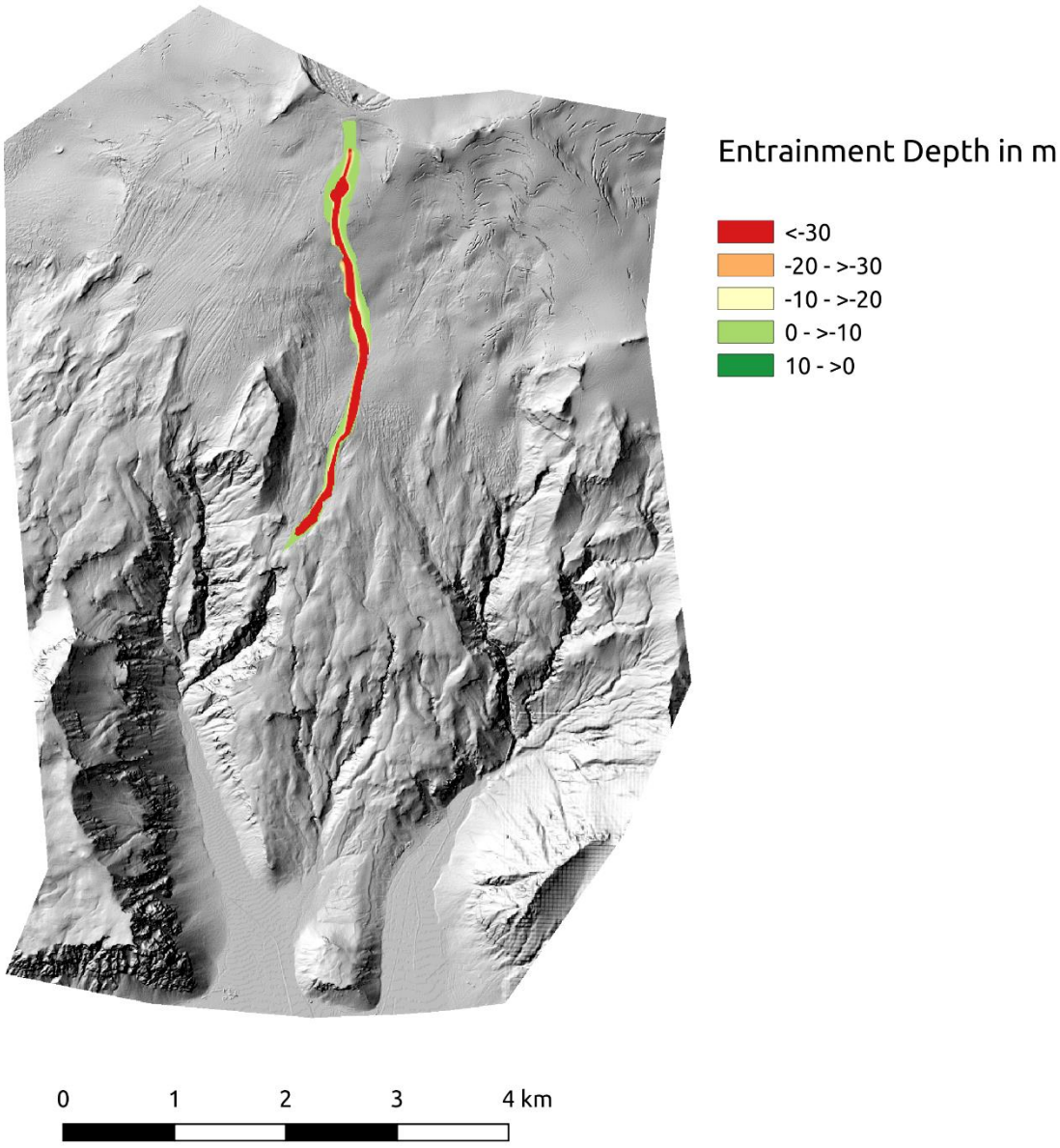

Figure 29: The overestimated simulation regarding the entrainment volume.

Simulation C (Input-hydrograph = 1.23m; C_e = -6 kg $^{-1}$) was chosen to represent the simulations, that overestimated the event. In contrast to the actual entrainment (Fig. 12), the entrainment areas with depths over 30m are considerably larger, covering ~ 80% of the total area. Areas with 0 – 10m entrainment depths appear mostly in the first half at the edges of the trench and almost disappear in the second half.

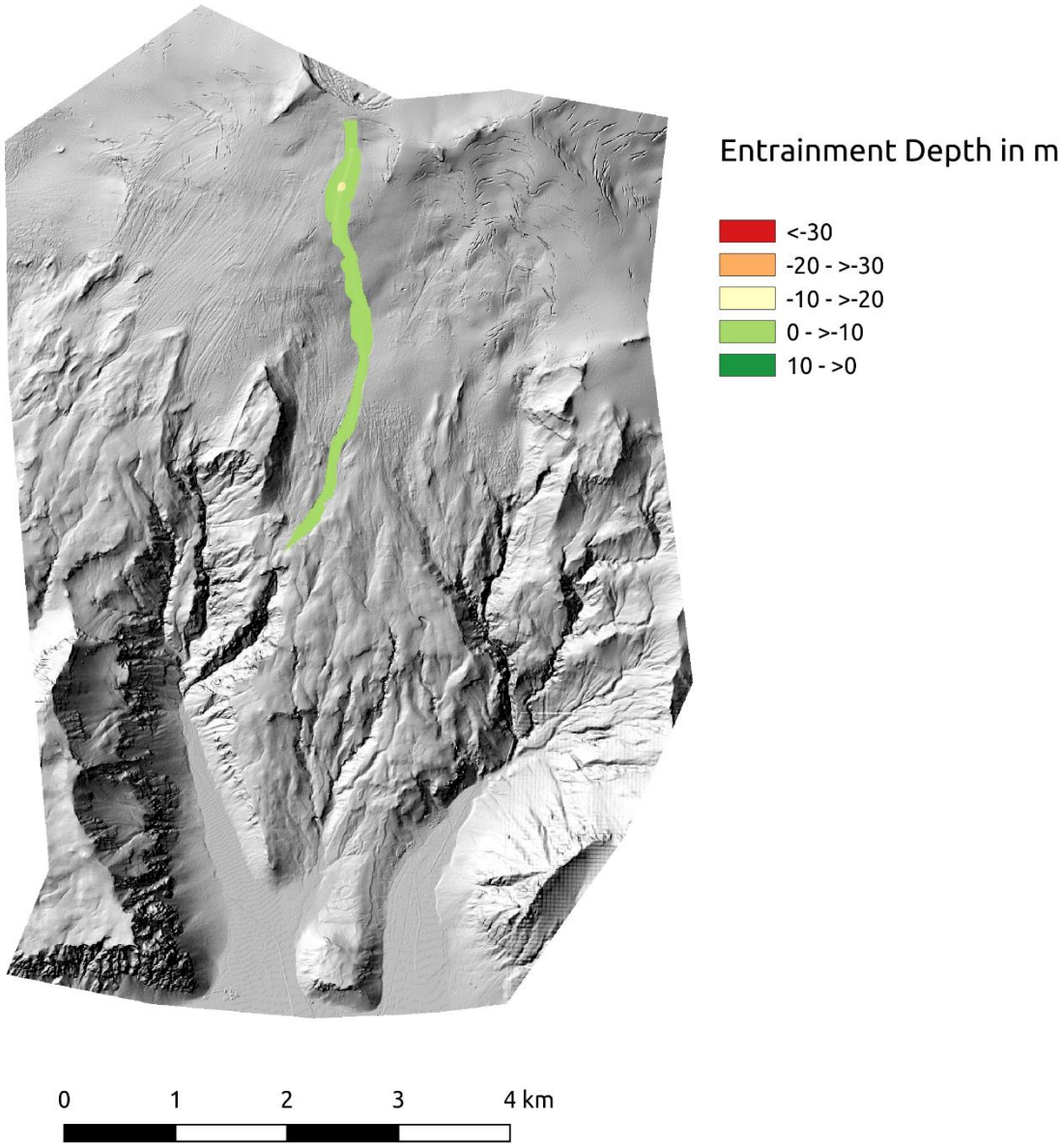

Figure 30: The underestimated simulation regarding the entrainment volume.

The underestimating simulation B (Input-hydrograph = 0.88m; C_e = -6.9 kg^{-1}) shows clearly the possible simulation differences. Entrainment depths over 10 m were only exceeded in the crater at the top of the slope in a very small area. The mediocre input-hydrograph combined with an entrainment-coefficient on the bottom of the scale lead to entrainment depths between 0 – 10 m at ~95% of the total entrainment area. Like the overestimated simulation shown in Fig. 29, the entrainment was quite homogeneous with one dominant depth-range.

5.3 Flow Height

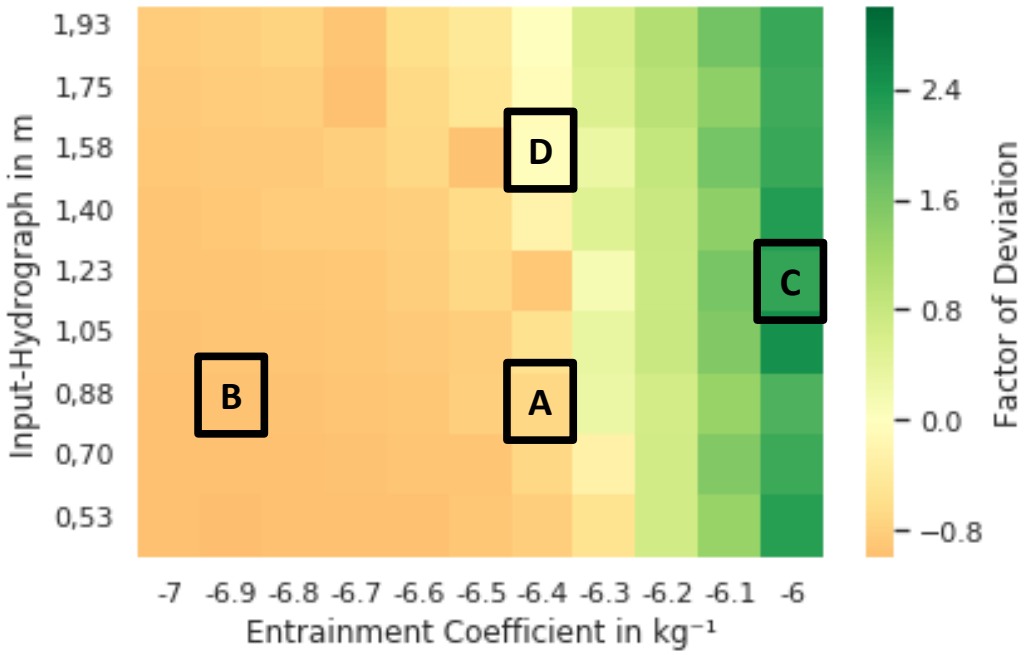

Figure 31: Heatmap of the deviation regarding the flow-height.

The flow-height results will be also represented by four simulations, whereat the best overall, the underestimating and the overestimating simulation are the same as for the entrainment. Only the best simulation, regarding the deviation of the entrained volume, is changed. In this case the simulation D (Input-hydrograph = 1.58m; C_e = -6.4 kg^{-1}) has the least deviation, with the closest value to 0.

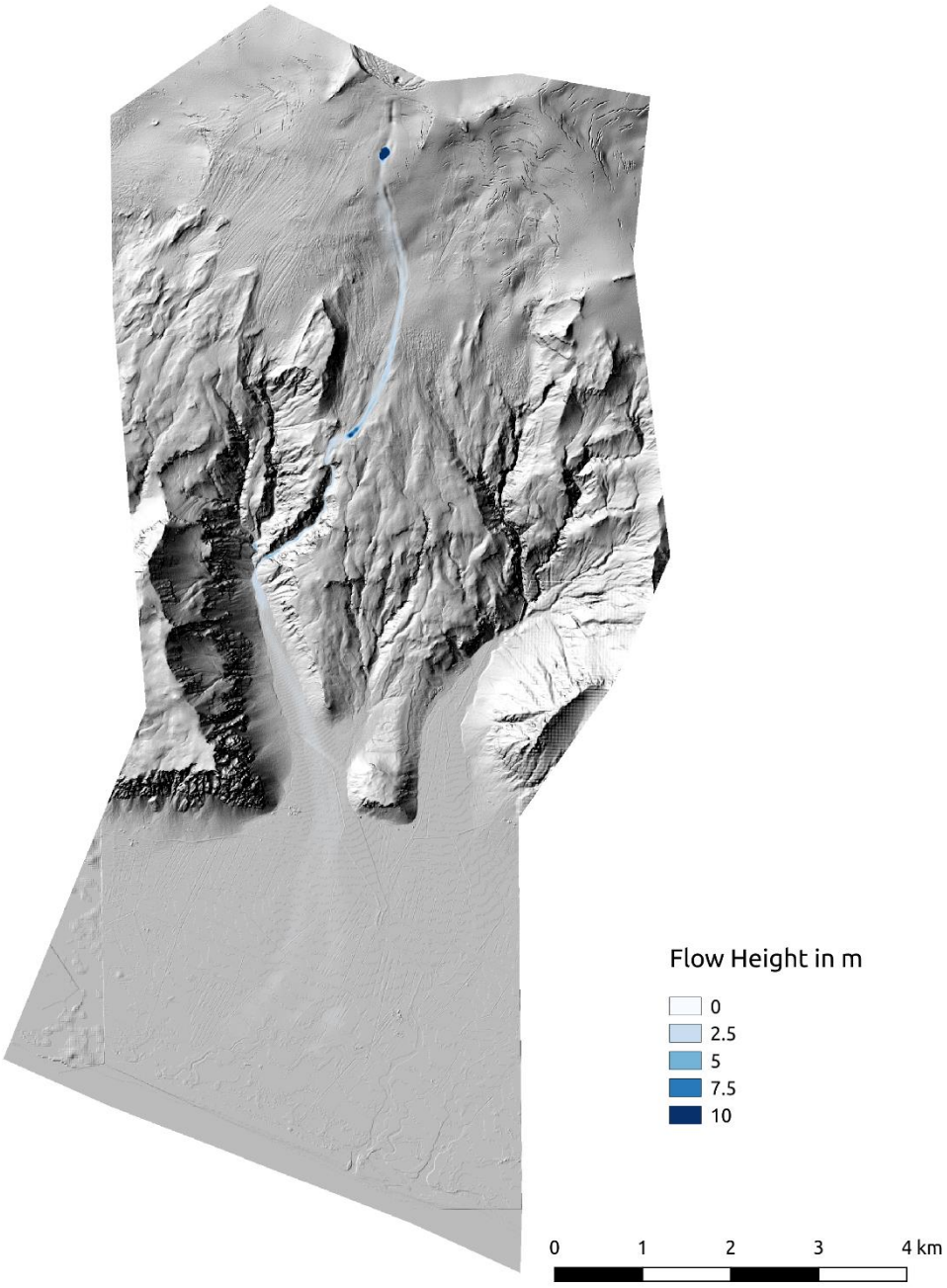

Figure 32: The maximum flow height for the overall best simulation (Input-hydrograph = 0.88m; Ce = -6.4 kg-1).

Figure 32 shows that the maximum flow heights, for the best simulation, were attained in the formed crater and right before the flow reached the southern gully. The flow canalized in the gully and expanded again after it left the gully and reached the beginning of the lowlands, right where the flow height was measured during the event. Another validation for this simulation, is the fact that the flow also streamed down the northern gully. After reaching the lowlands the flow heights quickly decrease, not exceeding 2.5m. The flow does not follow the dam, like in the assumed deposition area, instead overtopping it and streaming further south until it stops completely.

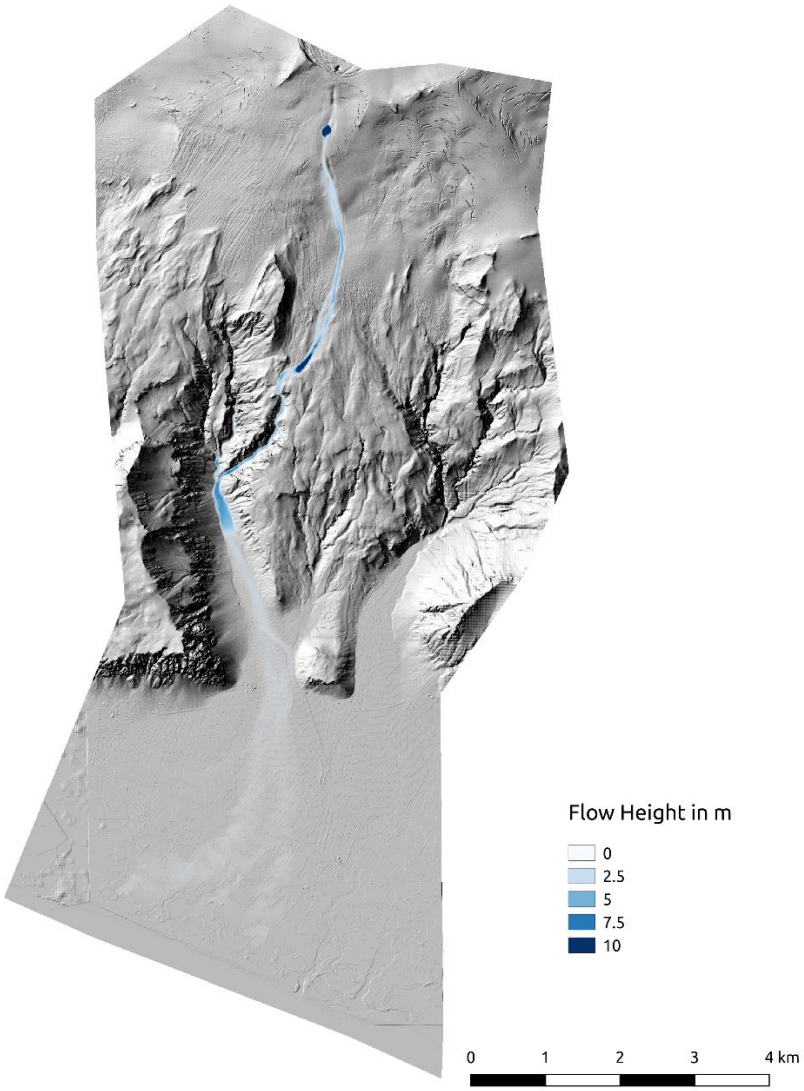

Figure 33: Simulation d (Input-hydrograph = 1.58m; Ce = -6.4 kg-1) with the least deviation, regarding the flow height.

The best simulation, regarding the flow height, shows quite similar results, to the overall best simulation. Maximum flow heights were obtained in the crater and right before the flow reached the southern gully. The decreasing and spreading of the flow beyond the point it reached the lowlands also looks similar to the simulation A (Input-hydrograph = 0.88m; C_e = -6.4 kg^{-1}). Both simulations have the same entrainment-coefficient but the maximum flow height, of the input-hydrograph, of simulation D (Input-hydrograph = 1.58m; C_e = -6.4 $kg^{-1)}$ is 0.6m higher. This probably explains the similar structure of the flow. Differences are, that the areas with high flow heights are larger at simulation D (Input-hydrograph = 1.58m; C_e = -6.4 kg^{-1}) and that some areas, like the middle part of the trench, display higher flow heights than in simulation A (Input-hydrograph = 0.88m; C_e = -6.4 kg^{-1}). Also, induced by the higher maximum flow height of the input-hydrograph, the runout-zone in the lowlands is bigger and exceeds farther south in simulation D (Input-hydrograph = 1.58m; C_e = -6.4 kg^{-1}). Although it is not displayed too well, some amounts of the flow went through the northern gully, as the assumed event.

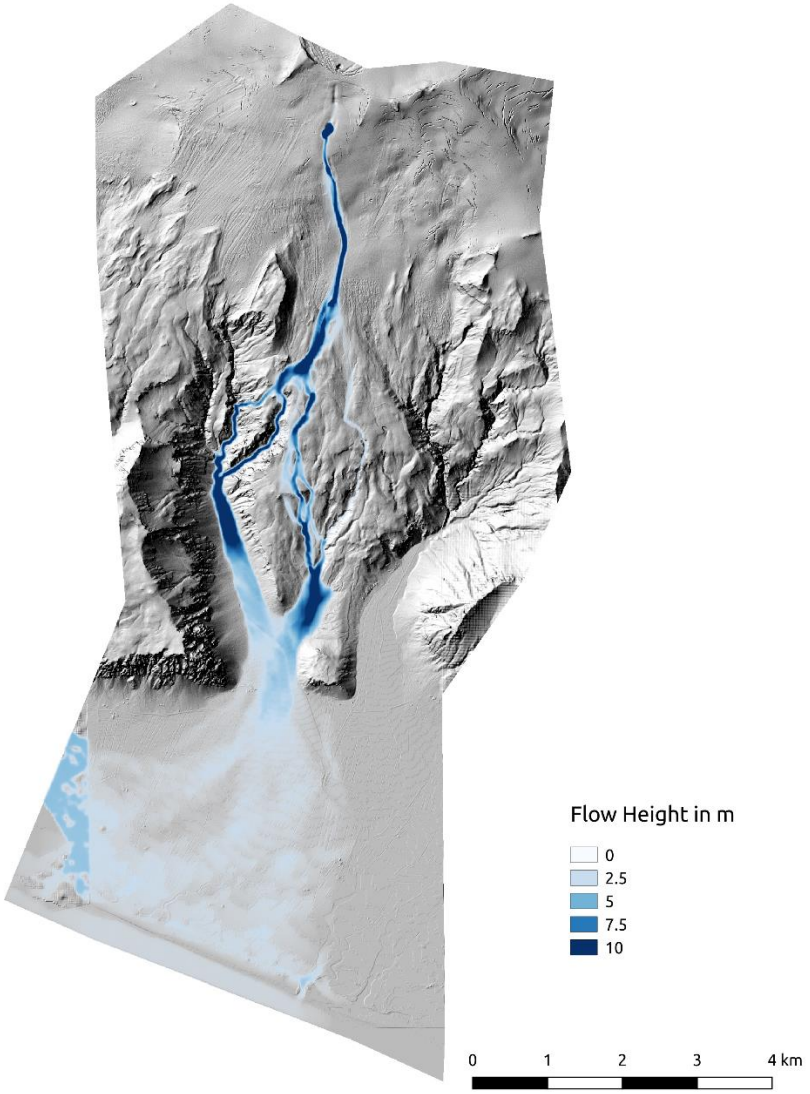

Figure 34: The overestimated Simulation C (Input-hydrograph = 1.23m; Ce = -6 kg-1), regarding the flow height.

The overestimating simulation clearly shows the impact of a high entrainment-coefficient combined with a mediocre maximum input flow height. From the crater downwards until the beginning of the lowlands, the maximum flow height constantly exceeds 10m, up to 70m. Still 10m were chosen for the visualization, for a better comparison of the simulations. Due to the immense heights of the flow, it develops new channels next to the southern gully. One channel is flowing down the northern gully, which has the same beginning and end as the southern gully. Eastwards of the southern gully originates another channel down the slope. The two flows reconnect in the lowlands, where they flood substantial amounts of the more southern area. After the flow height is between 0 – 2.5m for quite a distance, it rises in the bottom left corner up to 5m. This is caused by the fact, that the simulation hits its border here, and so the water “swaps” back from an imaginary wall in that area. This phenomenon can only be observed when the simulation drastically overestimates the assumed event.

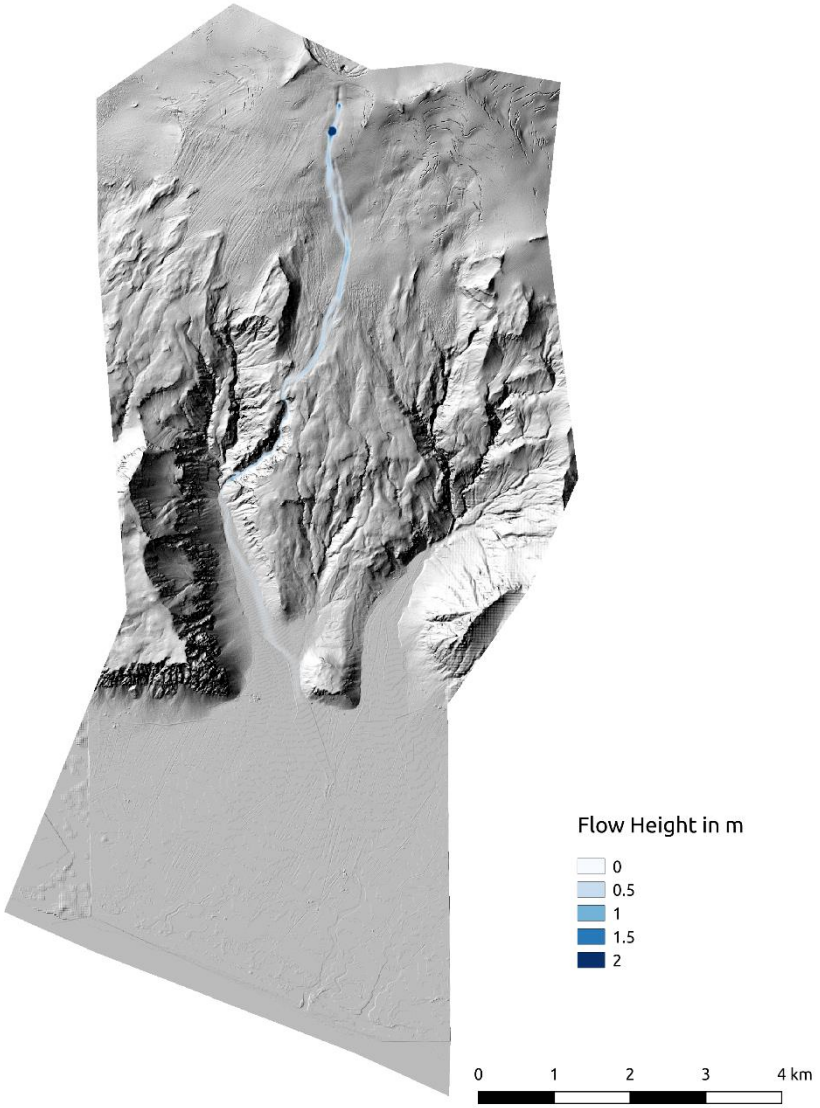

Figure 35: The underestimated Simulation B (Input-hydrograph = 0.88m; Ce = -6.9 kg-1), regarding the flow height.

The first thing was to downscale the legend for the underestimating simulation by a factor of 5, so that the results would be properly displayed. Due to the low flow heights, the results would not have been meaningful with the usual legend. As the other three simulations the maximum flow height was achieved at the crater, but at this simulation only here and not at the entrance of the southern gully or elsewhere. Due to the low entrainment-coefficient and input flow height the flow stops early in the lowlands, regarding the other simulations. However, the structure of the flow has some similarities to the simulations A (Input-hydrograph = 0.88m; C_e = -6.4 kg^{-1}) and D (Input-hydrograph = 1.58m; C_e = -6.4 kg^{-1}). The trench itself has mediocre flow heights and after the trench exits the southern gully into the lowlands, the flow heights quickly decreases and eventually stops.

5.4 Flow Time

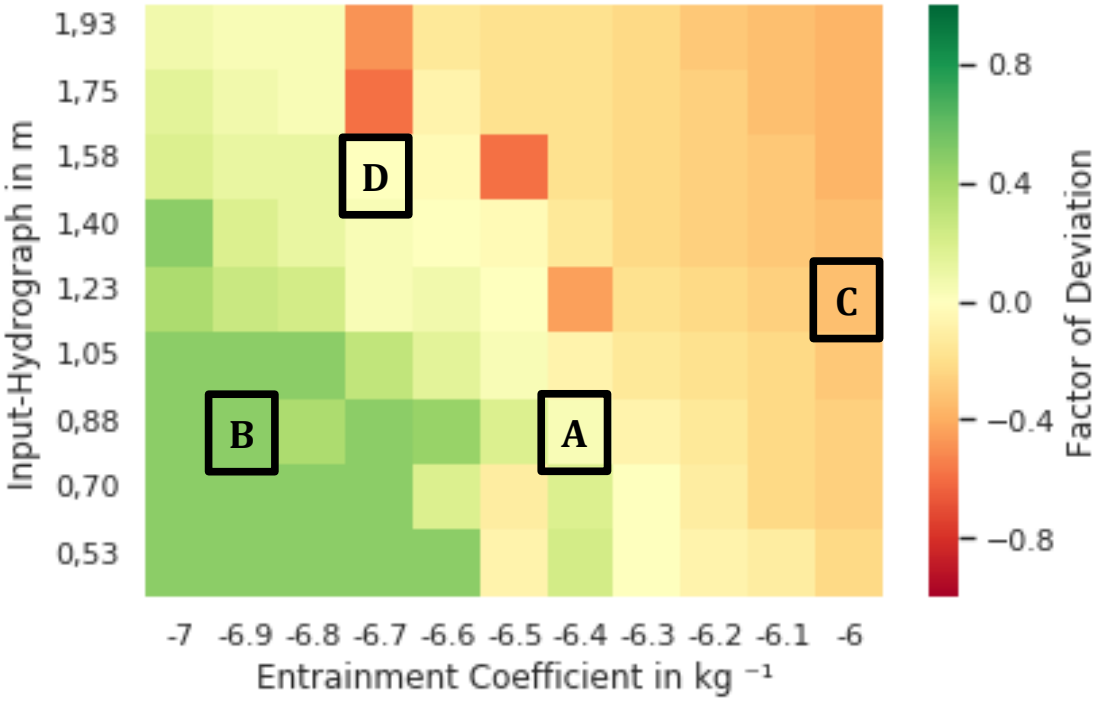

Figure 36: Heatmap of the deviation regarding the flow time.

Regarding the flow time the overall-best, the underestimating and the overestimating simulation remained the same (see Sect. 5.1). Since the overall-best simulation (simulation A) is also the simulation with the least deviation regarding the flow time, the second-best simulation was added, which in this case was simulation D(Input-hydrograph = 1.58m; C_e = -6.7 kg^{-1}).

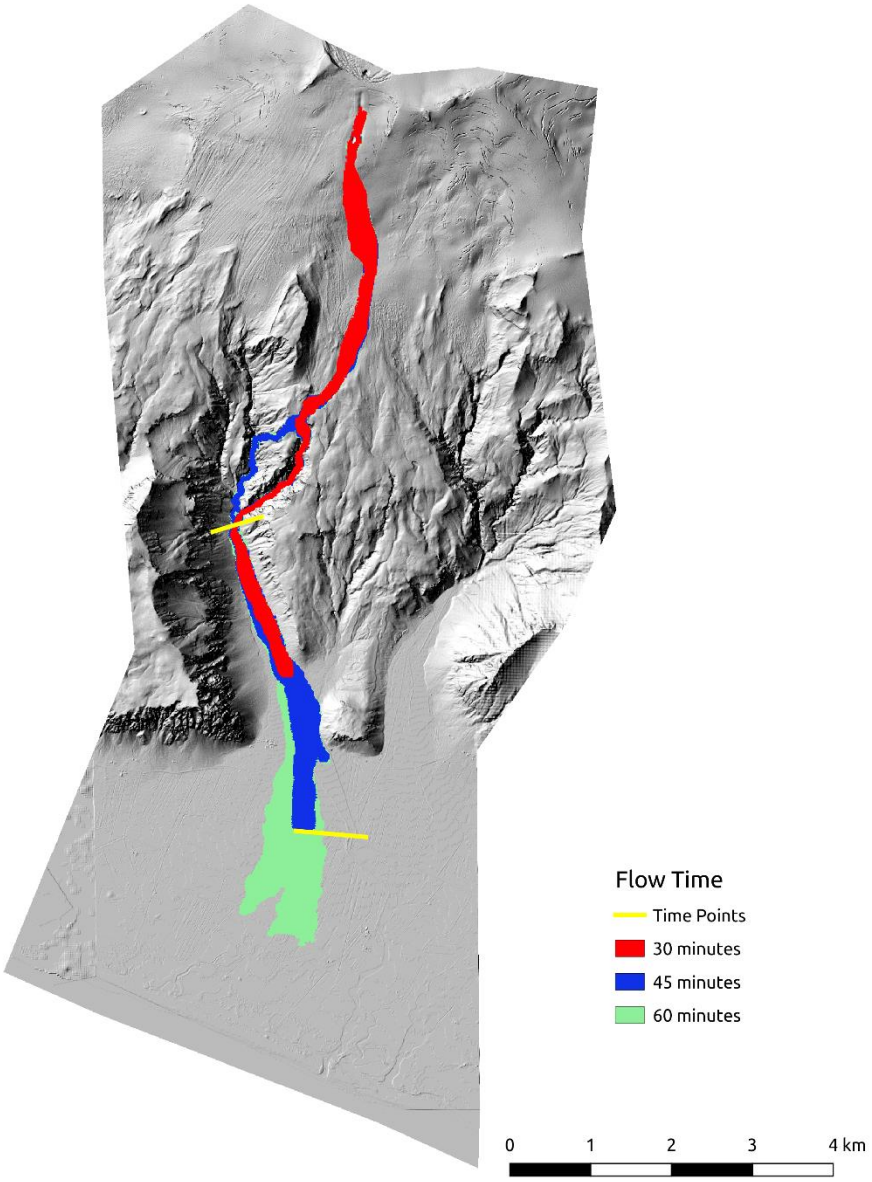

Figure 37: The flow times for the overall best simulation. The time points refer to the observed flow after 30, respectively 45 minutes.

After 30 minutes the simulated flow is farther downwards than the assumed flow, which is the case in most simulations. This may be due to the fact, that the basal friction angle was adjusted too low for the simulations. Another reason could be the composition of the flow, in which the solid rate was assumed too low for the simulations. However, after 45 minutes the flow is reaching exactly the same point as the assumed event. Since the second point, where the time of the flow was assumed, was in between the range of 45 – 60 minutes, maybe increasing the friction, respectively increasing the solid rate of the flow, would have shown results, where after 30 minutes the flow passed the first time point measurement and after 60 minutes the second time point measurement.

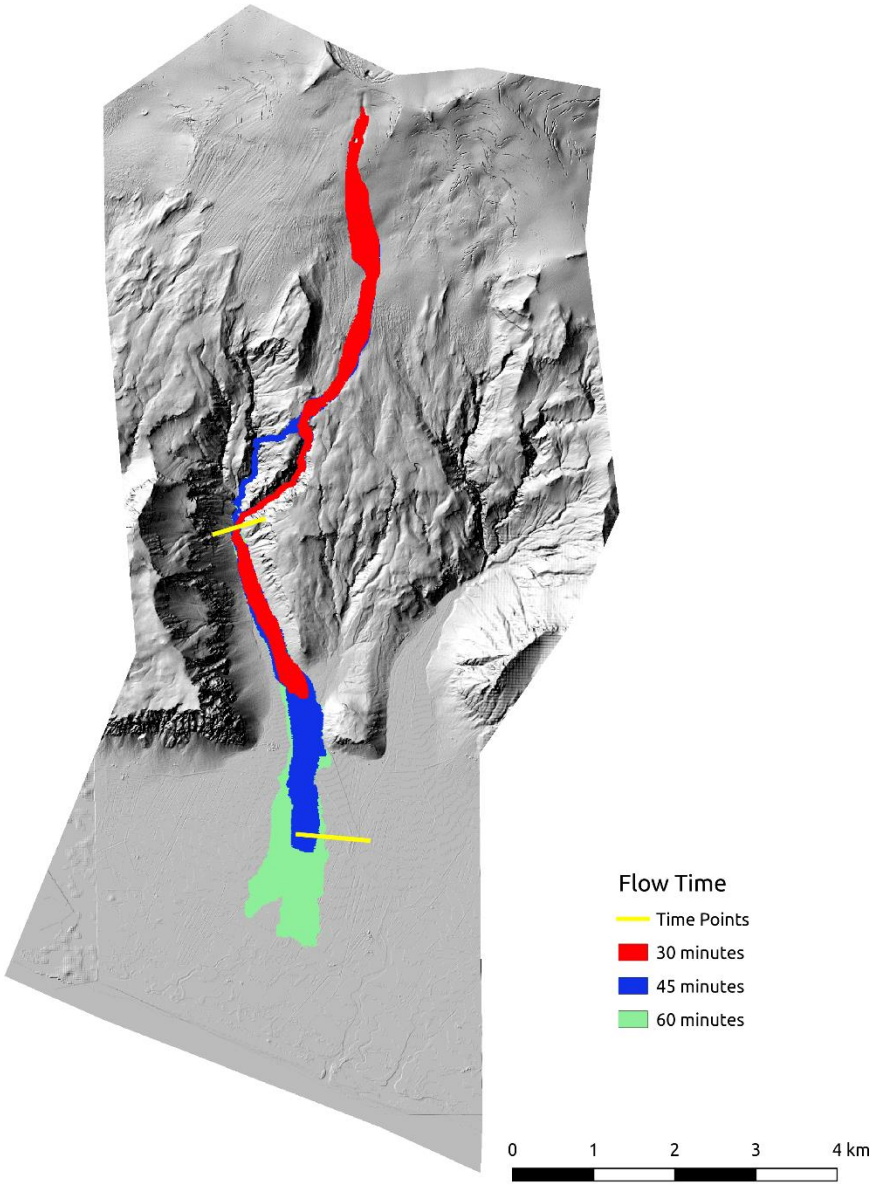

Figure 38: The flow times for the second-best simulation.

The second-best simulation shows quite similar results to the overall best simulation. After 30 minutes the flow is way ahead of the assumed event, though after 45 minutes the flow and the assumed event coincide rather well. Also, in both simulations, the flow runs through the northern gully and shortly before the flow stops it divides into two streams. What is different, is, that the flow, at every time step, is a little bit farther downwards, then in the overall best simulation.

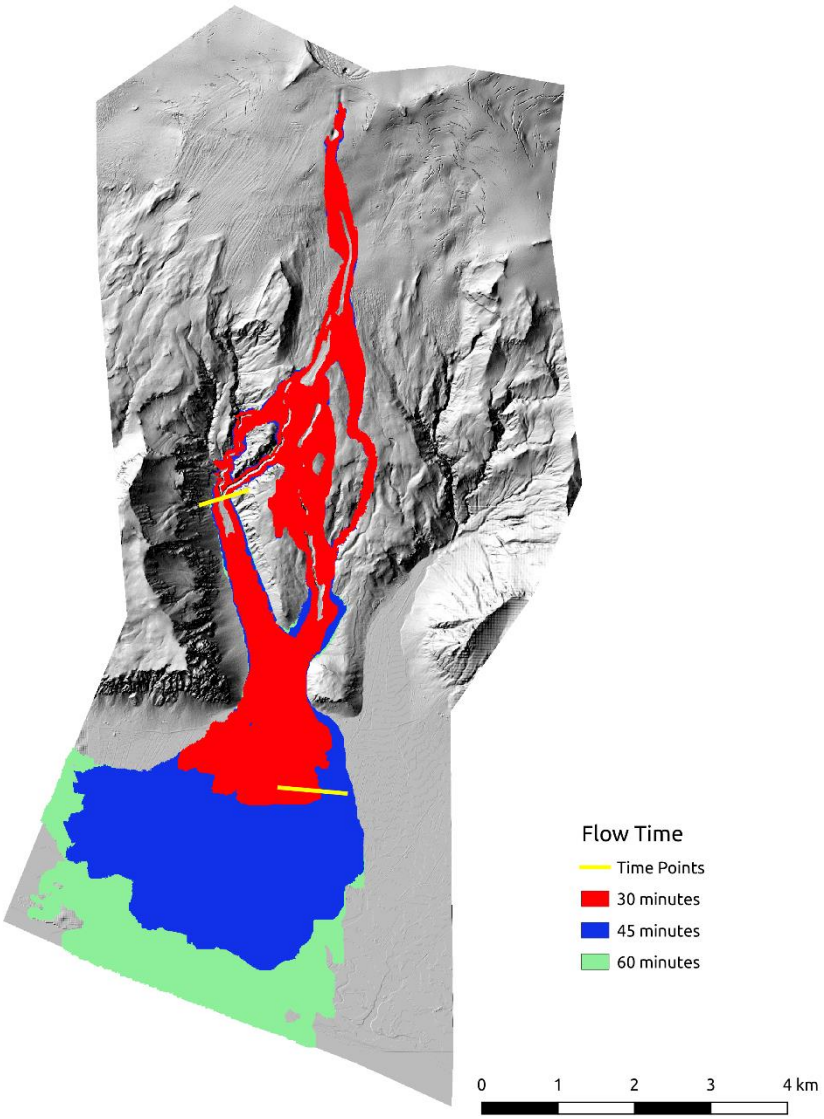

Figure 39: The flow times for the overestimated simulation.

Due to the combination of a high entrainment-coefficient and a mediocre maximum input-hydrograph flow height, the overestimating simulation is much faster as the assumed event. After 30 minutes the flow already passes the second time point measurement, with a volume much higher than the other presented simulations. After 45 minutes a vast area of the lowlands is inundated, but due to the low slope angle the distance between 30 and 45 minutes is not as big as expected. The difference between 45 and 60 minutes would usually be larger, but the flow got limited due to the boundaries of the DEM.

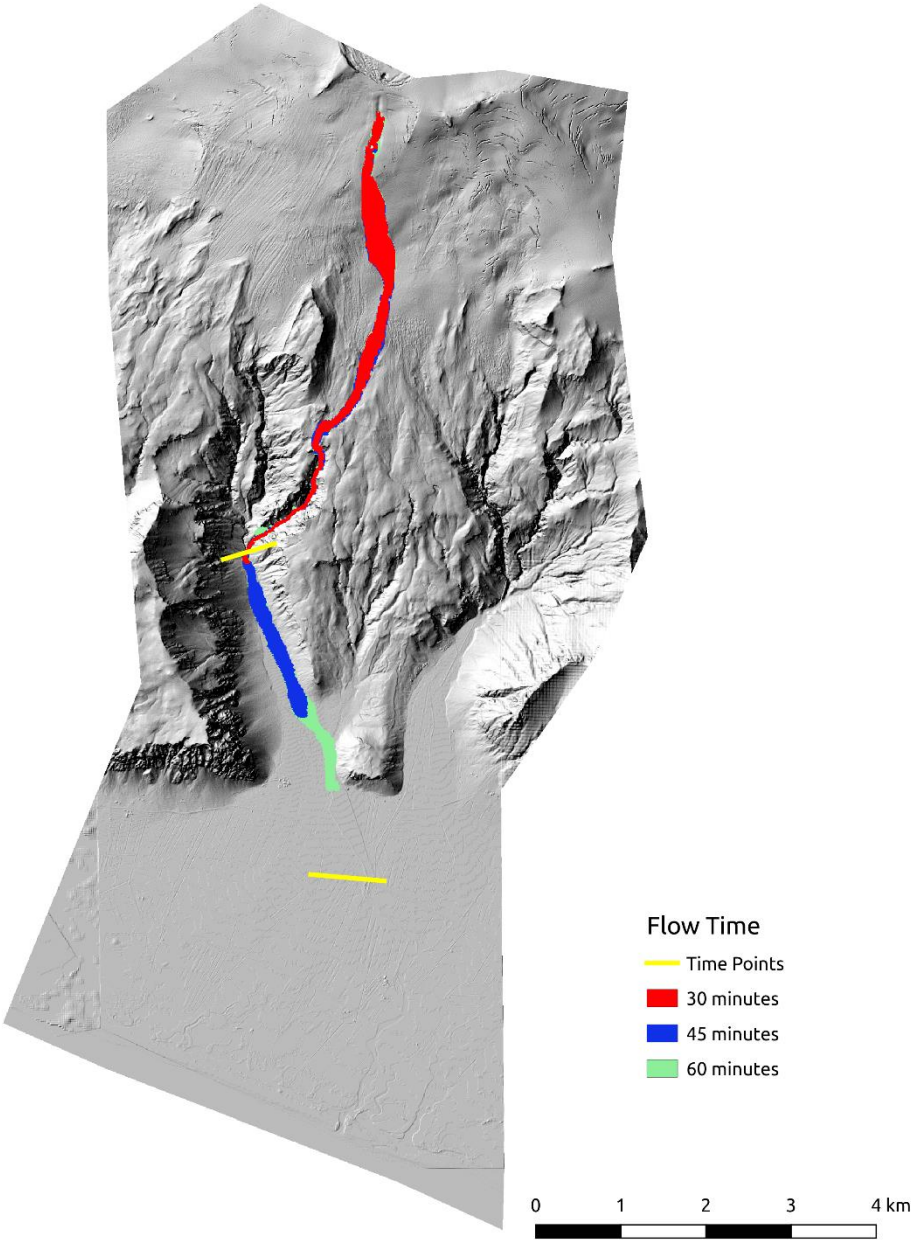

Figure 40: The flow times for the underestimated simulation.

Figure 40 illustrates the flow times after 30/45/60 minutes for the underestimating simulation. After 60 minutes the flow does not reach the second time point measurements, which indicates clearly that the input parameters of the simulation were picked way too low. In the assumed event the flow reached the second time point measurement after 45 – 60 minutes and still kept flowing after that. Despite that, after 30 minutes, the simulated flow is almost exactly at the first time point measurement, as the assumed event. Looking at Fig. 37, the overall best simulation, the flow was too fast after 30 minutes but exactly at the second time point measurement after 45 minutes. So, maybe to achieve ideal results, regarding the flow time, assigning two different basal friction angles, one for the upper part until the end of the gully and one for the lowlands, would lead to better results.

5.5 Best overall simulation

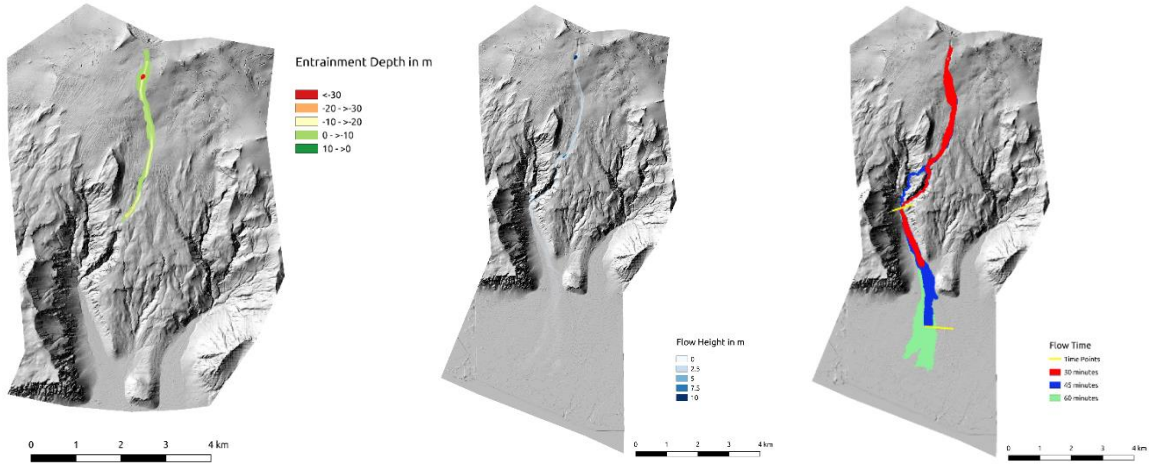

Figure 41: The entrainment depths, flow heights and flow time of the best-overall simulation.

Looking closer at the best overall simulation, by comparing the three different results, to verify to which extent the simulation coincides with the assumed event. Comparing the entrainment depths to the assumed entrainment depths (Fig. 26), the rough structure of the simulation looks quite similar to Figure 26. The crater shows entrained depths over 30 m, but contrariwise to the simulation the actual entrainment map shows entrainment depths not only in the crater, but in other areas upwards and downwards of the crater. Regarding the trench itself, the simulation and the observed entrainment look quite similar. Another slight difference is, that right before the gully, material, up to 10m got deposited during the actual event, which is not the case for the simulation. Reasons for that might be a basal friction angle too low for the simulation or a wrong solid-fluid ratio.

The flow times of the simulation, especially the one after 45 minutes, look not to bad either. As mentioned above for the entrainment, increasing the basal friction angle or changing the solid-fluid composition, could make the flow move slower. By doing that, the flow times for 30 and 60 minutes will probably move a little bit upwards. Another cause for this change might be, that the second time point measurement was chosen to be after 45 minutes, but the observations were not very clear, and the estimations ranged from 45 to 60 minutes.

Regarding the flow height, the simulation quite underestimated the assumed event. In order, for the simulation, to approach the assumption, the maximum flow height of the Input-hydrograph must be raised, for example to 1.58m as shown in Fig. 33. This raise would converge the simulation to the assumed event, regarding the flow height.

Combining the raise of the flow height, the increasing of the basal friction angle and changing the solid-fluid ratio could lead to a simulation fitting the assumption quite well in all three categories.

5.6 Equifinality

One of the main questions of this thesis was, if equifinality issues arise using the underlying model implemented in r.avaflow and to which extent equifinality appears. The results are four heatmaps: entrainment, flow height, flow time and a combination of these three outcomes. These maps indicate, whether r.avaflow is competent of equifinality or not. The focus of these results is the general pattern of these heatmaps. If there is a visible line or random combinations of input parameters, which state that it is possible to attain the same outcome with several different inputs with r.avaflow. And to which extent? In the present work, a diagonal was visible in the heatmaps. Furthermore, if equifinality is not shown, outline reasons why this might be the case. Outliers may always appear in computational modelling due to the complex numerical models, that is implied in r.avaflow.

5.6.1 Equifinality for Entrainment

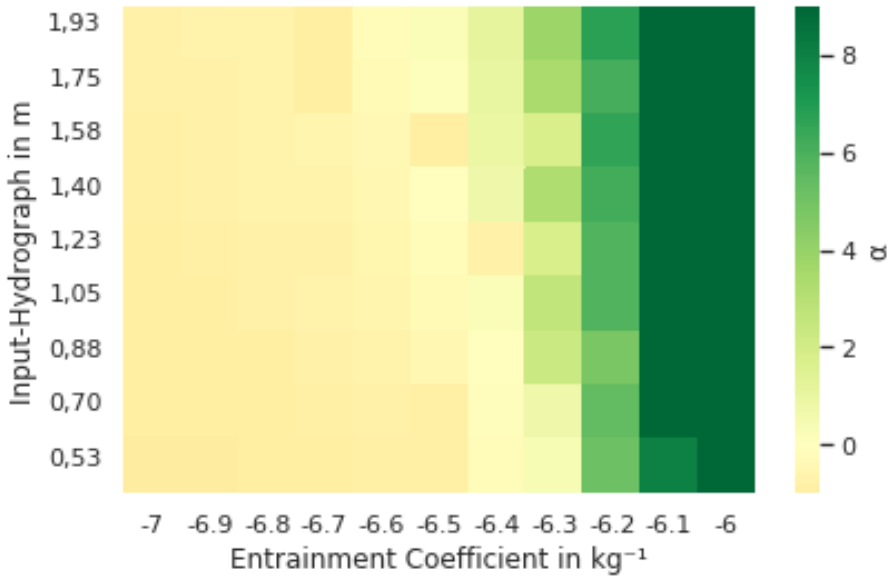

Figure 42: Heatmap for entrainment.

In this heatmap for the entrainment, the scale for the deviation ratio α_entrainment ranges from -1 to 9. The reason for this unbalanced scale is, that -1 is the minimum, as it means there was no entrainment and some simulations, with a high entrainment coefficient, entrained vastly more material than the assumed event. So, if the maximum of the scale would have been set, for example to two, the right third of the heatmap would have been displayed all in the same colour. A diagonal is existing, but it is not ranging from the top left to the bottom right. Rather, it is arranged in the middle third of the heatmap. However, the diagonal is inclined, which indicates equifinality. If the middle third of the heatmap would be stretched over the whole frame, the

equifinality would probably be displayed quite well. One option to achieve this result would be the same procedure, but with a smaller range of entrainment-coefficients, for example from C_e = -6.6 to C_e = -6.3 with intervals of 0.03 and leave the maximum flow heights of the Input-hydrograph as they are.

As soon as the entrainment-coefficient gets smaller than C_e = -6.6, α_entrainment reaches the minimum -1 quite quickly. Because of the logarithmic nature of the entrainment-coefficient the flow barely entrains material below C_e = -6.6. That this is the result for all flow heights could lead to the conclusion, that the entrainment-coefficient weighs in more in the resulting entrainment than the maximum flow height of the input-hydrograph.

On the other side of the diagonal, the α_entrainment values near 0 are relatively sparse and then quickly reach values of 4 and higher, which also is the result of the logarithmic nature of the entrainment-coefficient. The difference to the underestimating side of the diagonal is, that here the maximum flow height of the input-hydrograph does significantly change the result, so the assumption of the loading must be thought through carefully. The difference between the overestimating and the underestimating side is, that the overestimating side has no limit. To display this loading of the maximum flow height of the input-hydrograph the maximum of the scale would have to be way higher, but this would destroy the overall impression of the heatmap.

5.6.2 Equifinality for Flow Height

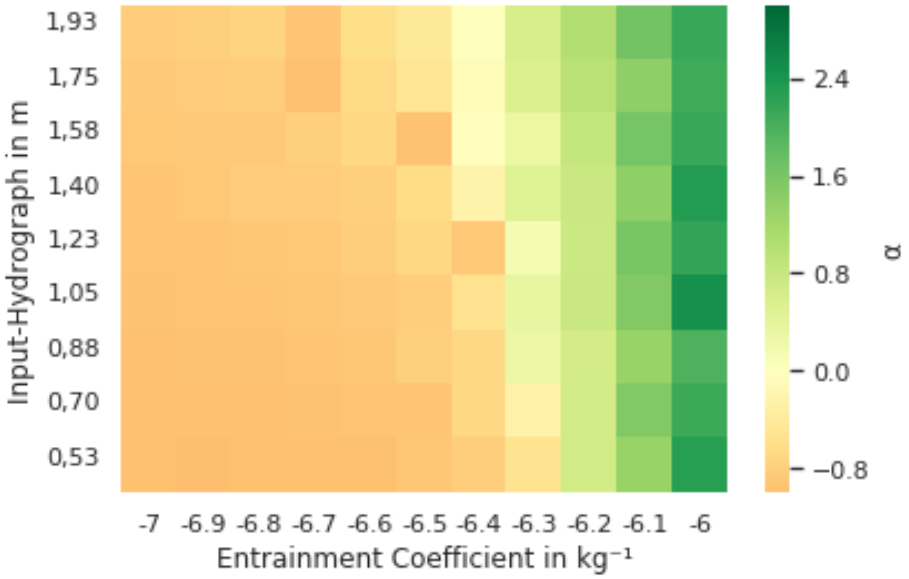

Figure 43: Heatmap for flow height.

In order to gain a meaningful image with reasonable colour distribution the scale for α_depth, like in the heatmap for entrainment, is unbalanced from -1 to 3. The reason is the same as for Fig. 42, that a balanced scale would have produced a meaningless heatmap.

The diagonal in this heatmap is even harder to recognize as in the map before, but there is a slight projection of it, to the right of the middle of the map. From top C_e = -6.4 to bottom C_e = -6.2 the values for α_depth range between -0.5 to 0.5, which indicates equifinality in this part of the map. As for Fig. 42 the range for the entrainment-coefficient would have to be shortened in order to display the equifinality better.

For the underestimating side of the diagonal, the results are similar to Fig. 42 but the gradation of α_depth is a little bit more distinct. Next to the diagonal, two or three rows show simulations with considerably different values for α_depth because the colour difference is displayed very clear. In the bottom left corner, the values for α_depth are exclusively -1, which again indicates, that a low entrainment-coefficient produces barely any entrainment along the path of the flow. One possible way to determine the actual influence of low entrainment-coefficients would be an analysis of the same event with the entrainment-coefficient only with a range from -7 to -6.8/-6.7, to determine at which point exactly the basal material won't be entrained any more.

Because of the location of the diagonal the overestimating side is considerably smaller than the underestimating one. Due to that fact and that theoverestimating range is 3 times as big as the underestimating one, this side is structured quite well. Choosing a range up to 3 was again necessary for this heatmap to achieve visually appealing results. However, the gradation progresses slower than in Fig. 42. Also notable is, that the values for α_depth do not progress gradually until reaching its peak at the top right corner. For entrainment-coefficients C_e = -6.1 and C_e = -6 the values for α_depth rise and fall with each maximum flow height of the input-hydrograph and not rise continuously.

5.6.3 Equifinality for Flow Time

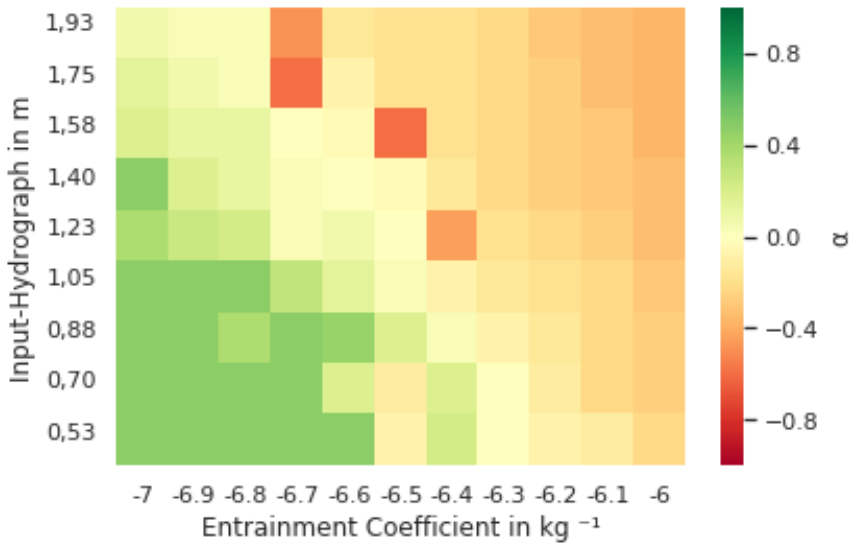

Figure 44: Heatmap for flow time.

Regarding the flow time, it was not necessary to unbalance the scale, because a balanced scale already produced a visually attractive heatmap. One thing to mention here is, that the underestimating side and overestimating side are switched. Considering that high entrainment and flow heights also mean, that the flow has more volume and due to this probably moves faster, this makes absolute sense because the flow then passes the time point measurements earlier than the flows with less entrainment/flow height and therefore less speed.
The diagonal in this heatmap is nearly perfectly moving from the top left to the bottom right. Only the minimum and the maximum of the entrainment-coefficient range, C_e = -7 and C_e = -6, could be removed in order to gain an even better result. In the middle/upper part of the diagonal, four outliers are remarkable, more than in Fig. 42 or Fig. 43.
Overestimating and underestimating side of the diagonal both show a slow evolving gradation. This could indicate, that the flow time is not as essential as the entrainment and flow height for the evaluation for this event. When entrainment and flow height clearly over- and underestimate the assumed event, the flow time still is in range of -0.5 to 0.5. Notable is the clean gradual gradation of the underestimating side. Until the top right corner, the values for α_time almost equally change, with close values forming lines parallel to the diagonal, which can be considered the optimum regarding the equifinality. The overestimating side shows this gradual gradation up to a certain point, after which the values in the bottom left corner almost all show the equal result.

5.6.4 Equifinality for the combination of entrainment, flow height and flow time

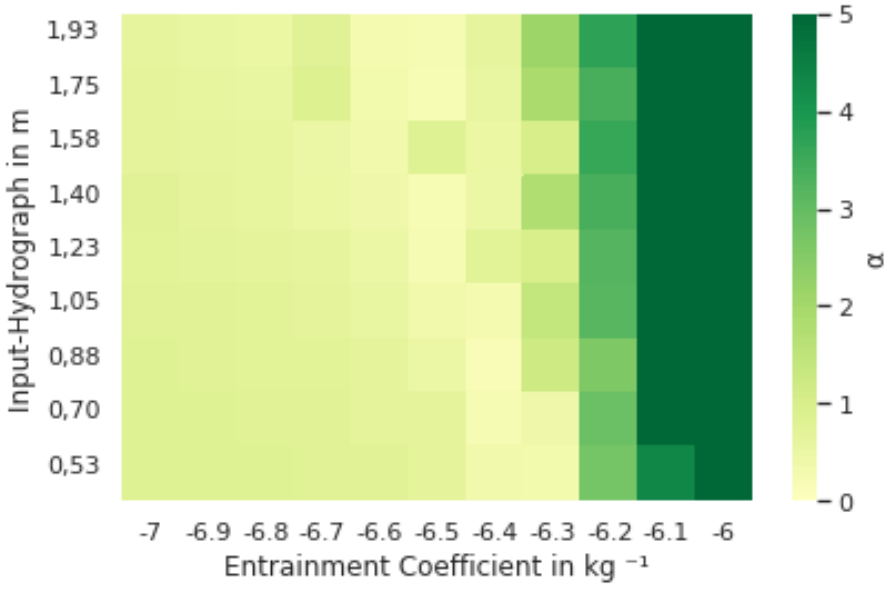

Figure 45: Heatmap for the combination of entrainment, flow height and flow time.

This heatmap takes the entrainment, flow height and flow time into consideration and with the method explained in Sect. 4 an absolute deviation is created, which only allows positive values for α_combined.
From C_e = -6.6 top to C_e = -6.3 bottom a diagonal is recognizable which can be translated to equifinality. With the same method explained in Sect. 5.6.1 and 5.6.2, to reproduce this heatmap only in the range of C_e = -6.6 to C_e = -6.3, this diagonal could be displayed more accurately.
Left of the diagonal the values are mostly similar, around 0.5 to 1.5. On the other side of the diagonal the values go up to 5 and still almost all fields of C_e = -6.1 and C_e = -6 have the maximum value. Raising the maximum would have ruined the visual effect of the heatmap and would have been useless, because simulations with an absolute deviation of 5 or more are already vastly overestimating the assumed event, and it is not relevant if the factor is 5 or, for example, 8.
This difference between the left and the right side of the diagonal is generated because for the other heatmaps, no absolute deviations were calculated, so overestimating and underestimating values were possible. Underestimating values were limited with a minimum of -1, whilst overestimating values did not have a fixed maximum. For the entrainment and flow height map the overestimating values were displayed on the right of the diagonal and lots of fields gained values of 5 and more. The flow time however was switched up, so the overestimating values were on the left of the diagonal, however for this heatmap only maximum values of ~0.5 were reached. All these facts together lead to a combined heatmap like the one above.

6. Discussion

The following chapter is discussing and critically analysing the results of this thesis. One of the first topics is the choice of validation criteria, namely entrained volume, flow height and flow time. These three categories were chosen, because it was possible to reconstruct the observation values. With the post-event DEM, furthermore the pre-event DEM, it was possible to estimate the entrained volume, the flow height was measured during the event, and with pictures and eye-/earwitnesses it was possible to gain an overview regarding the flow time. Predestined validation criteria, using r.avaflow, would be the observed impact or deposition area, as r.avaflow includes built-in functions to validate the model results against observation (M. Mergili, Fischer, Krenn, et al., 2017). However, using these functions was not possible due to lack of accuracy regarding the DEMs in usage. The post-event DEM was created several weeks after the event. In the meantime a lahar and several floods streamed down the same path as the jökulhlaup, changing the topography significantly, especially in the lowlands where a lot of debris deposited. Since there

was no pre-event DEM available and impossible to change the whole area of the lowlands in the post-event DEM, this validation criteria could not be used for this event.

6.1 Entrainment

r.avaflow was able to simulate the encarved trench quite well looking at the total entrained volume. Due to the fact, that there was no existing pre-event DEM, the only possibility was to create one using the post-event DEM. Different methods were used to estimate the entrained volume and the mean was chosen for the comparison with the simulations. So, the observation values might be not completely accurate, hence the simulation values which supposedly fit well, are not as correct as assumed. However, there are simulations over- and underestimating the observed values only by a small factor, so even if the observed entrained volume was not estimated completely accurate, r.avaflow would probably still be able to simulate the entrained volume to an acceptable extent. Well documented two-phase events are scarce, but do exist (Fischer et al., 2015; Krenn et al., 2016; M. Mergili, Emmer, et al., 2018; M. Mergili, Frank, et al., 2018; M. Mergili, Jaboyedoff, et al., 2020; M. Mergili, Pudasaini, et al., 2020; Martin Mergili et al., 2016) and are essential to further develop simulation tools for gravitational mass flows and consequently entrainment. One way to improve entrainment simulation would be the implementation of a mechanical model for erosion, entrainment and deposition (Pudasaini & Fischer, 2016).

6.2 Flow Height

As for the entrainment, r.avaflow was able to deliver promising results for the flow height of the jökulhlaup. Again, the pre-event DEM, developed from the post-event DEM could be the resource of uncertainties. The post-event DEM was rendered some time after the event, during which a couple of floods of lahar came down the flow path, depositing debris and leading to changes in topography (Roberts et al., 2011). Comparing the simulation values with the observation values, this fact has to be considered, as this part of the post-event DEM was not changed, due to the potential excessive effort. However, as stated for the entrained volume, some simulations over- and underestimated the observation values, so it probably would be possible, to attain the correct flow height values, comparing the simulations to differing observation values.

6.3 Flow time

The observation values for the flow time resulted from pictures taken out of a helicopter during the event and statements from eye/-earwitnesses. Two output-hydrographs were installed to measure

the time of the simulated flow. Because for comparison with the observations, the second measurement point was chosen, the best simulation, in the heatmap, is the one, which came closest to the second measurement point after 45 minutes. It is reaching the second measurement point exactly after 45 minutes, however after 30 minutes the simulated flow is farther downwards than the assumed flow. This is the case for most of the simulations. One reason for that might be, that the basal friction angle was adjusted too low for the simulations. Also, the observations regarding the flow time were not precise, and the estimations for the second time measurement point ranged from 45-60 minutes. Another reason might be the composition of the flow. After consulting Tómas Jóhannesson from the Icelandic Meteorological Office, a solid amount of 35% was set. Increasing the solid amount would increase friction and potentially decelerate the flow. Since the time measurement points could only be guessed and not determined precisely maybe decelerating the flow plus increasing the time of the second time measurement point cause more accurate results. Or dividing the flow path into two parts, an upper and lower part, with two different basal friction angles, as the topography differs along the flow path, with glacier on top and rocky lowlands on the bottom (Gíslason, 2012).

6.4 Combination of entrainment, flow height and flow time

An absolute ratio of deviation was elaborated to rate the simulations combining all three results of entrainment, flow height and flow time leading to an overall best simulation. Looking at that simulation the entrained volume and flow time provide satisfying results. The rough structure of the entrainment depths looks quite similar to the observations, as do the entrainment depths. For the second time measurement point, after 45 minutes, the results fit quite well. Regarding the flow height, the simulation quite underestimated the observations. For the simulation to fit the observations properly, the maximum flow height of the input-hydrograph would have to be raised. A raise of the flow height, combined, as stated above, with an increase of the basal friction angle and a change of the solid-fluid ratio of the flow could lead to a fitting simulation.

6.5 Equifinality

It was possible to show equifinality to a certain extent, analysing the 121 simulations conducted with the underlying model implemented in r.avaflow. However, some limitations could be observed throughout the results. The most obvious factor was the range of input-parameters, especially for the entrainment-coefficient. Looking at the Heatmaps the top right corner and the bottom left corner overestimate the observed values by a factor up to over 8, respectively underestimate the observed values down to -1, which pictures zero entrainment, flow height and therefore no flow time measurements.

Looking at the entrainment-coefficient, the two highest/lowest values almost lead to no meaningful results at all throughout all heatmaps. One exception is the heatmap for the flow time, which will be discussed further down the chapter. Decreasing the range of the entrainment-coefficient with smaller intervals could lead to better heatmaps, regarding the showing of equifinality, because more input-combinations would potentially lead to meaningful results (Beven, 1993).

The input-hydrographs apparently do not have as great an impact as does the entrainment-coefficient. When looking at the heatmaps, almost every input-hydrograph is able to produce results similar to the observed values, when paired with the correct entrainment-coefficient. What could be changed is the solid-fluid ratio, as mentioned above, to produce a simulation which would fit the observed values of the jökulhlaup in all three categories to a satisfying extent.

While the heatmap for the entrained volume and the flow time show clear under-/overestimation of the observed values, the heatmap for the flow time shows quite fitting results throughout all input-parameter combinations. Overestimating and underestimating side of the diagonal both show a slow evolving gradation with factors only up/down to 0.5 of the observed values. One explanation would be, that the flow time is not as crucial as the entrained volume and flow height for the evaluation of this event. While for certain simulations, the entrained volume and flow height clearly over-/underestimate the event, the flow time is still showing reasonable results. Especially the underestimating side of the heatmap is showing promising results regarding equifinality. From the middle diagonal outward the values for α_time almost equally change, with similar values forming lines parallel to the middle diagonal. The overestimating side is also showing similar results up to a certain extent, but at some point, the values in the bottom left corner all show similar results, regarding α_time.

7. Conclusion and outlook

7.1 Conclusions

Equifinality, although well-known throughout the scientific community, is treated sceptical since it is still a relative new thesis and not used frequently. In the field of simulating gravitational mass flows, equifinality is still under investigation, because there are still side effects and uncertainties to be considered. Therefore, this thesis aimed to establish a deeper understanding of the equifinality thesis by simulating a jökulhlaup with 121 different input combinations with the simulation tool r.avaflow. The two main objectives of this thesis were, if equifinality is plays an

important role simulating jökulhlaups with the underlying model implemented in r.avaflow and if r.avaflow is able to simulate the 2010 jökulhlaup at Eyjafjallajökull in an empirically adequate way.

Q1: Is equifinality an important aspect simulating jökulhlaups with the underlying model implemented in r.avaflow, with respect to initial and boundary conditions?

Evaluating the 121 simulations conducted, it can be stated that the underlying model implemented in r.avaflow is showing equifinality to a certain extent, with some limitations. As the heatmaps show, equifinality is only visible with input parameters in the middle of the selected range. Using extreme input values (on the bottom and top of the spectrum) the simulations differ more and more from the observation. Looking at the heatmaps the process under investigation is also a crucial factor regarding equifinality, due to their different complexities. When looking at the heatmap for the entrained volume, only a small section in the middle is showing simulations, which got close to the observation. Looking at the flow height and especially the flow time, the sections of simulations fitting the observation to some extent are bigger. A reason for that circumstance could be, that entrainment is quite a complex process, which is still not completely understood, hence implementing entrainment in simulation tools is an intricate task. For all three heatmaps of entrained volume, flow height and flow time it was possible to conduct multiple simulations with different input combinations that almost attained the exact same values as the observations. The combined heatmap of these three parameters, is also showing some simulations in the middle section which fit the observations very well. Summarizing all these observations, it is safe to say, that equifinality is an important aspect simulating jökulhlaups with r.avaflow, although further investigation is needed to gain better understanding of the topic. What can be said, is the fact, that no extreme parameter combinations led to a reasonable result which indicates a stability of the underlying model implemented in r.avaflow. Combinations of extreme parameters do not lead to an empirically adequate result, which could lead to wrong predictions, compared to observations, for similar events using r.avaflow.

Q2: Can the software tool r.avaflow be used to simulate the 2010 jökulhlaup at Eyjafjallajökull in an empirically adequate way, and how large are the accompanying uncertainties and how can we quantify them?

121 simulations were conducted to simulate the 2010 jökulhlaup at Eyjafjallajökull. The main focus was to determine, if the underlying model implemented in r.avaflow is able to show equifinality. Furthermore, this thesis is investigating if it is possible to simulate the 2010 jökulhlaup descending down the south of Eyjafjallajökull with r.avaflow. No simulation is fitting the observations in all three categories entrained volume, flow height and flow time. The overall best

simulation with the least deviation is showing good results in flow time and entrained volume, while the flow height is quite underestimated. However, looking at the categories separately, there is at least one simulation which fits the observations quite well. r.avaflow was able to simulate the entrained volume, flow height and flow time almost exactly, if we focus on only one category. What has to be considered, is the fact that the observations for the entrained volume and the flow time could only be estimated and not be defined precisely. For the third category, the flow height measured observations were available. This could lead to uncertainties in interpreting the simulations, because the observed values do not have to be one-hundred percent accurate. Especially the flow time could only be roughly guessed, as the observation values relied on pictures and witnesses, who heard the flow at a certain time in a certain location. Overall, r.avaflow was able to simulate the jökulhlaup quite well, when looking at the categories individually and solid when taking the combination of all three categories into consideration.

7.2 Outlook

r.avaflow was able to simulate the three categories, which were used to evaluate the event, in an empirical adequate way. In order to conduct simulations, which also fit the combination of the three categories, it would be necessary to run multiple simulations with different input parameters, changing the solid-fluid ratio and the basal friction angle, which was out of the scope of the present work. Furthermore, in order to detect if r.avaflow is able to simulate jökulhlaups in general, other events need to be back-calculated which should be well-documented. In the best case, the area of extent is well-known and digitalized to use the built-in functions of r.avaflow to compare the area of extent with the simulations.

Regarding the equifinality, the next steps would be to (i) to run the same event with different input-parameters, changing the range of the entrainment-coefficient to, for example C_e = -6.6 to C_e = -6.3 with intervals of 0.03 with the maximum flow heights of the input-hydrographs staying the same, (ii) using the same approach as in the present work for back-calculating another jökulhlaup to verify the results of this thesis and (iii) use the same, or a similar, approach for another type of gravitational mass flow, e.g. avalanche, debris flow or rock fall, to examine if similar results are possible with different types of mass flows.

8. References

Anacona, P. I., Mackintosh, A., & Norton, K. (2015). Reconstruction of a glacial lake outburst flood (GLOF) in the Engaño Valley, Chilean Patagonia: Lessons for GLOF risk management. *Science of the Total Environment*, *527*, 1–11.

Anderson, S. P., Walder, J. S., Anderson, R. S., Kraal, E. R., Cunico, M., Fountain, A. G., & Trabant, D. (2003). Integrated hydrologic and hydrochemical observations of Hidden Creek Lake jökulhlaups, Kennicott Glacier, Alaska. *Journal of Geophysical Research: Earth Surface*, *108 (F1)*(6003). https://doi.org/10.1029/2002JF000004

Armanini, A., Fraccarollo, L., & Rosatti, G. (2009). Two-dimensional simulation of debris flows in erodibloe channels. *Computational Geosciences*, *35*, 993–1006.

Awal, R., Nakagawa, H., Fujita, M., Kawaike, K., Baba, Y., & Zhang, H. (2010). Experimental study on a glacial lake outburst floods due to waves overtopping and erosion of moraine dam. *Annual Disaster Prev. Res. Inst. Kyoto University*, *53B*, 583–594.

Bajracharya, B., Shrestha, A., & Rajbhandari, L. (2007). Glacial Lake Outburst Floods in the Sagarmatha Region. *Mountain Research and Development*, *27(4)*, 336–344.

Berger, C., McArdell, B. W., Fritschi, B., & Schlunegger, F. (2010). A novel method for measuring the timing of bed erosion during debris flows and floods. *Water resources research*, *46(2)*, W02502. https://doi.org/10.1029/2009WR007993

Beven, K. (1993). Prophecy, reality and uncertainty in distributed hydrological modelling. *Advances in water resources*, *16(1)*, 41–51.

Beven, K. (2006). A manifesto for the equifinality thesis. *Journal of hydrology*, *320(1-2)*, 18–36.

Beven, K. (2012). Causal models as multiple working hypotheses about environmental processes. *Comptes Rendus Geoscience*, *344(2)*, 77–88.

Beven, K. (2018). On hypothesis testing in hydrology: Why falsification of models is still a really good idea. *Wiley Interdisciplinary Reviews: Water*, *5(3)*, e1278.

Beven, K., & Freer, J. (2001). Equifinality, data assimilation, and uncertainty estimation in mechanistic modelling of complex environmental systems using the GLUE methodology. *Journal of hydrology*, *249(1-4)*, 11–29.

Bird, D., & Gisladottir, G. (2012). Residents' attitudes and behaviour before and after the 2010 Eyjafjallajökull eruptions-a case study from southern Iceland. *Bulletin of Volcanology*, *74(6)*, 1263–1279.

Björnsson, H. (1976). Marginal and supraglacial lakes in Iceland. *Jökull*, *26*, 40–51.

Björnsson, H. (1988). Hydrology of Ice Caps in Volcanic Regions. *Soc. Sci. Isl.*, *Univ. of Iceland*(Reykjavík).

Björnsson, H. (1992). Jökulhlaups in Iceland: Prediction, characteristics and simulation. *Annals of Glaciology*, *16*, 95–106.

Björnsson, H. (2003). Subglacial lakes and jökulhlaups in Iceland. *Global and Planetary Change*, *35(3-4)*, 255–271.

Boon, S., & Sharp, M. (2003). The role of hydrologically-driven ice fracture in drainage system evolution on an Arctic glacier. *Geophysical Research Letters*, *30(18)*(1916). https://doi.org/10.1029/2003GL018034

Bottino, G., Chiarle, M., Joly, A., & Mortara, G. (2002). Modelling rock avalanches and their relation to permafrost degradation in glacial environments. *Permafrost and Periglacial Processes*, *13(4)*, 283–288.

Bouchut, F., Fernandez-Nieto, E. D., Mangeney, A., & Lagree, P.-Y. (2008). On new erosion models of Savage-Hutter type for avalanches. *Acta Mechanica*, *199*, 181–208.

Breien, H., de Blasio, F. V., Elverhøi, A., & Høeg, K. (2008). Erosion and morphology of a debris flow caused by a glacial lake outburst flood, Western Norway. *Landslides*, *5(3)*, 271–280.

Brufau, P., Garcia-Navarro, P., Ghilardi, P., Natale, L., & Savi, F. (2000). 1-D Mathematical modelling of debris flow. *Journal of Hydraulic Research*, *38*, 435–446.

Carrivick, J. (2006). Application of 2D hydrodynamic modeling to high-magnitude outburst floods: An example from Kverkfjöll, Iceland. *Journal of hydrology*, *321(1-4)*, 187–199.

Carrivick, J. (2011). Jökulhlaups: Geological importance, deglacial association and hazard management. *Geology Today*, *27(4)*, 133–140.

Cenderelli, D., & Wohl, E. (2003). Flow hydraulics and geomorphic effects of glacial-lake outburst floods in the Mount Verest region, Nepal. *Earth Surface Processes Landforms*, *28*, 385–407.

Chen, H., Crosta, G. B., & Lee, C. F. (2006). Erosional effects on runout of fast landslides, debris flows and avalanches: A numerical investigation. *Geotechnique*, *56*, 305–322.

Chen, H., & Lee, C. F. (2000). Numerical simulation of debris flows. *Canadian Geotechnical Journal*, *37(1)*, 146–160.

Christen, M., Bartelt, P., & Kowalski, J. (2010). Back calculation of the In den Arelen avalanche with RAMMS: interpretaion of model results. *Annals of Glaciology*, *51(54)*, 161–168.

Clague, J. J., & Evans, S. G. (2000). A review of catastrophic drainage of moraine-dammed lakes in British Columbia. *Quaternary Science Reviews*, *19(17-18)*, 1763–1783.

Clarke, G. K. C. (1982). Glacier outburst floods from „Hazard Lake“, Yukon Territory, and the problem of flood magnitude prediction. *Journal of Glaciology*, *28(98)*, 3–21.

Costa, J. E., & Schuster, R. L. (1988). The formation and failure of natural dams. *Geological society of America bulletin*, *100(7)*, 1054–1068.

Crosta, G. B., Chen, H., & Frattini, P. (2006). Forecasting hazard scenarios and imoplications for the evaluation of countermeasure efficiency for large debris avalanches. *Engineering Geology*, *83(1-3)*, 236–253.

Crosta, G. B., Imposimato, S., & Roddeman, D. (2009). Numerical modelling of entrainment/deposition in rock and debris-avalanches. *Engineering Geology*, *109(1-2)*, 135–145.

De Jong, C. (1992). *Measuring Changes in Micro and Macro Roughness on Mobile Gravel Beds*. Proceedings of the Oslo Symposium, IAHS Publ., 210.

Dean, S., Freer, J. E., Beven, K. J., Wade, A. J., & Butterfield, D. (2009). Uncertainty assessment of a process-based integrated catchment model of phosphorus (INCA-P). *Stochastic Environmental Research and Risk Assessment*, *23(7)*, 991–1010.

Doty, D. H., Glick, W. H., & Huber, G. P. (1993). Fit, equifinality, and organizational effectiveness: A test of two configurational theories. *Academy of management journal*, *36(6)*, 1196–1250.

Dunning, S., Large, A., Russell, A., Roberts, M., Duller, R., Woodward, J., Mériaux, A.-S., Tweed, F., & Lim, M. (2013). The role of multiple glacier outburst floods in proglacial landscape evolution: The 2010 Eyjafjallajökull eruption, Iceland. *Geology*, *41(10)*, 1123–1126.

Ebel, B. A., & Loague, K. (2006). Physics-based hydrologic-response simulation: Seeing through the fog of equifinality. *Hydrological Processes: An International Journal*, *20(13)*, 2887–2900.

Einstein, H. A. (1937). *The bed load transport as probability problem* [Mitt. Versuchsanstalt Wasserbau]. Eigenössische Technische Hochschule Zürich.

Fischer, J.-T., Kofler, A., Fellin, W., Granig, M., & Kleemayr, K. (2015). Multivariate parameter optimization for computaional snow avalanche simulation in 3d terrain. *Journal of Glaciology*, *61(229)*, 875–888.

Fischer, J.-T., Kowalski, J., & Pudasaini, S. (2012). Topographic curvature effects in applied avalanche modeling. *Cold Regions Science and Technology*, *74*, 21–30.

Fisher, D. (1973). Subglacial leakage of Summit Lake, British Columbia, by dye determinations. *Symposium on the Hydrology of Glaciers*, *95*, 111–116.

Fraccarollo, L., & Capart, H. (2002). Riemann wave description of erosional dam-break flows. *Journal of Fluid Mechanics*, *461*, 183–228.

Fread, D. L. (1988). *BREACH: An erosion model for earthen dam failures*. Hydrologic Research Laboratory, National Weather Service, NOAA.

Gíslason, M. B. (2012). *Straumfræðileg hermun jökulhlaups niður suðurhlíðar Eyjafjallajökuls í apríl 2010: Ákvörðun Manningsstuðla*.

Gottlieb, G. (2001). The relevance of developmental-psychobiological metatheory to developmental neuropsychology. *Developmental Neuropsychology*, *19(1)*, 1–9.

GRASS Development Team. (2016). *Geographic Resources Analysis Support System (GRASS) Software, Version 7.0.* Open Source Geospatial Foundation. http://grass.osgeo.org

Griswold, J. P., & Iverson, R. M. (2008). *Mobility statistics and automated hazard mapping for debris flows and rock avalanches*. U.S. Geological Survey Scientific Investigations Report 2007-5276. http://pubs.usgs.gov/sir/2007/5276/.

Gruber, U., & Margreth, S. (2001). Winter 1999: A valuable test of the avalanche-hazard mapping procedure in switzerland. *Annals of Glaciology*, *32*, 328–332.

Gudmundsson, M. (2015). *The Encyclopedia of Volcanoes*. Academic Press.

Gudmundsson, M., Pedersen, R., Vogfjörd, K., Thorbjarnardóttir, B., Jakobsdóttir, S., & Roberts, M. (2011). *Eruptions of Eyjafjallajökull Volcano, Iceland*.

Haeberli, W. (1983). Frequency and characteristics of glacier floods in the Swiss Alps. *Annals of Glaciology*, *4*, 85–90.

Haines-Young, R. H., & Petch, J. R. (1983). Multiple Working Hypotheses: Equifinality and the Study of Landforms. *Transactions of the institute of British Geographers*, 458–466.

Hauffe, C., Müller, R., Winkler, P., Baldy, A., Schwarze, R., & Wagner, M. (2016). Strategie zur Kalibrierung großräumiger Wasserhaushaltsmodelle sowie Ergebnisse für Ist-Zustand und Klimaszenarien in Sachsen. *Hydrologie und Wasserbewirtschaftung*, *60(1)*, 57–77.

Huggel, C., Kääb, A., Haeberli, W., & Krummenacher, B. (2003). *Regional-scale GIS models for assessment of hazards from glacier lake outbursts: Evaluation and application in the Swiss alps*.

Hungr, O., & Evans, S. G. (2004). Entrainment of debris in rock avalanches: An analysis of a long run-out mechanism. *Geological Society of America Bulletin*, *116(9-10)*, 1240–1252.

Hungr, O., McDougall, S., & Bovis, M. (2005). Entrainment of material by debris flows. In *Debris-flow hazards and related phenomena.* (S. 135–158). Springer.

Iorgulescu, I., Beven, K. J., & Musy, A. (2007). Flow, mixing, and displacement in using a data-based hydrocheical model to predict conservatice tracer data. *Water resources research*, *43(3)*.

Issler, D. (2014). Dynamically consistent entrainment laws for depth-averaged avalanche models. *Journal of Fluid Mechanics*, *759*, 701–738.

Iverson, R. M. (2012). Elementary theory of bed-sediment entrainment by debris flows and avalanches. *Journal of Geophysical Research: Earth Surface*, *117*, F03006.

Iverson, R. M., & Ouyang, C. (2015). Entrainment of bed material by Earth-surface mass flows: Review and reformulation of depth-integrated theory. *Reviews of Geophysics*, *53(1)*, 27–58.

Iverson, R. M., Reid, M. E., Logan, M., LaHusen, R. G., Godt, J. W., & Griswold, J. G. (2011). Positive feedback and momentum growth during debris-flow entrainment of wet bed sediment. *Nature Geoscience*, *4*, 16–121. https://doi.org/10.1038/NGEO1040

Jensen, E., Helgason, J., Einarsson, S., Sverrisdottir, G., Höskuldsson, A., & Oddsson, B. (2013). Lahars, Floods and Debris Flows Resulting from the 2010 Eruption of Eyjafjallajökull: Observations, Mapping, and Modelling. In *Landslide science and practice* (S. 435–440). Springer, Berlin, Heidelberg.

Johannesdottir, G., & Gisladottir, G. (2010). People living under the threat of volcanic hazard in southern Iceland: Vulnerability and risk perception. *Natural Hazards and Earth System Sciences*, *10(2)*, 407–420.

Kamb, B., Raymond C. F., Harrison, W. D., Engelhardt, H., Echelmeyer, K. A., Humphrey, N., Brugman, M. M., & Pfeffer, T. (1985). Glacier surge mechanism: 1982-83 surge of Variegated Glacier, Alaska. *Science*, *227(4686)*, 469–479.

Karlsdottir et al. (2012). *The 2010 Eyjafjallajökull eruption, Iceland*. Report to ICAO, 209p.

Kattel, P., Khattri, K. B., Pokhrel, P. R., Kafle, J., Tuladhar, B. M., & Pudasaini, S. P. (2016). Simulating glacial lake outburst floods with a two-phase mass flow model. *Annals of Glaciology*, *57(71)*, 349–358.

Kattelmann, R. (2003). Glacial lqke outburst floods in the Nepal Himalaya: A manageable hazard? *Natural Hazards*, *28*, 145–154.

Kershaw, J. A., Clague, J. J., & Evans, S. G. (2005). Geomorphic and sedimentological signature of a two-phase outburst flood from moraine-dammed Queen Bess Lake, British Columbia, Canada. *Earth Surface Processes Landforms*, *30*, 1–25.

Kingslake, J., & Ng, F. (2013). Modelling the coupling of flood discharge with glacier flow during jökulhlaups. *Annals of Glaciology*, *54(63)*, 25–31.

Kirkby, M. J. (1996). *A role for theoretical models in geomorphology?* The Scientific Nature of Geomorphology: Proceedings of the 27thBinghamton Symposium in Geomorphology. Held 27-29 September, 1996 (Vol. 27, p. 257). John Wiley & Sons

Krenn, J., Mergili, M., Fischer, J.-T., Frattini, P., & Pudasaini, S. (2016). *Proceedings of the 12th International Symposium on Landslides*. 12th International Symposium on Landslides, Napoli, Italy, 12-19 June 2016.

Le, L., & Pitman, E. B. (2009). A model for granular flows over an erodible surface. *Siam journal on applied mathematics*, *70(5)*, 1407–1427.

Lecomte, I., Thollet, I., Juliussen, H., & Hamran, S. E. (2008). Using geophysics on a terminal moraine damming a glacial lake: The Flatbe debris flow case, Wetsern Norway. *Advances in Geosciences*, *14*, 301–307.

Legros, F. (2002). The mobility of long-runout landslides. *Engineering Geology*, *63*, 301–331.

Leopold, L. B., Emmet, W. W., & Myrick, R. M. (1966). Channel and hillslope processes in a semi-arid area. *U.S. Geological Survey Professional Paper*, *352G*, 193–253.

Leopold, L. B., Wolman, M. G., & Miller, J. P. (1964). *Fluvial Processes in Geomorphology*. *522 pp.*, W. H. Freeman, San Francisco, California.

Liestøl, O. (1956). Glacier-dammed lakes in Norway. *Nor. Geogr. Tidsskr.*, *15*, 122–149.

Lisle, E., & Eads, R. E. (1991). Methods to measure sedimentation of spawning gravels. *Reservoir Note PSW-411*, *7 pp.*, Pacific Southwest Reservoir St. For. Serv., U.S. Dep. of Agric., Berkeley, California.

Liu, Y., Freer, J. E., Beven, K. J., & Matgen, P. (2009). Towards a limit of acceptability approach to the calibration of hydrological models: Extending observation error. *Journal of hydrology*, *367(1-2)*, 93–103.

Magnusson, E., Gudmundsson, M., Roberts, M., Sigurdsson, G., Höskuldsson, F., & Oddsson B. (2012). Ice-volcano interactions during the 2010 Eyjafjallajökull eruption, as revealed by airborne imaging radar. *Journal of Geophysical Research: Solid Earth*, *117(B7)*.

Mangeney, A. (2011). Landslide boost from entrainment. *Nature Geoscience*, *4(2)*, 77–78.

Mangeney, A., Roche, O., Hungr, O., Mangold, N., Faccanoni, G., & Lucas, A. (2010). Erosion and mobility in granular collapse over sloping beds. *Journal of Geophysical Research: Earth Surface*, *115*, F03040. https://doi.org/10.1029/2011JF002278

Mangeney, A., Tsimring, L., Volfson, D., Aranson, I., & Bouchut, F. (2007). Avalanche mobility induced by the presence of an erodible bed and associated entrainment. *Geophysical Research Letters*, *34(22)*.

McCoy, S. W., Kean, J. W., Coe, J. A., Tucker, G. E., Staley, D. M., & Wasklewicz, T. A. (2012). Sediment entrainment by debris flows: In situ measurements from the headwaters of a steep catchment. *Journal of Geophysical Research: Earth Surface*, *117*, F03016. https://doi.org/10.1029/2011JF002278

McDougall, S., & Hungr, O. (2005). Dynamic modelling of entrainment in rapid landslides. *Candadian Geotechnical Journal*, *42(5)*, 1437–1448.

Mergili, M., Emmer, A., Juricová, A., Cochachin, A., Fischer, J.-T., Huggel, C., & Pudasaini, S. P. (2018). How well can we simulate complex hydrogeomorphic process chains? The 2012 multi-lake outburst flood in the Santa Cruz Valley (Cordillera Blanca, Perú). *Earth surface processes and landforms*, *43(7)*, 1373–1389.

Mergili, M., Fischer, J.-T., Krenn, J., & Pudasaini, S. P. (2017). R.avaflow v1, and advanced open-source computational framework for the propagation and interaction of two-phase mass flows. *Geoscientific Model Development*, *10(2)*, 553.

Mergili, M., Fischer, J.-T., & Pudasaini, S. P. (2017). *Process chain modelling with r.avaflow: Lessons learned for multi-hazard analysis*. *Workshop on World Landslide Forum*, (pp. 565-572). Springer, Cham.

Mergili, M., Frank, B., Fischer, J.-T., Huggel, C., & Pudasaini, S. P. (2018). Computational experiments on the 1962 and 1970 landslide events at Huascarán (Peru) with r.avaflow: Lessons learned for predictive mass flow simulations. *Geomorphology*, *322*, 15–28.

Mergili, M., Jaboyedoff, M., Pullarello, J., & Pudasaini, S. P. (2020). Back-calculation of the 2017 Piz-Cengalo-Bondo landslide cascade with r.avaflow. *Natural Hazards and Earth System Sciences*, *20*, 505–520. https://doi.org/10.5194/nhess-20-505-2020

Mergili, M., Pudasaini, S. P., Emmer, A., Fischer, J.-T., Cochachin, A., & Frey, H. (2020). Reconstruction of the 1941 multi-lake outburst flood at Lake Palcacocha (Cordillera Blanca, Peru). *Hydrology and Earth System Sciences*, *24*, 93–114. https://doi.org/10.5194/hess-24-93-2020

Mool, P. K., Bajracharya, S. R., & Joshi, S. P. (2001). *Inventory of glaciers, glacial lakes and glacial lake outburst floods.* Nepal International Centre for Integrated Mountain Development, Kathmandu, Nepal.

Moring, J. R., & Lantz, R. L. (1975). The Alseawatershed study: Effects of logging on the aquatic resources of three headwater streams of the Alsea River, Oregon. *Fish. Res. Rep.*, *9*, 66 pp., Oregon Depratment of Fish and Wildlife, Corvallis.

Naaim, M., Faug, T., & Naaim-Bouvet, F. (2003). Dry granular flow modeling including erosion and deposition. *Surveys in Geophysics*, *24*, 569–585.

Nawa, R. K., & Frissell, C. A. (1993). Measuring scour and fill of gravel streambeds with scour chains and sliding-bead monitors. *North American Journal of Fisheries Management*, *13*, 634–639.

Neteler, M., & Mitasova, H. (2007). *Open source GIS: a GRASS GIS approach*. (Vol. 689) Springer Science & Business Media.

Nye, J. F. (1976). Water flow in glaciers: Jökulhlaups, tunnels and veins. *Journal of Glaciology*, *17(76)*, 181–207.

Osti, R., & Egashira, S. (2009). Hydrodynamic characteristics of the Tam Pokhari glacial lake outburst flood in the Mt. Everest region, Nepal. *Hydrological Processes: An International Journal*, *23(20)*, 2943–2955.

Pappenberger, F., Frodsham, K., Beven, K. J., Romanovicz, R., & Matgen, P. (2007). Fuzzy set approach to calibrating distributed flood inundation models using remote sensing observations. *Hydrological Earth Systems Science Discussion*, *3*, 2243–2277.

Pierson, T. C. (1989). Hazardous hydrologic consequences of volcanic eruptions and goals for mitigative action: An overview, in „Hydrology of disasters“, edited by Ö. Starosolszky and O. M. Melder. *World Meteorol. Org.*, *Geneva*(Switzerland), 220–236.

Pirulli, M., & Pastor, M. (2012). Numerical study on the entrainment of bed material into rapid landslides. *Geotechnique*, *62*, 959–972.

Pudasaini, S., & Hutter, K. (2007). *Avalanche dynamics: Dynamics of rapid flows of dense granular avalanches.* Springer Science & Business Media.

Pudasaini, S., & Krautblatter, M. (2014). A two-phase mechanical model for rock-ice avalanches. *Journal of Geophysical Research: Earth Surface*, *119(10)*, 2272–2290.

Pudasaini, S. P. (2012). A general two-phase debris flow model. *Journal of Geophysical Research: Earth Surface*, *117(F3)*.

Pudasaini, S. P., & Fischer, J.-T. (2016). *A mechanical erosion model for two-phase mass flows.* arXiv preprint arXiv:1610.01806

R Core Team. (2016). *R: A Language and Environment for Statistical Computing*.

Roberts, M. (2005). Jökulhlaups: A reassessment of floodwater flow through glaciers. *Reviews of Geophysics*, *43(1)*.

Roberts, M., Sigurdsson, G., Sigurdsson, O., Pagneux, E., Jóhannesson, T., Zóphóníasson, S., Gudmundsson, M., Russell, A., Gylfason, Á., Höskuldsson, F., & Björnsson, B. (2011). *The April 2010 Eruption of Eyjafjallajökull Volcano: Glacial Flooding and Attendant Hazards*. IAVCEI-IUGG, Melbourne, Australia, 28.

Rogers, A. R. (2000). On equifinality in faunal analysis. *American Antiquity*, *65(4)*, 709–723.

Rogers, J. D., Watkins, C. M., & Chung, J.-W. (2010). The 2005 upper Taum Sauk dam failure: A case history. *Environmental & Engineering Geoscience*, *16(3)*, 257–289.

Schneider, D., Bartelt, P., Caplan-Auerbach, J., Christen, M., Huggel, C., & McArdall, B. W. (2010). Insights into rock-ice avalanche dynamics by combined analysis of seismic recordings and a numerical avalanche model. *Journal of Geophysical Research: Earth Surface*, *115(F4)*.

Schneider, D., Huggel, C., Cochachin, A., Guillén, S., & García, J. (2014). Mapping hazards from glacier lake outburst floods based on modelling of process cascades at Lake 513, carhuaz, Peru. *Advances in Geosciences*, *35*, 145–155.

Scott, K. M., Vallance, J. W., Kerle, N., Macías, J. L., Strauch, W., & Devoli, G. (2005). Catastrophic precipitation-triggered lahar at Casita volcano, Nicaragua. *Earth Surfaces Processes Landforms*, *30*, 59–79.

Sosio, R., Crosta, G. B., Chen, J. H., & Hungr, O. (2012). Modelling rock avalanche propagation onto glaciers. *Quaternary Science Reviews*, *47*, 23–40.

Sovilla, B., Burlando, P., & Bartelt, P. (2006). Field experiments and numerical modeling of mass entrainment in snow avalanches. *Journal of Geophysical Research: Earth Surface*, *111*, F03007. https://doi.org/10.1029/2005JF000391

Sparks, R. S. J., Gardeweg, M. C., Calder, E. S., & Matthews, S. J. (1997). Erosion by pyroclastic flows on Lascar Volcano, Chile. *Bulletin of Volcanology*, *58(7)*, 557–565.

Spring, U., & Hutter, K. (1981). Numerical studies of jökulhlaups. *Cold Regions Science and Technology*, *4(3)*, 227–244.

Tai, Y.-C., & Kuo, C. Y. (2008). A new model of granular flows over general topography with erosion and deposition. *Acta Mechanica*, *199*, 71–96.

Thórarinsson, S. (1939). The ice-dammed lakes of Iceland with particular reference to their value as indicators of glacier oscillations. *Geografisker Annaler*, *21A*, 216–242.

Vallance, J. W., & Scott, K. M. (1997). The Osceola mudflow from Mount Rainier: Sedimentology and hazard implications of a huge clay-rich debris flow. *Geological Society of America Bulletin*, *109*, 143–163.

Vilímek, V., Zapata, M. L., Klimes, J., Patzelt, Z., & Santillán, N. (2005). Influence of glacial retreat on natural hazrds of the Palcacocha Lake area, Peru. *Landslides*, *2*, 107–115.

Voellmy, A. (1955). Über die Zerstörungskraft von Lawinen. *Schweizerische Bauzeitung*, *Jahrg., 73*, 159–162.

Vrugt, J. A., ter Braak, C. J. F., Gupta, H. V., & Robinson, B. A. (2008). Equifinality of formal (DREAM) and informal (GLUE) Bayesion approaches in hydrologic modeling? *Stochastic Environmental Research and Risk Assessment*, *23(7)*, 1011–1026.

Walder, J. S., & Costa, J. E. (1996). Outburst floods from glacier-dammed lakes: The effect of mode of drainage on flood magnitude. *Earth Surface Processes Landforms*, *21*, 701–723.

Wang, G., Sassa, K., & Fukuoka, H. (2003). Downslope volume enlargement of a debris slide-debris flow in 1999 Hiroshima, Japan, rainstorm. *Engineering Geology*, *69*, 309–330. https://doi.org/10.1016/S0013-7952(02)00289-2

Wilcock, P. R., Barta, A. F., Shea, C. C., Kondolf, G. M., Matthews, W. V., & Pitlick, j. (1996). Observations of flow and sediment entrainment on a large gravel-bed river. *Water resources research*, *32(9)*, 2897–2909.

Worni, R., Stoffel, M., Huggel, C., Volz, C., Casteller, A., & Luckman, B. (2012). Analysis and dynamic modeling of a moraine failure and glacier lake outburst flood at Ventisquero Negro, Patagonian Andes (Argentina). *Journal of hydrology*, *444*, 134–145.

Xin, W., Shiyin, L., Wanqin, G., & Junli, X. (2008). Assessment and Simulation of Glacier Lake Outburst Floods for Longbasaba and Pida lakes, China. *Mountain Research and Development*, *28(3)*, 310–317.

Young, P., Parkinson, S., & Lees, M. (1996). Simplicity out of complexity in environmental modelling: Occam´s razor revisited. *Journal of applied statistics*, *23(2-3)*, 165–210.

9. Attachment A:

Attachment A shows the script written in Python 3.7, which was used to create the heatmaps. Four scripts were written in order to create heatmaps regarding the entrained volume, flow height, flow time and a heatmap combining these three parameters in one absolute ratio of deviation.

```
import numpy as np; np.random.seed(0)
import seaborn as sns; sns.set()
import matplotlib.pyplot as plt
```

```
abspath = '/home/simulation/avalanche_simulation/uli_simulation/Iceland_simulations/'
sim_list = np.zeros(121)
for i in
(0,1,2,3,4,5,6,7,8,9,10,11,12,13,14,15,16,17,18,19,20,21,22,23,24,25,26,27,28,29,30,31,32,33,34,35,3
6,37,38,39,40,41,42,43,44,45,46,47,48,49,50,51,52,53,54,55,56,57,58,59,60,61,62,63,64,65,66,67,68
,69,70,71,72,73,74,75,76,77,78,79,80,81,82,83,84,85,86,87,88,89,90,91,92,93,94,95,96,97,98,99,100
,101,102,103,104,105,106,107,108,109,110,111,112,113,114,115,116,117,118,119,120):

    filepath = abspath + '%s_results/%s_files/%s_validation.txt' %(i,i,i)

    a = [1, 2]

    with open(filepath, 'r') as fd:
        for n, line in enumerate(fd):
            if n == 1:
                string = line
                ves = float(string[27:-14])
            if n == 2:
                string = line
                vef = float(string[27:-14])

    entrainment = ves + vef
    sim_list[i] = (-entrainment-2000000)/2000000
```

```
entrainment = ["-7", "-6.9","-6.8", "-6.7", "-6.6", "-6.5", "-6.4", "-6.3", "-6.2", "-6.1", "-6"]
input_discharge = ["1,93", "1,75","1,58", "1,40", "1,23", "1,05", "0,88", "0,70", "0,53", "0,35", "0,18"]

sim_array = np.zeros((9,11))
#
================================================================================
# for idx, value in enumerate(sim_list):
#     j = range(11)
#     j =  idx//11 #TEILEN MIT REST
#     #if idx in range (0,10):
#       #  j = 0
#     #if idx in range (11,21):
#      #   j = 1c = length_list*0.25 + height_list*0.25 + sim_list*0.5
#     sim_array[j,idx]=(value)/-2300000
#     #j = int(idx/11)
#     #print(list(j))
#
================================================================,============

for j in range(9):
    for i in range(11):
        idx = (j*11+i)
        sim_array[j,i] = sim_list[idx]



#Index = np.array([[2300000/22600000, 2300000/23410000, 2300000/21680000],
                  #[2300000/19910000, 2300000/17400000, 2300000/20300000],
                  #[2300000/2111300, 2300000/10430000, 2300000/2281000]])

fig, ax = plt.subplots()
#im = ax.imshow(Index)

uniform_data = sim_array
ax = sns.heatmap(uniform_data, center=0, vmin=-1, vmax=9, cmap="RdYlGn")
ax.collections[0].colorbar.set_label("Ratio of relative Deviation")

#bounds = [0, 0.5, 0.75, 1.25, 1.5]
#cmap = "gist_earth"
#norm = colors.BoundaryNorm(bounds, cmap.N, clip=True)
#sns.heatmap(sim_array, cmap=cmap, norm=norm,)
```

```
#...and label them with the respective list entries
ax.set_xticklabels(entrainment)
ax.set_yticklabels(input_discharge)
# rotate the tick labels and set their alignment,
plt.setp(ax.get_yticklabels(), rotation=0, ha="right", rotation_mode="anchor")
plt.xlabel('Entrainment Coefficient in kg⁻¹')
plt.ylabel('Input-hydrograph in m')
# Loop over data dimensions and create text annotations
#for i in range(len(input_discharge)):
    #for j in range(len(entrainment)):
        #text = ax.text(j, i, Index[i, j],
                       #ha="center", va="center", color="w")


#ax.set_title("Entrainment")
fig.tight_layout()


import numpy as np; np.random.seed(0)
import seaborn as sns; sns.set()
import matplotlib.pyplot as plt




abspath = '/home/simulation/avalanche_simulation/uli_simulation/Iceland_simulations/'
height_list = np.zeros(121)
for j in
(0,1,2,3,4,5,6,7,8,9,10,11,12,13,14,15,16,17,18,19,20,21,22,23,24,25,26,27,28,29,30,31,32,33,34,35,3
6,37,38,39,40,41,42,43,44,45,46,47,48,49,50,51,52,53,54,55,56,57,58,59,60,61,62,63,64,65,66,67,68
,69,70,71,72,73,74,75,76,77,78,79,80,81,82,83,84,85,86,87,88,89,90,91,92,93,94,95,96,97,98,99,100
,101,102,103,104,105,106,107,108,109,110,111,112,113,114,115,116,117,118,119,120):
```

```
    filepath = abspath + '%s_results/%s_files/%s_ctrlpoints.txt' %(j,j,j)

    a = [1]

    with open(filepath, 'r') as fd:
        for n, line in enumerate(fd):
            #if n == 42:
            string = line
        fhmax = float(string[21:-1])
            #if n == 2:
                #string = line
                #vef = float(string[27:-14])

    flowheight = fhmax
    height_list[j] = (flowheight-7)/7

entrainment = ["-7", "-6.9","-6.8", "-6.7", "-6.6", "-6.5", "-6.4", "-6.3", "-6.2", "-6.1", "-6"]
input_discharge = ["1,93", "1,75","1,58", "1,40", "1,23", "1,05", "0,88", "0,70", "0,53", "0,35", "0,18"]

sim_array = np.zeros((9,11))
#
================================================================================
# for idx, value in enumerate(sim_list):
#     j = range(11)
#     j =  idx//11 #TEILEN MIT REST
#     #if idx in range (0,10):
#       #  j = 0
#     #if idx in range (11,21):
#      #   j = 1
#     sim_array[j,idx]=(value)/-2300000
#     #j = int(idx/11)
#     #print(list(j))
#
================================================================================

for j in range(9):
    for i in range(11):
        idx = (j*11+i)
        sim_array[j,i] = height_list[idx]
```

```
#Index = np.array([[2300000/22600000, 2300000/23410000, 2300000/21680000],
                   #[2300000/19910000, 2300000/17400000, 2300000/20300000],
                   #[2300000/2111300, 2300000/10430000, 2300000/2281000]])

fig, ax = plt.subplots()
#im = ax.imshow(Index)

uniform_data = sim_array
ax = sns.heatmap(uniform_data, center=0, vmin=-1, vmax=3, cmap="RdYlGn")
ax.collections[0].colorbar.set_label("Ratio of relative Deviation")

#bounds = [0, 0.5, 0.75, 1.25, 1.5]
#cmap = "gist_earth"
#norm = colors.BoundaryNorm(bounds, cmap.N, clip=True)
#sns.heatmap(sim_array, cmap=cmap, norm=norm,)




#...and label them with the respective list entries
ax.set_xticklabels(entrainment)
ax.set_yticklabels(input_discharge)
# rotate the tick labels and set their alignment
plt.setp(ax.get_yticklabels(), rotation=0, ha="right", rotation_mode="anchor")
plt.xlabel('Entrainment Coefficient in kg⁻¹')
plt.ylabel('Input-hydrograph in m')
# Loop over data dimensions and create text annotations
#for i in range(len(input_discharge)):
    #for j in range(len(entrainment)):
        #text = ax.text(j, i, Index[i, j],
                       #ha="center", va="center", color="w")


#ax.set_title("Flow Height")
fig.tight_layout()


import numpy as np
```

```
import seaborn as sns; sns.set()
import matplotlib.pyplot as plt

abspath = '/home/simulation/avalanche_simulation/uli_simulation/Iceland_simulations/'
length_list = np.zeros(121)
for h in
(0,1,2,3,4,5,6,7,8,9,10,11,12,13,14,15,16,17,18,19,20,21,22,23,24,25,26,27,28,29,30,31,32,33,34,35,3
6,37,38,39,40,41,42,43,44,45,46,47,48,49,50,51,52,53,54,55,56,57,58,59,60,61,62,63,64,65,66,67,68
,69,70,71,72,73,74,75,76,77,78,79,80,81,82,83,84,85,86,87,88,89,90,91,92,93,94,95,96,97,98,99,100
,101,102,103,104,105,106,107,108,109,110,111,112,113,114,115,116,117,118,119,120):

    filepath = abspath + '%s_results/%s_files/%s_hydinfo3.txt' %(h,h,h)



    data = np.loadtxt(filepath, skiprows=1)

   # if data[:,0]:
    #    print(1)

    z = data[:,0], data[:,5], data[:,9]
    time = np.array(z)
    np.shape(time)
    time_trans = time.transpose()

    for x in time_trans:
        if x[1] !=0 or x[2] != 0:
            break
        #if x.all() == 0:
         #   break

    y = x[:1]
    length_list[h] = (y-2700)/2700

entrainment = ["-7", "-6.9","-6.8", "-6.7", "-6.6", "-6.5", "-6.4", "-6.3", "-6.2", "-6.1", "-6"]
input_discharge = ["1,93", "1,75","1,58", "1,40", "1,23", "1,05", "0,88", "0,70", "0,53", "0,35", "0,18"]

sim_array = np.zeros((9,11))

for j in range(9):
    for i in range(11):
```

```
        idx = (j*11+i)
        sim_array[j,i] = length_list[idx]

fig, ax = plt.subplots()

uniform_data = sim_array
ax = sns.heatmap(uniform_data, center=0, vmin=-1, vmax=1, cmap="RdYlGn")
ax.collections[0].colorbar.set_label("Ratio of relative Deviation")

#...and label them with the respective list entries
ax.set_xticklabels(entrainment)
ax.set_yticklabels(input_discharge)

# rotate the tick labels and set their alignment
plt.setp(ax.get_yticklabels(), rotation=0, ha="right", rotation_mode="anchor")
plt.xlabel('Entrainment Coefficient in kg ⁻¹')
plt.ylabel('Input-hydrograph in m')

#ax.set_title("Flow Time")
fig.tight_layout()
```

```
c = ((length_list*length_list)**0.5)*0.25 + ((height_list*height_list)**0.5)*0.25 +
((sim_list*sim_list)**0.5)*0.5


c_array = np.zeros((9,11))

for j in range(9):
    for i in range(11):
        idx = (j*11+i)
        c_array[j,i] = c[idx]
```

```
fig, ax = plt.subplots()

uniform_data = c_array
ax = sns.heatmap(uniform_data, center=0, vmin=0, vmax=5, cmap="RdYlGn")
ax.collections[0].colorbar.set_label("Ratio of absolute Deviation")

#...and label them with the respective list entries
ax.set_xticklabels(entrainment)
ax.set_yticklabels(input_discharge)

# rotate the tick labels and set their alignment
plt.setp(ax.get_yticklabels(), rotation=0, ha="right", rotation_mode="anchor")
plt.xlabel('Entrainment Coefficient in kg ⁻¹')
plt.ylabel('Input-hydrograph in m')

#ax.set_title("combination")
fig.tight_layout()
```

10. Erklärung/Affirmation

Hiermit bestätige ich, dass:

- ich die vorliegende Masterarbeit selbstständig verfasst habe,
- ich keine anderen Quellen und Hilfsmittel benutzt habe als die angegebenen und mich keiner unerlaubten Hilfe bedient habe,
- ich dieses Masterarbeitsthema bisher weder im In- noch im Ausland in irgendeiner Form als Prüfungsarbeit vorgelegt habe,
- diese Arbeit mit der vom Begutachter beurteilten Arbeit vollstädnig übereinstimmt.

Hereby I certify, that:

- the master thesis was written by me, not using sources and tools other than quoted and without use of any other illegitimate support.
- I clearly marked and separately listed all of the literature and all of the other sources which I employed when producing this academic work, either literally or in content.
- I have not submitted this master thesis either nationally or internationally in any form.
- The version of this thesis is the same as the work judged by the supervisor.

Mäder 05.05.2020